BRNO UNIVERSITY OF TECHNOLOGY
VYSOKÉ UČENÍ TECHNICKÉ V BRNĚ

FACULTY OF MECHANICAL ENGINEERING
FAKULTA STROJNÍHO INŽENÝRSTVÍ

HEAT TRANSFER AND FLUID FLOW LABORATORY
LABORATOŘ PŘENOSU TEPLA A PROUDĚNÍ

LOW-COST FILTRATION BARRIERS FOR ULTRAFINE PARTICLES SEPARATION

LEVNÉ FILTRAČNÍ PŘEPÁŽKY PRO SEPARACI ULTRAJEMNÝCH ČÁSTIC

DOCTORAL THESIS
DIZERTAČNÍ PRÁCE

AUTHOR — Ing. Pavel Kejík
AUTOR PRÁCE

SUPERVISOR — prof. Ing. Tomáš Svěrák, CSc.
ŠKOLITEL

BRNO 2019

ABSTRACT

A lot of applications use inorganic filtering media based on materials that use primary resources and their production is energy-intensive and thus costly and environmentally harmful. The aim of this study is to verify whether alkali-activated materials based on secondary resources, namely blast furnace slag (BFS) and fly ash (FA), can be used to produce porous media which could possibly replace ceramic and other inorganic filters.

The research question was addressed using an experimental design based on an in-house developed MATLAB calculation scheme for composition mixtures based on the most important oxide ratios in the input raw materials. This way, the greatest control of the variable composition of the inputs was ensured. In addition, the work is more relevant in general because this computational tool takes the basic oxide composition of the resources into account, so the results can be generalized. The author also designed a pure one solid component mixture series for a comparison and better characterization of the effects of composition changes on the resulting product properties.

The findings show that the strength of the 24-hour, 70 °C cured materials can exceed 7.6 MPa under a four point bending tensile test (in accordance with ČSN EN 12390-5), but to achieve a good porosity, the strength is always decreased. In the final composition slightly above 6.3 MPa was achieved. In general, the results show that the SiO_2/Al_2O_3 ratio and the amount of alkali activator affect the strength the most. Pure BFS-based mixtures show more than twice the strength of the pure FA-based samples within the given compositions used for the experiments.

The fineness of the pores achieved using fractionated raw materials (particle sizes in the range of tens to slightly over a hundred microns) is in the order of tenths to units of microns in most cases and approximately 0.2 microns in the final composition.

The total porosity of the pressed bodies is closely under 40% which compared to the unclassified resource based materials, is nearly twice that much. Pure BFS-based samples show lower total porosities than the FA-based samples, apparently due to their entirely different particle morphology – irregularly angular in BFS and round in FA.

The efflorescence phenomenon was mostly observed on FA-based materials. Energy-dispersive spectrometry (EDS) confirmed sodium hydroxide crystals undergoing gradual carbonation by atmospheric CO_2.

Permeability testing required asymmetrical barriers preparation due to the very fine porosity of the material. The asymmetrical barriers achieved water permeability of 138 L/h.m^2.bar and air permeability of 1320 L/h.m^2.bar.

KEYWORDS

Alkali activation, alkali-activated materials, geopolymer, blast furnace slag, fly ash, filtration, separation

ABSTRAKT

V mnoha oborech jsou stále využívána anorganická filtrační media založená na materiálech, jejichž výroba využívá primární suroviny. Jejich výroba je tedy energeticky náročná a v důsledku nákladná a neohleduplná k životnímu prostředí. Cílem této práce je ověřit možnost využití alkalicky aktivovaných materiálů na bázi sekundárních surovin, především vysokopecních strusek (BFS) a popílků z uhelných elektráren (FA), pro výrobu porézních médií schopných v budoucnosti nahradit keramické a jiné anorganické filtry.

Výzkum je rozvinut skrze experimentální design založený na výpočetním schématu samostatně vyvinutém s pomocí programu MATLAB. Toto schéma počítá vhodná složení směsí na základě poměrů obsahu nejdůležitějších oxidů ve vstupních surovinách. Tak je zajištěno zohlednění proměnlivého složení vstupních surovin a práce je tím hodnotnější, že její výsledky jsou skrze početní nástroj zohledňující základní oxidové složení surovin zobecnitelné. Zároveň byly však pro srovnání a lepší názornost závislostí vlastností na složení navrhnuty a připraveny i série vzorků založené vždy pouze na jedné ze surovin.

Z výsledků vyplývá, že pevnost vzorků z těchto směsí (vytvrzených 24 hodin při 70 °C) ve čtyřbodové ohybové zkoušce dle ČSN EN 12390-5 může přesáhnout 7,6 MPa. Dosažením co možná nejvyšší porozity však zákonitě negativně ovlivňuje pevnost materiálu a výsledný materiál tedy dosahuje pevnosti těsně nad hranicí 6,3 MPa. Výsledky obecně dokazují, že nejvíce je pevnost materiálů ovlivněna poměrem SiO_2/Al_2O_3 a množstvím alkalického aktivátoru. Z výsledků vyplývá, že alkalicky aktivované materiály (AAM) na bázi strusky dosahují i více než dvojnásobné pevnosti analogických materiálů na bázi elektrárenského popílku.

Velikost pórů materiálů připravených z tříděných surovin s velikostí zrna od desítek po lehce přes sto mikronů se ve většině případů pohybuje v rozmezí desetin ž jednotek mikronů, v případě výsledného materiálu je to pak přibližně 0,2 mikronu.

Celková porozita lisovaných těles se pohybuje těsně pod 40 %, což je v tomto případě téměř dvojnásobek ve srovnání s totožnými materiály na bázi netříděných surovin. Výsledky rovněž ukazují, že materiály na bázi strusky vykazují nižší porozitu než ty na bázi popílku, což je patrně způsobeno rozdílnou morfologií částic obou materiálů – částice strusky jsou nepravidelně hranaté a částice popílku kulaté.

V průběhu experimentální činnosti byla pozorována tvorba výkvětů u materiálů na bázi elektrárenských popílků. Pomocí Energo-disperzní spektroskopické analýzy (EDS) byly výkvěty identifikovány jako hydroxid sodný procházející karbonatací za účasti vzdušného CO_2.

Test permeability vyžadoval, kvůli velmi jemné povaze porézní struktury, přípravu asymetrických filtračních přepážek. Tyto přepážky dosáhli propustnosti 138 L/h.m^2.bar pro vodu a 1320 L/h.m^2.bar pro vzduch.

KLÍČOVÁ SLOVA

Alkalická aktivace, alkalicky aktivované materiály, vysokopecní struska, elektrárenský popílek, filtrace, separace

KEJÍK, P. Low-cost filtration barriers for capture of ultrafine particles from media. Brno: Brno University of Technology, Faculty of Mechanical Engineering, 2018. 136 s. Supervisor of the doctoral thesis prof. Ing. Tomáš Svěrák, CSc..

KEJÍK, P. Levné filtrační přepážky pro separaci ultrajemných částic. Brno: Vysoké učení technické v Brně, Fakulta strojního inženýrství, 2018. 136 s. Vedoucí dizertační práce prof. Ing. Tomáš Svěrák, CSc..

DECLARATION

I hereby declare that I have written the PhD thesis on my own according to advice of my supervisor Prof. Ing. Tomáš Svěrák, Csc. and all the literary sources are quoted correctly and completely. This dissertation thesis is the property of the Faculty of Mechanical Engineering, Brno University of Technology and it can be used for commercial purposes only with consent of the doctoral thesis supervisor and the dean of FME.

…… ……

(Place, date) (Signature)

ACKNOWLEDGEMENT

Firstly, I would like to express my sincere gratitude to my supervisor prof. Ing. Tomáš Svěrák, CSc. for his patience, motivation, friendly attitude and encouragement.

My sincere thanks also goes to prof. Ing. Jaroslav Horský, CSc. (in memoriam) and prof. Ing. Miroslav Raudenský, CSc. who have allowed the establishment of our associated chemical engineering group and supported as well as inspired me.

I thank all my fellow labmates for the stimulating discussions, for the long evenings we were working together before deadlines, and for all the fun we have had in the last years.

Great thanks to my university colleagues for their help, namely: Ing. Jan Komínek, Ph.D. and Ing. Jakub Kůdela for their big help with the mathematical issues, Ing. Vlastimil Bílek, Ph.D. for help with the practical issues and measurements, Ing. et Ing. Pavel Bulejko for his numerous help and advice, Ing. Ondřej Krištof and Ing. Josef Kalivoda Ph.D. for the productive talks on the topic, all guys from the Heat Transfer and Fluid Flow Laboratory workshop for their help on the experimental work apparatus and especially for teaching me operating the workshop facilities.

Finally, my biggest thanks belong to my parents for the best support conceivable in life.

CONTENT

1 INTRODUCTION 9

2 THEORETICAL PART 10

2.1 Filtration 10
2.2 Porosity and porous media 11
2.3 Filtration barrier properties 14
2.4 Types of filtration media 14

2.4.1 Beds of granular material 16
2.4.2 Filter paper 16
2.4.3 Textile fabrics and geotextiles 17
2.4.4 Polymer porous barriers 17
2.4.5 Stoneware, ceramic and glass barriers 17
2.4.6 Sintered metal barriers 18

2.5 Alkali-activated materials and geopolymers 18

2.5.1 History of alkali activation 23
2.5.2 Alkali activation 24
2.5.3 Structures and Mechanism 25

3 STATE OF ART 31

4 METHODS 35

4.1 Spiral jet mill ALPINE Aeroplex 100 AS 35
4.2 Air jet sieve ALPINE E200 LS 36
4.3 Powder ultrafine classifier alpine 50 atp turboplex 37
4.4 Optical microscope Olympus BX41 38
4.5 Scanning electrone microscope 39
4.6 Laser granulometer MALVERN Mastersizer 2000 40
4.7 Planetary centrifugal vacuum mixer Thinky ARV-310 41
4.8 Porometer Quantachrome 3Gzh 42
4.9 Labortech tensile testing machine 43
4.10 Siemens D5005 X-RAY powder diffraction analysis 44
4.11 Experimental filtration post 45

5 EXPERIMENTAL PART 46

5.1 Materials 46

5.1.1 Particular materials *46*
5.1.2 Activators *52*
5.1.3 Material costs *53*
5.2 Composition calculation parameters 54
5.2.1 SiO_2:Al_2O_3 ..... *54*
5.2.2 M_2O:Al_2O_3 ..... *54*
5.2.3 H_2O:M_2O *55*
5.3 Composition calculation methods 56
5.3.1 MS Excel Solver *56*
5.3.2 MATLAB *58*
5.4 Mixtures compositions 63
5.5 Preparation procedure 65
5.6 Mechanical testing 73
5.7 Porosity 81
5.8 Microstructure 89
5.9 Final porous material composition 99
5.10 Permeability testing 101
6 DISCUSSION 106
7 CONCLUSION 109
8 REFERENCES 111
9 LIST OF FIGURES 126
10 LIST OF TABLES 129
11 LIST OF ABREVIATIONS AND SYMBOLS 130
12 AUTHOR'S CURRICULUM VITAE 131
13 AUTHOR'S RESEARCH ACTIVITIES 132
13.1 Publications and Conference attendances 132
13.2 patent 136
13.3 Creative activities 136

1 INTRODUCTION

Filtration and separation techniques are vital to the world as we know it. A very basic principle of the whole field is to reduce the entropy of the world around us, which tends to self-increase towards a state of complete equilibrium (the state with the lowest energy), which is incompatible with life. The first definition of life taught in basic school is that living organisms are spatially and temporally bounded, open (to the flow of matter, energy and information) and substantive (very similar chemical composition) systems with a high degree of organization, with the ability to independently exist, metabolize, reproduce and evolve. None of the aforementioned is possible without the capability to separate particles from one another based on some of their qualities.

To be less philosophical, separation techniques are widely used in various fields of human activity as well as industry in large scales. Separation techniques become more and more important since the growing human population needs to recycle and be more effective in extraction and production to achieve the oft-stated goal of sustainable development.

The filtration of water is today already crucial in order to remove suspended solids, pathogenic bacteria, and toxins from drinking water. The filtration of air has also become important, especially in big cities, due to the recent increase in various particles pollution and the associated need to meet increasingly stringent regulations for suppressing particulate matter releases. Apart from the very basic human needs as water and air, there are porous material applications in diverse areas such as gas and liquid separators, fluid filters, catalyst carriers, heat exchangers, thermal insulators, solid oxide fuel cells, combustion burners etc.

The facts mentioned above gave the author a motivation to put effort into a filtration-oriented study dedicated to porous materials. The novelty that should be brought to the field is using secondary raw materials recently utilized almost only in the construction industry for their notable properties and low cost. The author believes they have the qualities for future filtering media production. The simplest name for these materials is ‘alkali-activated materials’ (AAMs) and there are very few references about their utilization in filtration and separation techniques.

AAMs are materials with qualities suitable to replace e.g. ceramic materials in many applications, one of which could be the production of porous filtering media. The main advantages of these, mostly secondary raw source based, materials are their fewer primary raw materials requirements, lower costs, and less energy, and in the future when properly engineered these filters can compete with conventional products.

Note 1: *Due to Davidovits the term ‘alkali-activated materials’ should not be interchanged with ‘geopolymers’. He postulates that geopolymers are only materials based on metakaolin (Al peak in position 55 in the NMR spectrum). The other related materials mostly based on other resources are called plainly AAMs. The background of their formation and their substantial composition are however the same in most aspects. The author uses both terms carefully due to his best knowledge and belief, but in some cases it can be confusing due to interchanging the terms in literature and the need to quote these sources correctly or simply because most of the processes valid for all AAMs were explained on geopolymers and the literature deals with them accordingly.*

Note 2: *All the preparation procedures as well as instrumental tools and methodology for this work had been designed by the author during the ongoing research of the topic.*

2 THEORETICAL PART

2.1 FILTRATION

The simplest definition of filtration is an operation designed to separate suspended particles from fluid media by passing the solution through a porous medium. As the fluid of a suspension is forced through the pores of the filter, the solid particles are retained on the filter medium surface (or on the walls of the pores) while the fluid passes through. The outcoming fluid is then referred to as a filtrate (Cheremisinoff et al., 1998). But to be more precise, the wider background has to be mentioned in the first place. Filtration specifically, and separation generally, refer to the act of separating one or more distinct phases from another in a process which uses physical differences in the phases (such as particle size, density or electric charge). The whole of the phase separation spectrum is illustrated in Table 1 which covers the separation of distinct phases as well as completely mixed ones (Sutherland, 2008).

Table 1: The separation processes spectrum (Sutherland, 2008).

Completely mixed phases	
Vaporization	Distillation
	Evaporating and drying
	Sublimation
Condensation	
Sorption	Absorption
	Adsorption
Phase transfer	Diffusion
	Leaching and extraction
Distinct phases	
Solid from solid	Screening and elutriation
	Classification
Solid from fluid	Filtration
	Sedimentation
	Flotation
	Scrubbing (wet or dry)
	Electrostatic precipitation
Liquid from liquid	Sedimentation
	Coalescing
Liquid from gas	Demisting
	Sedimentation
Gas from liquid	Defoaming
	Sedimentation

From Table 1 is clear that the flow of fluids through a porous medium is of interest not only by filtration, but also other processes such as adsorption, chromatography, ion exchange, and various reactor engineering applications often including surface-mediated catalysis. In petroleum industry the application lies in the separation of oil from gas, water and miscible solvents. In hydrology interests are in the removal of trace pollutants from water systems, the recovery of water for drinking and irrigation and saltwater intrusion into freshwater reservoirs. In soil physics the main objective is in the movement of water and nutrients into (and pollutants into or out of) plants. In biophysics the subject relates to vital processes such as the flow of fluids in lungs and kidneys. And there are many more examples of filtration and generally fluid flow through porous media applications, the above mentioned should only explain and uphold the great importance of this field of research (King, 1980).

Filtration has a long history and irreplaceable role in the chemical engineering and it gains in value for increasingly important production of high purity products as well as for technologies extensively used in all kinds of pollution control and prevention.

2.2 POROSITY AND POROUS MEDIA

The Elsevier Handbook of Filter Media has a precise definition of a filter medium:

A filter medium is any material that, under the operating conditions of the filter, is permeable to one or more components of a mixture, solution or suspension, and is impermeable to the remaining components.

The retained components, the ones to which the medium is impermeable, may be particles of solid, droplets of liquid, colloidal material, or molecular or ionic species in solution, while the permeate (or filtrate) will normally be the suspending fluid or solvent, possibly together with some of the other components. (Sutherland, 2008)

Filter medium has to have a certain arrangement to fulfill the above mentioned - it has to be porous. A porous medium may be in the simple terms described as a piece of solid containing many holes, voids and tubules - these are referred to as pores. The overall content of pores is so large that a volume ratio is needed to estimate relevant properties of the mass. Pores that occupy a definite fraction of the bulk volume form a complex network. The fashion in which holes or pores are arranged, their interconnection extent, their size, shape and position characterize the particular porous medium.

The term porosity refers to the fraction of the apparent volume of the sample that is attributed to the pores (Espinal et al., 2002):

$$\varepsilon = \frac{V_{Pores}}{V_{Total}}$$

The experimental value is dependent on the method used to determine the total volume of the sample bulk and the volume of the pores (e.g. fluid displacement, gas sorption, scattering methods). The volume of pores in the equation above may refer either to open pores and lead to the open porosity, to closed pores leading to the closed porosity, or to total volume of pores together - total porosity. When the closed pores which are not accessible to fluid passing through

the material, plus the fraction of the open pores that do not contribute to the flow, are neglected, the resulting value is referred to as the effective porosity (Rouquerol et al., 1994). To have an overview of these and some other terms Table 2 was compiled.

Table 2: Porous solids - definitions of selected important terms (Rouquerol et al., 2008).

Term	Definition
Pore	Cavity deeper than wide
Porous solid	Solid containing cavities deeper than wide
Open pore	Cavity or channel with access to the surface
Closed pore	Cavity not connected to the surface
Interconnected pore	Pore which communicates with other pores
Blind/dead-end pore	Pore with a single connection to the surface
Void	Space between particles
Pore size	Pore width / diameter
Pore volume	Volume of pores determined by stated method
Porosity	Ratio of total pore volume to apparent particle/powder vol.
Total porosity	Ratio of volume of voids and pores (open and closed) to volume occupied by solid
Open porosity	Ratio of volume of voids and open pores to volume occupied by solid
Surface area	Extent of surface assessed by a given method (experimental or theoretical) under stated conditions
Specific surface area	Surface area of unit mass of powder under stated conditions
External surface area	Area of surface outside all pores
Internal surface area	Area of all pore walls
True density	Density of solid, excluding pores and voids
Apparent density	Density including closed and inaccessible pores, as determined by stated method

Terms micropores, mesopores and macropores are used differently many times, therefore the classification of pores according to size has been under discussion for many years. In order to clarify the situation, the sizes of the different categories of pores were proposed by IUPAC (Everett, 1972; Sing et al., 1985) and very good overview of contemporary theories is summarized by Zdravkov et al. in the paper *Pore classification in the characterization of porous materials: A perspective*, 2007. The pore size is mostly characterized as the pore width, in other words a distance between the two opposite walls. Although to define it precisely, the geometrical shape has to be defined and that would be unnecessarily complicated for most purposes. The limiting and defining size is therefore ordinary that of the smallest dimension as it generally represents the effective pore size. In the recent decade using the term ‘nanopores’/’nanoporous’ has become fashionable but it is not recommend for pores wider than 100 nm.

The idealized types of pores in Figure 1 relate to the definitions in Table 2. Pores can be divided to closed pores and open pores, and also blind (or dead-end) pores and interconnected pores. Pores open at both sides of matter are termed ‘through pores’. (Rouquerol et al., 2008)

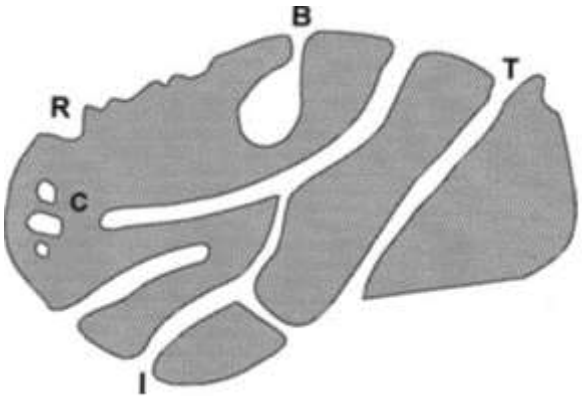

Figure 1: *Hypothetical porous grain cross section showing various types of pores: closed (C), blind (B), through (T), interconnected (I), together with some roughness (R) (Rouquerol, 1990).*

There is a bottomless list of natural and synthetic materials that can be classified as, artificially prepared, modified or even tailored to porous media of specific pore properties (Medri et Ruffini, 2012; Nasvi et al., 2014), however, not all of them are of interest to the subject of filtration.

In general, these materials as a porous media can be divided to unconsolidated and consolidated and/or as ordered and random. Examples of unconsolidated media are sand, glass beads, catalyst pellets, column packings, soil, gravel and packing such as charcoal. Examples of consolidated media are most of the naturally occurring rocks such as sandstones and limestones. Materials like concrete, cement, bricks, paper and cloth belong to the same group as they plainly are manmade consolidated materials. Ordered media are regular formations of various materials such as spheres or structure of wood. Random media have no specific correlation factor (Cheremisinoff, 1998).

Porous media can be further categorized in terms of geometrical or structural arrangement best represented by average properties related to flow properties.

The structure of pores can be described by microscopy. The main objective of pore-structure analysis is to provide a characterization that is related to the macroscopic bulk or flow properties. The major bulk properties that correlate with pore description or characterization are porosity, permeability, tortuosity and connectivity. Because even in studying different samples of the same medium the number of pore sizes, shapes, orientations and interconnections is enormous, it is impossible to precisely cover and characterize the structure and arrangement. Due to this complexity, pore-structure description is most often a statistical distribution of apparent pore sizes. Apparent because models that provide average or statistical pore sizes have to be used to convert measurements to pore sizes. A common approach to defining a characteristic pore size distribution is to model the porous medium as a bundle of straight cylindrical capillaries. The diameters of the model capillaries are defined on the basis of a convenient distribution function. Pore structure for unconsolidated media is inferred from a particle size distribution, the geometry of the particles and the packing arrangement of particles. The theory of packing is though well-established only for symmetrical geometries such as spheres. Information on particle size, geometry and the theory of packing allows relationships between pore size distributions and particle size distributions to be established (Dullien, 1979).

The overall macroscopic description is then based on average or bulk properties at sizes much larger than a single pore. A simplified but many times unexpectedly accurate approach

is to assume the medium to be ideal in terms of homogeneity, uniformity and isotropy. If this presumption proves to be false (the theoretical characterization do not correlate with experimental results) more complex and computationally demanding approaches have to be involved to get closer to the real state of things (Cheremisinoff, 1998).

2.3 FILTRATION BARRIER PROPERTIES

Finally, when some of the separation and porosity basics were discussed, the true interest lies in the field of porous filtration barriers, namely their properties in the first place.

The main characteristics of filtration barriers due to their filtration properties are fluid media penetrability and solid particles impenetrability. Every filter, if made of natural or synthetic material, metal, ceramics, fabric or paper, has to be specified in number of factors because nowadays applications are often advanced and can have very unique needs. These aspects can be basically divided into three categories:

1. Mechanical properties based on material and manufacturing of the filter predetermining the applicability in certain construction type of filter,
2. Application properties deciding about chemical, biochemical and physical properties of propitious substrates (also properties required by ecological and sanitary standards and final cost are important at this point),
3. Process characteristics concerning separated suspension phases – flow resistance, porosity, pore size, permeability, sludge capacity, pores clogging, filtration cake removing etc. (Bulejko, 2014).

2.4 TYPES OF FILTRATION MEDIA

It is true to say that any material that is porous, can be rendered porous or can be anyhow made into a porous structure can serve as a filter medium, doesn't matter whether the pores are the size of a fist or smaller than a micrometer. However, as far as it is reasonable, a filter medium should be strong (in tension at least), flexible, resistant to corrosion and abrasion, easily manipulated into the required shapes and capable of being made in a range of porosities. These requirements cut down on the number of possible media but still leave plenty of potential materials: inorganic (minerals, carbon, glass, metals and metal oxides/ceramics etc.) and organic (natural and synthetic materials). Each of these basic materials lends itself to one or more formats of filter media, as shown in Table 3, which gives the media formats for each of the materials from which media can be made, and further described below. A variant of this information is given in Table 4, relating material form to the types of media in that format (Sutherland, 2008).

Table 3: The overview of filter media types by material (Sutherland, 2008).

Material	Format
Natural fiber: wool, cotton etc.	Felt: loose, bonded, needled
Natural filament: silk	Woven yarn, filament
	Wound yarn
Processed natural fiber: cellulose	Wet-laid (paper, filter sheets)
Man-made org: regenerated cellulose	Granule: loose, bonded, sintered
synthetic polymers	Fibers and Filaments: felted, woven, dry-laid (spun), wet-laid (paper), rigidized, sintered
	Foam
	Extruded mesh (‘Netlon’)
	Sheet: perforated, stretched (fibrillated), porous, membrane
	Tubular: rigid porous, hollow fiber
Metals: ferrous and non-ferrous	Rod or bar structures
	Granules or powder: loose, sintered
	Fibers: loose, sintered
	Sheets: perforated (punched, etched)
	Wire: wound cartridge, woven mesh, sintered mesh, expanded mesh (‘Expamet’)
	Foam
Glass	Fibers: wet-laid (paper)
	Porous tube
	Granules
Carbon: natural	Granules or powder: loose, bonded, embedded
activated	Fibers: loose, felted, woven, embedded
	Porous block
Ceramics: metal oxides	Granule or powder: loose, sintered
others	Formed blocks, with tubular holes
	Fibers: loose, sintered
	Foam
Other minerals: mineral wools	Fibers: wet-laid (filter sheet), pads
sand, anthracite, garnet	Granules
Various mat. (metal, paper, plastic)	Solid fabrications: stacked discs, edge filters wedge wire, wire wound
Paper-like materials	Pleated sheet
Inert granules of all kinds	Packeted beds (deep bed filters)
Mixture of inert and active materials	Combination media

Table 4: The overview of filter media types by format (Sutherland, 2008).

Basic media format	Types of media
Loose granules	Deep bed
Loose fibers	Felts, pads
Structured granules	Bonded, sintered
Structured fiber	Needle felts, bonded, wet-laid (paper)
	spun (spun bonded, melt down)
Sheet	Perforated, microporous (including membrane)
Woven/knitted	Spun yarn, monofilament (including wire)
Tubular	Rigid porous, hollow fiber/capillary
Block	Rigid (with interior channels), foam
Wound on core	Spun yarn, monofilament (including wire)
Structure array	Ribbon, stacked discs, rod and bar structures
Extruded mesh	'Netlon' type

It should be mentioned at this point that most of the above (Table 4) listed forms of filters are interchangeable with some other different kinds in most applications. One of the most universal types are 'deep bed' or 'granular bed' filters which are made out of loose particles or granules of various diameters, morphology and materials. Due to this arrangement disposition deep bed filters can be tailored according to nearly any specific application. Some of the crucial groups of filters will be briefly discussed in this part of the text.

2.4.1 Beds of granular material

Beds of granular material are the oldest and the most widespread filtering media because that is the way rainwater becomes groundwater in nature from the beginning of our world. The artificial way this type of filters is prepared by e.g. sand, diatomite, expanded perlite or activated carbon layers sandwiched one upon another all topped on suitable macroporous support. One of the biggest advantages of this group is that these layers can be easily regenerated because the media is not solid (Šnita, 2005). The disadvantage however is based on the same fact. The finest particles can be easily washed away if the supporting barrier and the nearest adjacent material contain too wide pores.

2.4.2 Filter paper

The filter paper has to be mentioned among the first groups because filters of many different shapes and sizes based on paper are used in inexhaustible number of applications e.g. chemical laboratories, kitchen extractor fans, all kinds of car filters etc., and all of us come into contact with them a lot. Their advantages are low cost, simplicity of production a recycling possibility. The main handicap comes from the fact that cellulose fibers from which paper is made are not really durable and resistant material. That limits the use of paper filters in chemically, thermally or biologically inhospitable applications. It is a basic type of filter medium for laboratory purposes

but is widespread in all the industry as well. It is a typical material for surface filtration (Čerňanský et Peciar, 2008).

2.4.3 Textile fabrics and geotextiles

There are also many types of textile-based filters on the market. Main groups are woven and nonwoven textile fabrics differing in terms of material, structure and properties.

Woven textile fabrics are the most widely used filtration material. They are manufactured by weaving of various types of fibers, either natural or most recently synthetic. The main reason for more frequent use of them is that barriers made of synthetic fibers like polyester, polyamide, polypropylene etc. have better mechanical properties as well as chemical and biological resistance compared to the natural materials such as wool, cotton, hemp, flax etc.

Nonwoven textile fabrics called 'felts' are being made of variously arranged and compacted fibers that afterward make relatively integral structure. Felts have been used for long time mainly for depth filtrations (Čerňanský et Peciar, 2008)

Geotextiles are special branch of this large group of filters and include woven and unwoven (often spun-bonded), natural and synthetic textile-like fabrics. Geotextiles in general have good strength, resistance to blight, bacteria, various chemicals and UV light. On top of that they have controlled permeability used to provide filtration and separation. Some types can provide also reinforcement and drainage functions. Geotextiles are commonly used as filters between soil and drainage gravel where they are preventing soil particles from being carried away by the filtered water. The drainage gravel has otherwise a tendency to become clogged by these particles and the upper soil is then washed away. The role of geotextiles as a filter is to minimize this phenomenon (Swicofil, 2015)

2.4.4 Polymer porous barriers

Polymer materials are nowadays present in more or less every field of human activity. The same applies in the filtration- and separation-techniques sphere where new types of polymer barriers are being constantly developed for past decades. Polyurethane, polyethylene, polypropylene, polyvinylchloride, polyamide and many other polymers and their copolymers are used to form various filtration barriers, boards, discs, pipes, cartridges, and currently in research very popular porous hollow fibers. Ordinarily impermeable materials have to be made different way for the kind of applications – mostly foaming or specific thermal and/or stress treatment techniques resulting in continuous channels and pores presence in the product.

2.4.5 Stoneware, ceramic and glass barriers

These are widely used types of chemically and thermally resistant filtration barriers. Stoneware barriers are made of certain types of kaolin containing quartz (SiO_2), ceramic barriers are made from powders containing aluminum (mostly various types of Al_2O_3). Both types have to be sintered at high temperatures (1000 – 1400 °C). If they are being used only as a support of another filter media they have holes up to 6 mm in diameter. When using them as a filtration barrier itself, the sizes of pores can vary generally from 1 to 2500 μm. Recently, this kind of barriers is used for

filtration of liquids and gases at higher temperatures and for applications in corrosive conditions. Glass filters called frits are made of chemically and to certain extent also thermally resistant glasses (e.g. Simax or Pyrex) in the form of particulates pressed in molds or tubes packed together and afterwards sintered together. Finished frits can be slowly heated to maximal temperatures around 530 °C and they have to be also cooled down slowly, otherwise they crack due to uneven internal stresses combined with the fragility of glass (Medri et al., 2014).

2.4.6 Sintered metal barriers

Three different types of metal sintered barriers that are described below are widespread especially in chemical and food industry used for filtration various of liquids and gases.

Sintered metal powders – the initial material is a metal powder (often spherical particles made by inert atmosphere metal spraying or very fine grinding) with particle size between 0.5 and 100 μm. By pressing in a mold and consecutive sintering stainless steels, bronze, brass, nickel, monel, titanium and many other types of filters are made.

Sintered metal fibers – high porosity, low flow resistance and high sludge capacity filters made out of fibers of various diameters are often organized in a gradient structure. They can be found in petrochemicals, chemicals, hydraulics and hot gasses filtration processes among other things because of their long term on-stream life and good cleanability (as majority of metal-based filters).

Sintered woven sieves and composite sintered metal media are the last group of commonly used metal barriers to mention. These types of barriers are often used for elevated pressure filtrations of high viscous polymers.

2.5 ALKALI-ACTIVATED MATERIALS AND GEOPOLYMERS

Geopolymer materials will be mentioned a lot at this point as most of the background is the same for alkali-activated materials (AAMs). Literature often interchange these terms and more importantly most of the studies and knowledge about these materials in general can be found in the literature dedicated to geopolymers – the statements however are generally valid for AAMs. They have a lot of advantages for the filtration and separation applications and the main production advantage is that their porosity and thus a final structure can be well affected by temperature, particle morphology, admixtures and amount of water in the manufacturing process (Prud'homme et al., 2011; Rasouli et al., 2015). There are several possible materials and procedural ways for the purpose and the result could contain pores small enough for molecular filtration (Nasvi et al., 2013; Zhang et al., 2014) as well as several orders of magnitude bigger macropores (Prud'homme et al., 2010; Eom et al., 2013).

There are several definitions of AAM/geopolymer from different points of view and only their combination gives an integral explanation:

For chemists:

'...It is known that alkali-activated aluminosilicates are able to produce aluminosilicate geopolymers. The hardening mechanism involves the chemical reaction of geopolymeric precursors, such as aluminosilicate oxides, with alkali polysilicates yielding polymeric Si–O–Al bonds.' (Živica et al., 2011)

For geopolymer chemists:

'...Geopolymers consist of a polymeric Si–O–Al framework, similar to zeolites. The main difference to zeolite is geopolymers are amorphous instead of crystalline. The microstructure of geopolymers on a nanometer scale observed by TEM comprises small aluminosilicate clusters with pores dispersed within a highly porous network. The clusters sizes are between 5 and 10 nanometers.' (Huang et Han, 2011)

For geopolymer material chemists:

'...The reaction produces SiO_4 and AlO_4, tetrahedral frameworks linked by shared oxygens as poly(sialates) or poly(sialate–siloxo) or poly(sialate–disiloxo) depending on the SiO_2/Al_2O_3 ratio in the system. The connection of the tetrahedral frameworks is occurred via long-range covalent bonds. Thus, geopolymer structure is perceived as dense amorphous phase consisting of semi-crystalline 3-D aluminosilicate microstructure.' (Pimraksa et al., 2011)

For geopolymer ceramic chemists:

'...Although geopolymer is generally X-ray amorphous if cured at standard pressures and temperatures, it will convert into crystalline ceramic phases like leucite or pollucite upon heating.' (Peigang et al., 2011)

For alkali-cement scientists:

'... Geopolymers are framework structures produced by condensation of tetrahedral aluminosilicate units, with alkali metal ions balancing the charge associated with tetrahedral Al. Conventionally, geopolymers are synthesized from a two-part mix, consisting of an alkaline solution (often soluble silicate) and solid aluminosilicate materials. Geopolymerization occurs at ambient or slightly elevated temperature, where the leaching of solid aluminosilicate raw materials in alkaline solutions leads to the transfer of leached species from the solid surfaces into a growing gel phase, followed by nucleation and condensation of the gel phase to form a solid binder.' (Feng et al., 2011)

For ceramic scientists:

'...Geopolymers are a class of totally inorganic, aluminosilicate based ceramics that are charge balanced by group I oxides. They are rigid gels, which are made under relatively ambient conditions of temperature and pressure into near-net dimension bodies, and which can subsequently be converted to crystalline or glass-ceramic materials.' (Bell et al., 2009)

Aluminosilicates where repeatedly mentioned in the above definitions and there is another term to call exactly the part of aluminosilicates spectrum which meet the properties of interest – pozzolans.

The term 'pozzolan' derives from Pozzuoli area (on the territory of present-day Italy) where the ancient Romans found reactive materials of volcanic origin on the silicon- and alumina-oxides base. Pozzolans are defined as natural or industrial substances on silicate, aluminosilicate or a mixture base, with a content of reactive SiO_2. Although often presented separately, fly ash and silica fume also have pozzolanic properties. Pure pozzolans after mixing with water does not harden because they do not have hydraulic properties. However, they react in the presence of water at normal temperature with dissolved hydroxides to form silicate and aluminate compounds which are bearers of gradually increasing strength and the cohesive and adhesive properties. The resulting compounds are similar to those generated by the hardening of hydraulic substances.

Pozzolans should essentially contain the active silica and aluminum oxides. The rest then consists of iron or any other oxides. The content of active calcium oxide is negligible. The minimum content of active silica should be at least 25%wt, the activity for concrete practice is however set to be 47%wt (see Figure 2).

Figure 2 was taken over from technology of concrete mineral admixtures (Pytlík, 2000) and shows also hydraulicity of compounds depending on the amount of stated oxides. Compared to the next diagram in Figure 3 which namely shows the pozzolans directly in the picture, Figure 3 is more precise and shows understandable overlap of the materials oxide contents.

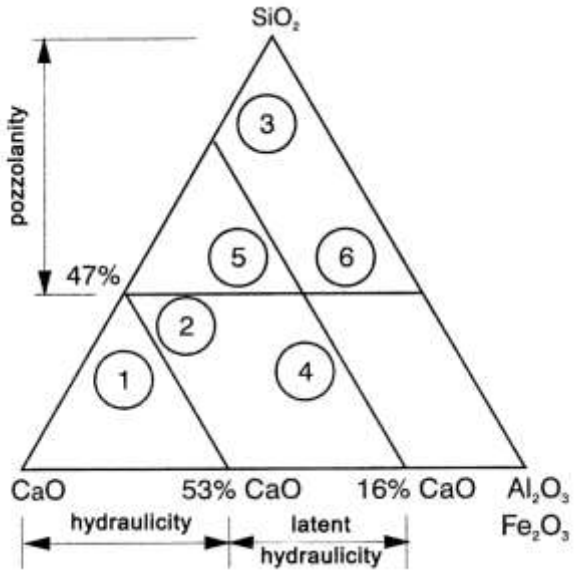

Figure 2: *Positions of hydraulic and pozzolan compounds in CaO-SIO_2-Al_2O_3(Fe_2O_3) ternary diagram of minerals. 1 – Portland cements, 2 – blast furnace slags, 3 – silica fumes, 4 – CaO-rich fly ash, 5 – SiO_2-rich (siliceous) fly ash, 6 – pozzolan fly ash. (Pytlík, 2000)*

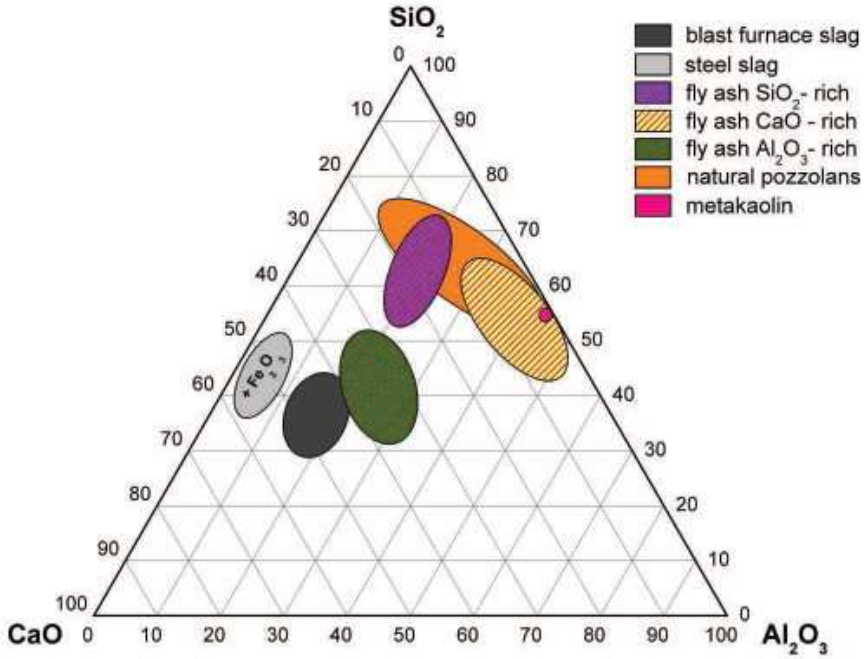

Figure 3: *Typical composition of pozzolanic materials (Šesták et al., 2009).*

Natural pozzolans are usually volcanic substances or sedimentary rocks of suitable chemical and mineralogical composition.

Industrial pozzolans are heat-treated, and activated clays and slates, air-cooled slags from the production of lead, copper, zinc, and other products of the metallurgical industry. Industrial pozzolans are gradually used in the construction materials industry but the requirements for them are to not substantially increase the water consumption in processing of cement, in any step they shall not reduce the resistance of the concrete or mortar, or reduce the reinforcement protection.

Fly ash (FA) in general refers to products from coal combustion processes today mostly from coal-fired power plants. These byproducts are used almost exclusively in cement industry and due to American Society for testing Materials (ASTM) are divided to class F (produced from high-rank coals) and class C (produced from low-rank coals). Coal rank, defined by ASTM D 388, is more of a concept then a property because it is not measured but assessed by physical and chemical properties that change during the process of coalification (degree of transformation from vegetation to coal). Coalification increases in this order: peat – lignite – subbitumens – bitumens – semi-anthracite – anthracite – meta-anthracite. Lignite and subbitumens are ranked low, bitumens and anthracite high (Fox, 2017). This classification is used very often despite the fact that it is not very accurate.

Siliceous fly ash (type 'V' due to EN 197) is very fine grained powder composed mainly of glassy spherical particles with pozzolanic properties. They consist mainly of active silicon dioxide and aluminum oxide, in the rest then iron and other oxides. The content of active calcium oxide has to be less than 5 %wt. The content of the active silicon dioxide in silica ash in accordance to preliminary European standard is not less than 25%wt.

Calcium fly ash (type 'W' due to EN 197) is fine grained powder with hydraulic or pozzolanic properties or both. It must mainly consist of active calcium oxide, then activated silica and aluminum oxides, and iron and other oxides in the rest. Active calcium oxide content shall be not less than 5%wt. Calcium fly ash containing 5%wt to 1%wt of active calcium oxide must contain at least 25%wt of active silica. Such finely ground calcium fly ash has to have at least 10 MPa in compressive strength after 28 days of hydration. The overall expansion of calcium fly ash is also very important factor.

Blast furnace slag (BFS or GBFS where G stands for granulated) is a byproduct from production of crude iron in blast furnaces how its name suggests. It is a latent hydraulic substance consisting of angular particles produced by fast water-cooling of flowing melt to prevent its crystallization and stabilize the glassy amorphous character and this way the latent hydraulic properties. Those are besides of its composition influenced also by method, temperature and rate of cooling. It is commonly used in finely ground state (GGBFS) as an admixture to cement where it improves reactivity and final strength of concrete but prolongs the hydration and setting time. Basically BFS divide due to basicity module M_b to acidic (M_b<1; used only as an aggregate in concrete) or alkaline (M_b>1; binder component in cement) (Pytlík, 2000):

$$M_b = \frac{CaO + MgO}{SiO_2 + Al_2O_3}$$

Table 5 compares the composition of a typical ground granulated blast-furnace slag to that of a typical Portland cement (type I), a typical Class C fly ash and a typical Class F fly ash to show that in basic terms the GGBFS and the two fly ashes have the same kinds of oxides as the cement only the ratios are different. Mineralogical composition however differs largely (GCPAT, 2016).

Table 5: Typical composition of FA, GGBFS and Portland cement comparison (GCPAT, 2016).

	Portland Cement	Type C Fly Ash	Type F Fly Ash	GGBFS
SiO_2	21.1	33.5	43.4	40.0
Al_2O_3	4.6	22.9	18.5	13.5
CaO	65.1	27.4	4.3	39.2
MgO	4.5	4.6	0.9	3.6
Fe_2O_3	2.0	6.1	29.9	1.8
SO_3	2.8	2.8	1.2	0.2
L.O.I.	1.4	1.2	1.2	0

Burnt shale, especially calcined oily shale is produced in a special furnace at about 800 °C. According to the natural raw material composition and the manufacturing process burnt shale contains clinker phases, in particular dicalcium silicate and monocalcium aluminate. Besides those, it contains small amounts of free calcium oxide and calcium sulfate, and a considerable proportion of pozzolanic reactive oxides, especially silica. Finely ground burnt shale has significant hydraulic as well as pozzolanic properties and it should have at least 25 MPa in compressive strength and low expansion after 28 days of hydration.

Silica fume consists of very fine spherical particles having a high content of amorphous silicon dioxide – more than 85%wt. Silica fume is formed when pure silicon or ferrosilicon is made in electric arc furnaces (Pozemní stavitelství, 2004). (Kejík, 2010)

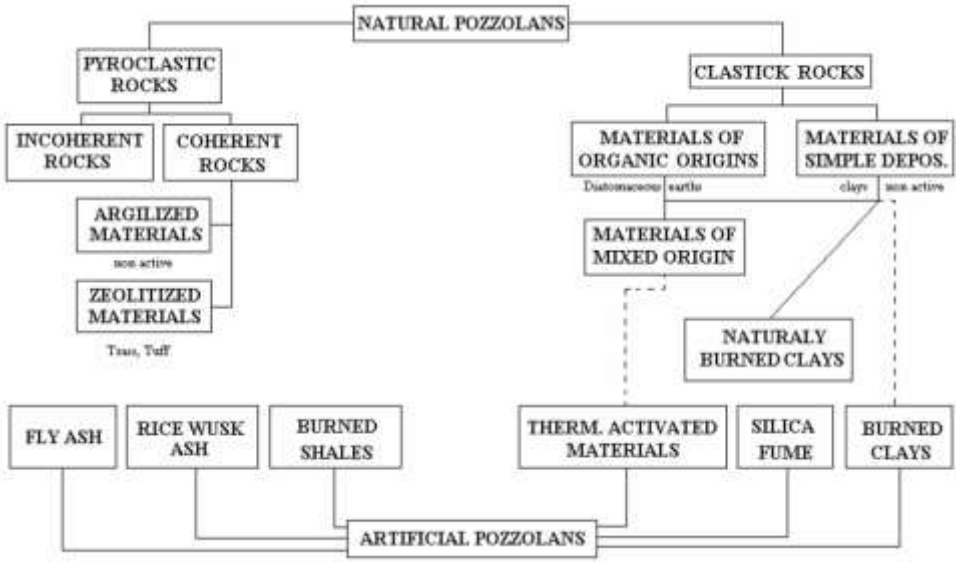

Figure 4: *Schematic diagram of pozzolan types due to Massazza (1993)*

There are many applications for porous ceramics and cement-based materials (and barriers in the subset) related to their properties of high permeability, low bulk density, high surface area and low thermal conductivity. Each of these properties is linked to the solid-part chemical composition and to the final pore volume fraction and structure in term of morphology, size and connectivity. In this respect processing has very important role (Ishizaki et al., 1998; Luyten et al., 2010, Rasouli et al., 2015). When ceramics is made, there is always at least one high-temperature step in the processing (that in many cases enables advantageous use of pore formers such as starch, saw dust, cotton thread, wheat flour etc. burnt in this step (Sarikaya et Dogan, 2013)) requiring lots of energy to be inserted. In cement-based materials the high energy-consuming step precedes the ingredient formation, because the clicker production takes place in kiln under more than 1300 °C and the production is also a big source of CO_2 emissions. Geopolymers are good candidates for replacement of some part of both of these materials in their common applications without mentioned disadvantages (Davidovits, 2008) – the processing can be performed at low temperature (<100 °C) and their manufacturing emits six times less CO_2 than standard cements (Duxson et al., 2007; Henon et al., 2012). There are also advantages of primary raw materials saving, secondary raw material cost, their processing instead of landfilling, and their post-recycling scope as well.

2.5.1 History of alkali activation

As already mentioned, pozzolans were probably known and widely used since the times of Egypt and Mesopotamia. So was the alkali activation and it has been even back then widely used in architecture and arts as it turns out from a chemical analysis of brick fragments from The Great Ziggurat of Ur (21st century B.C.) that at first appeared to consist of fired bricks but nobody could explain where could the builders get so much fuel for the firing. At given period of time and given place (the current Iraq) there were only lower plants and small amount of palm trees growing in a very wide area. It offers a solution in form of crude oil, but it would undoubtedly leave traces in the material which are not present. The only plausible theory supported also by the interpretation of old texts in the light of current knowledge is the preparation of the bricks by geopolymerization from sand, sodium and potassium salts and potash produced by combustion of certain lower plants (Svoboda et al., 2005). The most widely discussed is the use of re-agglomerated stone in the construction of pyramids in Giza. Egyptologists have developed the theories for construction using inclined ramps for years but prof. Davidovits questioned this theory by mineralogical and chemical analysis of the blocks that demonstrably contain water in the structure (which is not possible in natural stone) and on the basis of texts (e.g. Famine stela). This theory would explain the issue of transportation of huge blocks weighting several tons and also minimizing the joints between them (max. 2 mm). After the era, the techniques were probably forgotten and then rediscovered in ancient Rome and then lost again. In modern history the process of alkali activation was rediscovered in 1930 when H. Kuhl observed changes in slag behavior in the presence of potassium carbonate. During 1940s and 1950s this phenomenon was investigated (Purdon, 1940) and that resulted in the discovery of alkali-activated cement. In 1959 V. D. Glukhovsky presented his theory of using new materials named ‘soil binders’ based on natural aluminosilicate materials, or their alternatives in the form of secondary raw materials, with alkaline systems. Glukhovky was also the first researcher and author who studied the binders of ancient Roman and Egyptian structures. Later he was followed by P. Krivenko, who dealt

mainly with alkali-activated slags and he used for such materials the term ‘geocements’ for the first time. This was followed by a French scientist professor Josef Davidovits who in 1978 developed and patented a binders obtained by alkali activation of metakaolin entitled ‘geopolymers’. As mentioned above Davidovits is also the author of the theory that Egyptian pyramids are not made of natural stone but that those enormous blocks were made from a mixture of limestone sand, calcium hydroxide, sodium carbonate and water (Pacheco et al., 2008).

2.5.2 Alkali activation

Today geopolymers and AAMs, mostly used for construction purposes, are prepared by alkali activation of aluminosilicates – mostly metakaolin or some industrial by-products with a high content of aluminosilicate glass (e.g. baked clays). The most commonly used activators are concentrated solutions of alkali metal hydroxides or silicates (e.g. water-glass).

Under normal temperature it is a very slow process but is noticeably accelerated with increasing temperature. The basic principle of this reaction can be divided into three steps: rapid and exothermic initial dissolution, the induction period associated with heat generation decrease, and finally the reaction itself which is also exothermic. The heat development depends on alkaline activator concentration, water to solid phase ratio and the temperature. By increasing the ratio of water to the solid phase the induction period is prolonged and the total heat is reduced. The induction period is shortened with increasing temperature (Shi et al., 2006).

Glukhovsky proposed a classification of alkali activators into six groups according to their chemical composition as follows:

1. Alkaline hydroxides (MOH);
2. Low alkaline non-silicate nature salts (M_2CO_3, M_2SO_3, M_3PO_4, MF etc.);
3. Silicates ($M_2O.nSiO_2$);
4. Aluminates ($M_2O.nAl_2O_3$);
5. Aluminosilicates ($M_2O.\ Al_2O_3.(2-6)SiO_2$);
6. Neutral non-silicate nature salts (M_2SO_4, MCl).

Nature of the alkaline activator and its concentration is of course not the only thing that influences their use, it is also the price. Therefore mainly cheaper sodium compounds are used which are massively produced for various industrial applications – mainly sodium hydroxide (NaOH), sodium water glass ($Na_2O.nSiO_2$) or cheaply available alkaline to neutral salts such as sodium carbonate (Na_2CO_3) and sulphate (Na_2SO_4).

Otherwise activators based on cations from 1.-3. and 6. group can be also used but in real case the variety in use (an on top of that mostly only for laboratory purposes) is narrowed on the second cheapest possibility – potassium-based compounds. The issue with them apart from the fact they are more expensive is that they are less available. However there is also one big benefit to them which is their positive effect on the formation of efflorescence. Some people think they eliminate the efflorescence but due to the findings of prof. Škvára potassium based activators only decrease the amount of it and on top of that the products are not as much visible as the sodium based ones (based on live dialogue).

The rate of alkali activation is influenced by a number of factors – mixing, fineness of the particulate material, activator type and also the concentration as it is further discussed in the

experimental part. At this point it is only important to note that the 'power' of the activator, especially in terms of reaction rate and effecting mechanical characteristics of the product, cannot be interchanged for its concentration. Mostly there is a direct proportion between them but only up to a certain optimum where the mechanical properties start to decrease with further increasing the activator concentration.

2.5.3 Structures and Mechanism

Research in the field of geopolymers and AAMs in general has historically been strongly application-focused. The mechanisms and processes underlying geopolymer formation and controlling the out-coming structures of these reactions have in past few years become the subject of attention. However, more and more progress is being made in this area. The understanding that has been developed to date provides indications that AAM technology has, in fact, the potential for wide-scale utilization (Landi et al., 2013)

Naturally the activation mechanism of fly ash and blast furnace slag differs as slag contains more calcium-rich phases however it is believed that the basic mechanism is similar except the fact that the binding gel phase is mostly NASH (sodium aluminosilicate hydrate) in case of FA and CASH (calcium silicate hydrate that contains aluminum substitutions) in case of BFS, but it is not very clear yet. Introduction of calcium cause the system to undergo two separate and competing reactions and it is likely one reaction product is favored under certain conditions. Also an ordinary CSH known from hydration of cement can arise also but it is favored only when alkali hydroxide concentration is very low. When it is sufficiently high hydroxyl concentration hinders the Ca^{2+} dissolution forcing the dissolved silicates and aluminum species to form geopolymer gel. On the other hand, when the OH^- concentration is low, the amount of Ca^{2+} dissolving increases and causes more CSH to form.

Portland cement binders are mainly based on hydration reactions of calcium silicate phases that react with water to form calcium silicate hydrates. Water is an integral component for AAM but is not an essential component of the gel structure. For AAM, water is typically present to provide a medium for the aluminosilicate reaction to occur. However, for cement based materials, water is a not only necessity for the hydration reaction process but also is a part of the hydration product structure. Therefore, the chemistry of the Portland cement binder is intrinsically different in nature than that of AAM. AAM molecular structure is more closely aligned with zeolites and aluminosilicate gels, while CSH is comparable to tobermorite and jennite.

AAM on the atomic scale are composed of Si^{4+} and Al^{3+} cations linked by sharing O^{2-} anions. Both the silicon and aluminum form tetrahedral-coordinated structures. The tetrahedral groups exhibit short-range ordering. Short range ordering is typically constrained to nearest and next-nearest-neighbors of the atom under consideration. Short range ordering can be very helpful in understanding such structural characteristics as atomic connectivity, bond lengths, angles and correlation distances between non-covalently linked neighboring atoms (Barbosa et al., 2000). Figures 6, 7 and 9 show a basic conceptual model of short range ordering for geopolymers/AAMs.

Research in aluminosilicates minerals and zeolites produced a descriptive notation for the "backbone of alkali aluminosilicates systems" (Engelhardt et al, 1981). The notation developed was $Q^n(m\text{Al})$, where $0 \leq m \leq n \leq 4$, n is the coordination number of the silicon centers and m is

the number of Al neighbors surrounding the silicon connected through bridging oxygen bonds. Figure 5 illustrates the various three-dimensional $Q^4(m\text{Al})$ structures. The $Q^4(m\text{Al})$ notation is very useful for aluminosilicates (Kim, 2012).

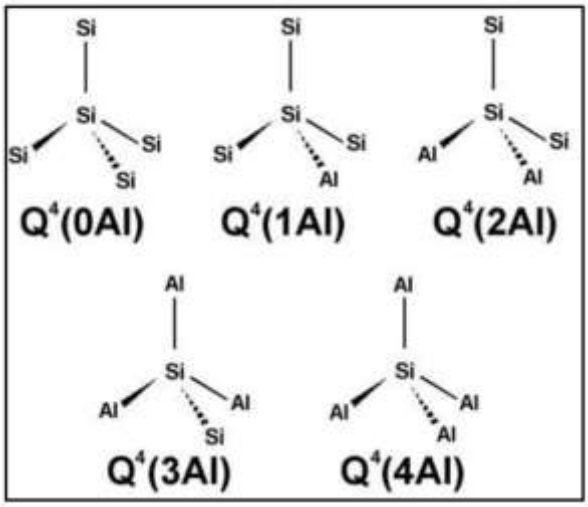

Figure 5: *$Q^4(m\text{Al})$ structures (Barbosa et al, 2000).*

According to Glukhovsky alkali activation mechanism is based on coupled reactions involving the decomposition of the primary material to the low stable structural units which interaction with coagulation structures gives rise to condensed structures (see Figure 6). First step is a hydrolysis of the solid surface of aluminosilicate by ion exchange for alkali metal cations (Na^+ and K^+) from the solution. From the structural damage point of view the first step is a disruption of covalent Si-O-Si and Al-O-Si bonds of $(SiO_4)^{4-}$ tetrahedrons and $(AlO_6)^{9-}$ octahedrons. This is due to the increased pH of the alkaline solution and aforementioned structures are via this process transformed into a colloidal phase.

It is known that up to eight hours after the mixing the liquid phase contains Ca^{2+}, K^+, Na^+, SO_2^{4-} and OH^- ions. Then, with decreasing concentration of Ca^{2+} and SO_2^{4-} the pH increase and so does the concentration of OH^-. This way leads to the grain surface negative charge development. This charge is then due to the alkalinity of the medium transported inwards by OH^- anions and progressively decomposes Si-O-Si and Si-O-Al bonds. Under constant pH the penetration of OH^- ions is the smaller the larger is the accompanying hydrated alkali cation (i.e. from Li^+, Na^+, K^+ and Ca^{2+} with Li^+ the penetration occurs most rapidly). At the same time the disintegration of each structural unit vacate the space for the next reaction since silicon and aluminum are released in the form of SiO^- and AlO_2^- ions into the solution due to the pressure inside the grains formed by penetrating other ions inside. These ions are in the solution involved in further reactions mostly in hydrated very reactive form $[Si(OH)_3]^-$ and $[Al(OH)_4]^-$.

$$\equiv Si–O–Si\equiv + 3OH^- \rightarrow [Si(OH)_3]^-$$

$$\equiv Si–O–Al\equiv + 7OH^- \rightarrow [Si(OH)_3]^- + [Al(OH)_4]^-$$

For better understanding the most probable intermediate steps will be shown. The disruption of siloxane bonds by OH^- ions is forming an alkali silicate and silicic acid:

$$\equiv Si–O–Si\equiv + R^+ + OH^- \rightarrow \equiv Si–O–R + H–O–Si\equiv$$

where R^+ stands for alkali Na^+ or K^+ ions.

Silicic acid is a weak acid and therefore immediately reacts with OH^- forming a silicate:

$$R^+ + OH^- + H–O–Si\equiv \rightarrow \equiv Si–O–R + H_2O$$

This silicate is in hygroscopic gel form and hydrate:

$$\equiv Si–O–R + n.H_2O \rightarrow \equiv Si–O^-\text{--}(H_2O)_n + R^+$$

This way R^+ cation is released again and can immediately enter next reaction of the same type (Ichikawa et Miura, 2007).

The polymerization occurs through the condensation of Si and Al while releasing water. The process gives formation of amorphous or semicrystalline three-dimensional structure of several types (see Figure 8 and 9):

• Poly(sialate) wherein the atomic ratio Si:Al = 1 forms a linear or cyclic polymers with the basic structural unit (-Si-O-Al-O-),

• Poly(sialate-siloxo) has an atomic ratio Si:Al = 2 and the basic unit is (-Si-O-Al-O-Si-O-),

• Poly(sialate-disiloxo) with atomic ratio Si:Al = 3 and contains (-Si-O-Al-O-Si-O-Si-O-) in the chain repeatedly,

• Poly(sialate-multisiloxo) wherein the Si:Al > 3 and chains are connected by Si-O-Al bridges between polysialate chains.

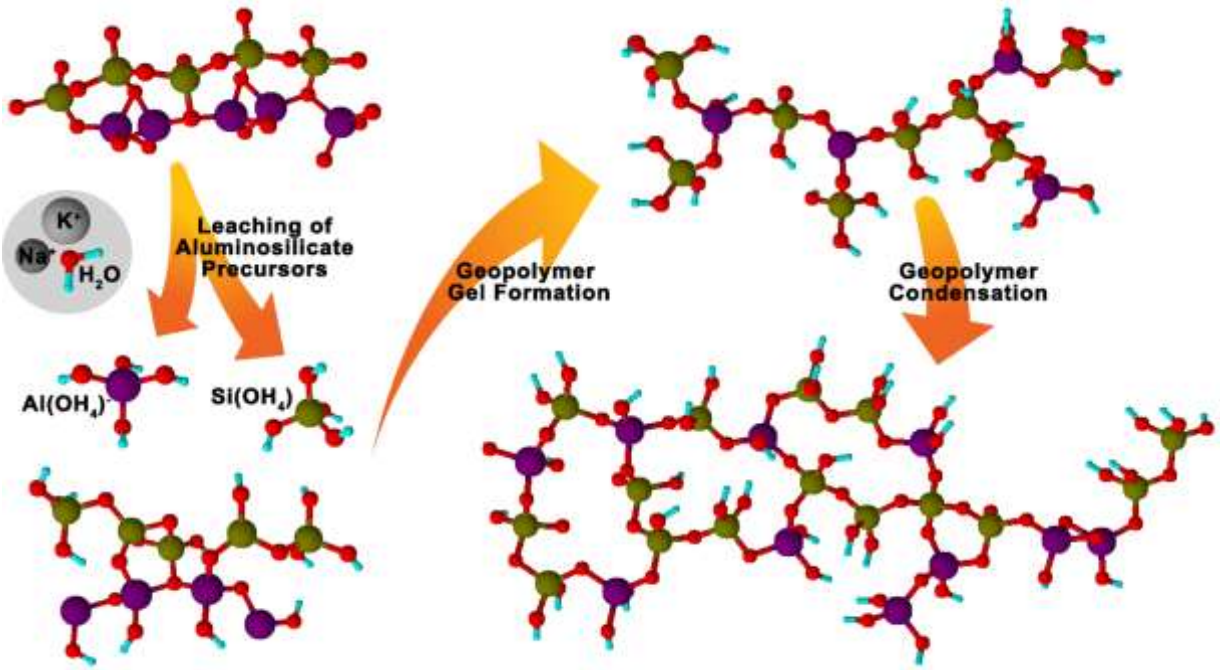

Figure 6: *Visualization of alkali activation mechanism. Note: the gel formation begins from supersaturated solution.*

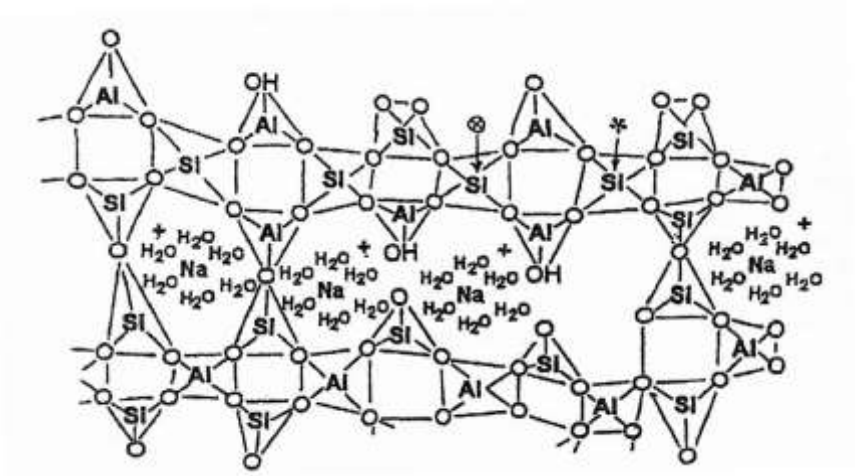

Figure 7: *A closer schematic look at randomly distributed and cross-linked tetrahedron polymeric structure of geopolymer (Barbosa et al., 2000).*

Sialate stands for silicon-oxo-aluminate (aluminosilicate oxide), see Figures 5, 6, 7 and 8 for a better understanding of the above described structures. The term was introduced by J. Davidovits. Gaps in the 3D network are filled with positively charged ions (Na^+, K^+, Li^+, Ca^{2+}, Ba^{2+}, NH_4^+ and H_3O^+) and compensate the negative charge of $(AlO_4)^-$ tetrahedrons (Davidovits, 2008). The presence of amorphous phase differentiates the material from zeolites that are crystalline.

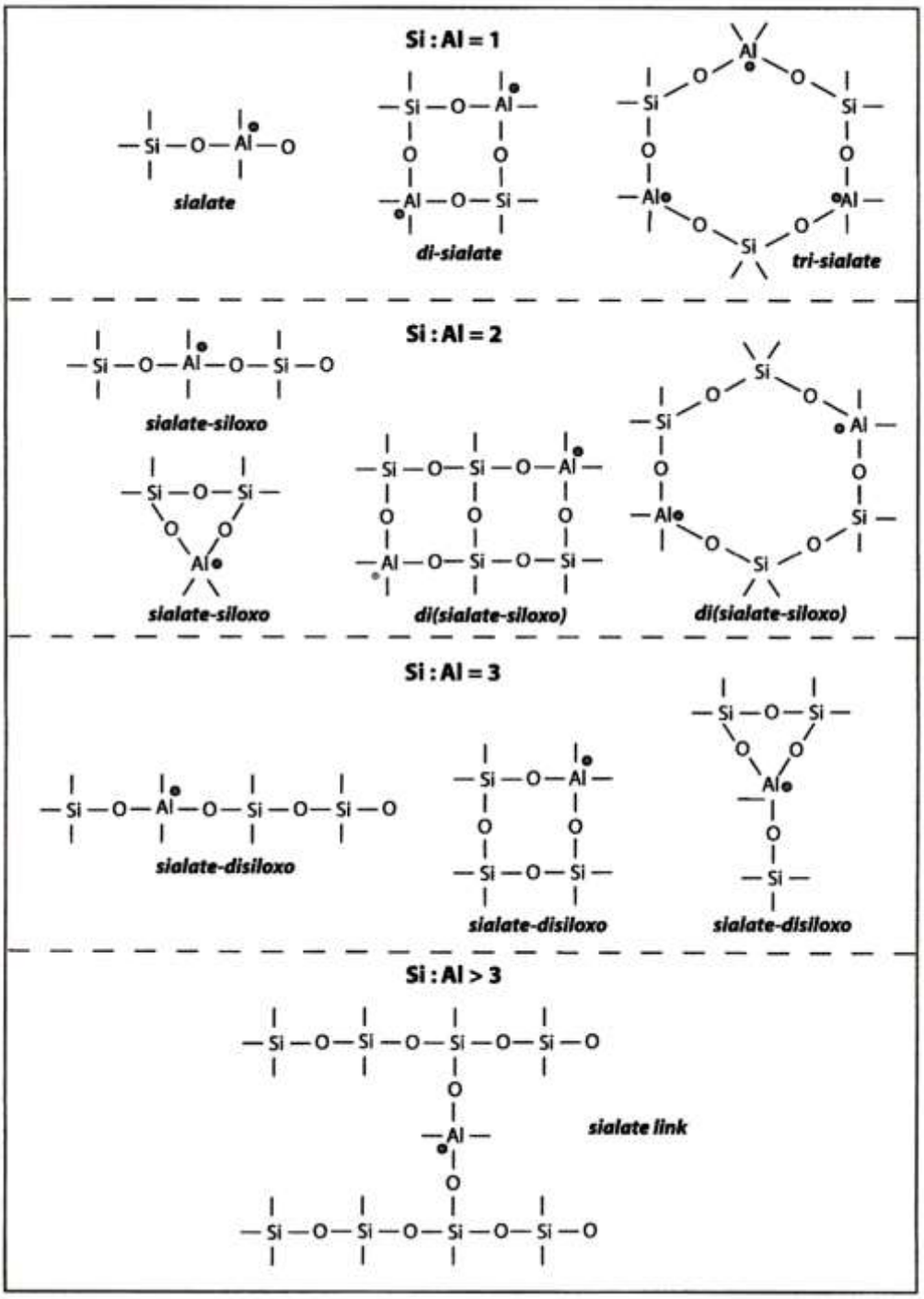

Figure 8: *Terminology of poly(sialate) geopolymers (Davidovits, 2008).*

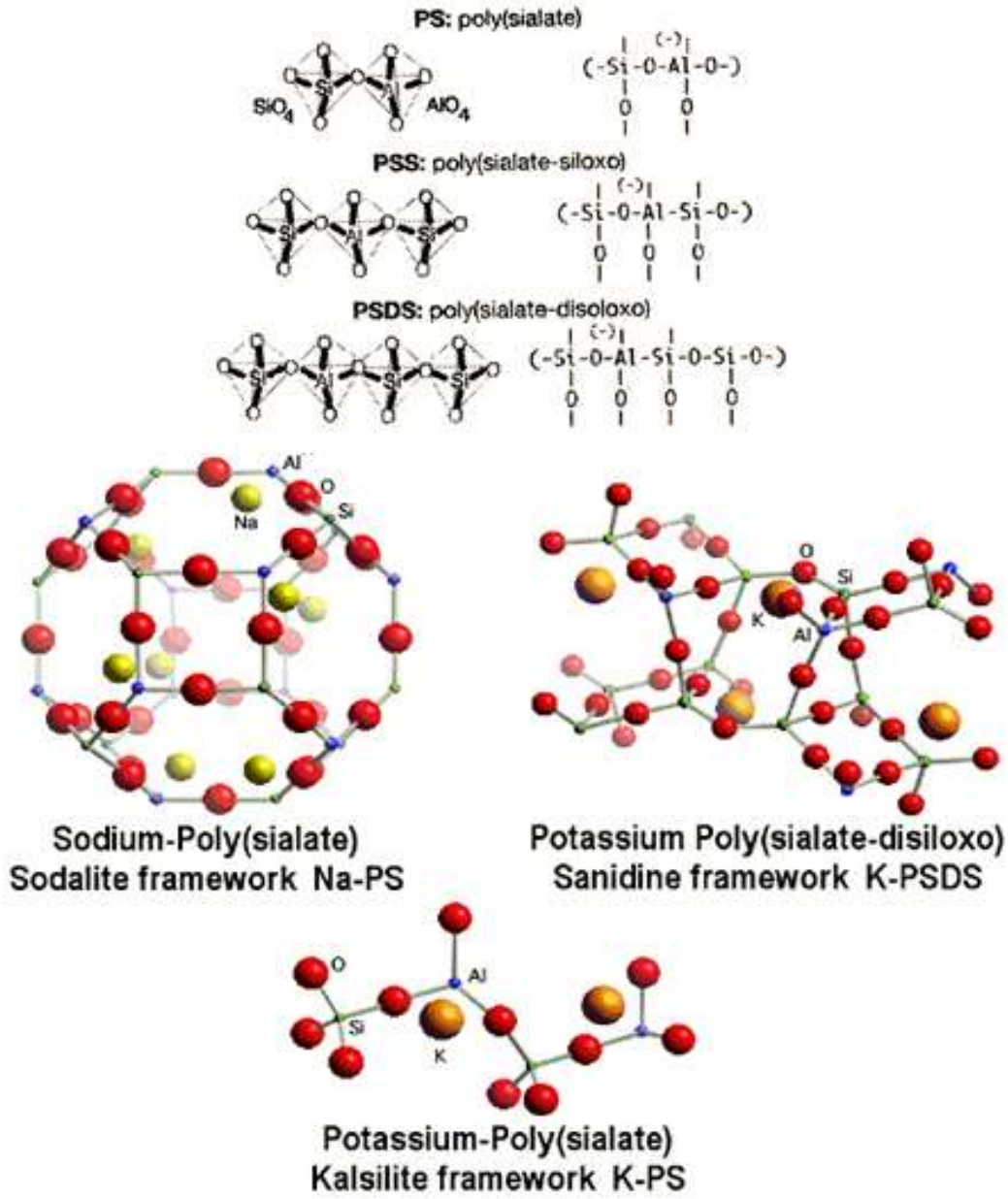

Figure 9: *Poly(sialate), poly(sialate-siloxo) and poly(sialate-disiloxo)structure illustrations (colorized)(Davidovits, 2008).*

The observations tend to point to a structure of the geopolymer (visible in Figures 7 and 9) consisting of tetrahedral Al and Si units randomly distributed along the polymeric chains which form cavities of sufficient size to accommodate the hydrated charge-balancing alkali metal ions. Despite its disorder, this type of structure possesses considerable thermal stability and shows very little tendencies for reordering or crystallizing at elevated temperatures (Šoukal et al., 2009; Sarker et al., 2014), and has chemically favorable mechanical properties compare to commonly used inorganic materials (Giasuddin et al., 2013).

There was a very interesting study concluded by Koleżyński et al (2018) presenting results of DFT and classical mechanics' calculations and theoretical analysis of geopolymer structures taking to account even the Si:Al ratio.

3 STATE OF ART

The main AAMs that are of growing interest in recent years are metakaolin-based geopolymers and subsequently the most research (and papers published) relates to geopolymers thus the technology, including the porous structures and even tailoring the porosity (Landi et al, 2013), is more advanced than in the case of other AAMs on the basis of secondary raw materials such as FA and BFS. This section therefore combines the results form papers dedicated to secondary raw materials based AAMs with relevant studies of the conventional geopolymers.

The first contemporary published attempts on similar aluminosilicate filtering media on the basis of industrial secondary raw materials come from 1990's, e.g. Jo et al (1996). These filters were however prepared by sintering and this line of research still continues parallel to the alkali-activation of these materials with very promising results (Jedidi et al, 2011; Tewari et al, 2010; Qin et al, 2015; Cao et al., 2014; Fang et al, 2013; Singh et Bularasa, 2013). However, if there is a way to achieve comparable results only by chemical reaction, a big amount of energy would be saved, which is the reason why studies like this dissertation are important.

Another direction of research directly in the field of alkali activated porous materials is their foaming mainly by adding silica fumes containing free silicon which is oxidized by water in the mixture releasing hydrogen (Prud'homme et al, 2010; 2011A; 2011B). However, the foams had not defined pore size because the bubbles tend to join together (which is not in most authors' main aim because the purpose of the studies is the material's light weight and favorable thermal insulation properties for future utilization in building industry). Recently, however, Zhang et al (2016) published a paper on controlling the foam porosity via two-step phase-conversion technique comprised of geopolymer foaming and hydrothermal crystallization. Previously, Henon et al. (2012) published a paper on possibility of controlling the porosity using various temperature cycles that also decreased the time of synthesis.

Medpelli et al (2014) introduced a very interesting technique for porous geopolymer preparation by mixing triglyceride oil into a freshly made geopolymer paste to form a reactive emulsion. During the curing process, the oil in the alkaline emulsion undergoes a saponification reaction to be decomposed to a water-soluble soap and glycerol molecules which are then extracted from the cured material simply using hot water.

The general history of alkali activation was further described above. The utilization of alkali-activated materials in preparation of filtration media has been of interest for only a decade or so if we do not take into account the alumino-silicate materials for immobilization of dangerous substances containing heavy metals by adsorption which has been researched since 1990s (Van Jaarsveld et al., 1997) and contain very interesting applications, for example Pb and Cu immobilization by FA-based AAM (Phair et al, 2004), removal of sulphates over barium-modified BFS AAM (Runtti et al, 2016), removal of cesium from aqueous solution by adsorption on mesoporous FA/BFS AAM (Lee et al, 2017), etc. Wang et al (2006) conducted work describing alkali-activation FA conversion into effective adsorbent for removal of heavy metals and dyes from wastewater. The true filtration separation techniques utilizing geopolymers/AAMs are e.g. gas oil in water emulsion separation on Taguchi method-synthesized BFS membrane (Mohammadi et Mohammadi, 2017), separation of water from ethanol on alkali activated BFS membrane (Azarshab et al, 2016).

Very interesting is the way of production and also the application of porous AAM prepared by Duan et al (2016). Porous material on the basis of FA was partially (30%wt.) replaced by iron ore tailings, H_2O_2 was added as a foaming agent, the mixture was activated by alkaline silicate solution and the material was tested (successfully) for spontaneous adsorption of Cu^{2+} from wastewater.

One of the first papers to address, among other things, directly the porosity of alkali-activated materials was published by Duxson et al. (2005) and it is named "*Undestanding the relationship between geopolymer composition, microstructure and mechanical properties"*. This paper inspired author of this work to study the porosity of the material directly through the ratio of the main oxides because the work shows the differences in structure based simply on the Si:Al ratio change.

There are not many articles on combination of fly ash and slag during alkali activation but there is a particularly important one recently published by Ye et Radlińska (2016) summarizing some of the key information about the microstructure formation.

A very good review on the topic of alkali-treatment recycling of fly ash and pozzolanic industrial by-products was recently published by Lee at al. (2017B). A zeolite framework synthesis and methods of appropriate research are presented in the paper. It also includes a chapter of fly ash acid pretreatment to remove CaO and Fe_2O_3 'impurities'.

Note: The fact was known when designing this works procedure but the pretreatment was not involved due to its complexity and energy- (and consequently cost-) demands especially for drying after the procedure as the intention of the work was to focus on the porous media preparation with the lowest theoretical cost possible. The level of CaO was however taken into account during the selection of the FA and the one with the lowest content was chosen for the experiments.

Another method of fly ash pretreatment, namely mechanical activation, was studied by Temuujin et al (2009) and Chindaprasirt et Rattanasak (2010) both concluding that the mechanical activation improves the compressive strength of the resulting AAM material to 40MPa on average.

Note: Mechanical activation was studied experimentally in this work and the strength results seem to be convincing. It was however not involved into the experimental procedure because of the fineness of the material - fly ash has very fine granulometry even in unaffected state and the classification has to be done to get rid of the finest portions (which embody a significant part of the bulk) to obtain fractions that can be used to prepare defined porous material via 'dry' press-molding of defined particle fractions. After series of grinding experiments on stirred media mill and then air jet mill in various regimes it was concluded that the processing was either not effective enough to substantially support the activity of the material or in other cases it meant an increase in the finest portions (that are not applicable for the porous material production) in a scale that do not justify the demand for energy spent on comminution and classification procedures neither the amount of extra material becoming useless for the work after this pretreatment.

Every year more and more authors study the factors affecting the mechanical properties, microstructure and composition of alkali-activated materials on the basis of secondary raw materials (e.g. relatively detailed study on red mud and FA gepolymers by Zhang et al., 2014).

A study conducted by Görkhan et Görkhan (2014) researched the influence of NaOH concentration on the mechanical properties of FA based AAM mortar cured at different temperatures and different curing times. They concluded that the increase in the curing time and the activator concentration affects the compressive strength as well as the porosity and consequently bulk density.

AAMs based on FA were also studied from the technological point of view by Nematollahi et Sanjayan (2014). The research was on use and effectivity of different commercial superplasticizers to increase workability of alkali-activated fly ash pastes.

Another recent study by Nedeljković et al (2018) investigates natural carbonation of AAS and FA pastes after one year and its influence on elastic modulus and porosity. The study concludes the fact that increasing BFS content decreases the occurrence of carbonation, so it is mainly an issue of FA-based AAMs.

On the other hand purely BFS-based AAMs have a different technological issue which is their shrinkage. Ye et Radlińska (2017) did the research of the polymerization shrinkage and came with a conclusion that the high-magnitude shrinkage in AAS is attributed to the high visco-elastic/visco-plastic pliability of calcium aluminosilicate hydrate (C-A-S-H) in the material and it can be considerably reduced via high-temperature curing. This would however unfortunately lead back to the energy-intensive treatment. Tthere are apparently better options concerning in particular shrinkage reducing admixtures (Bílek et al., 2016).

A study on how elevated temperatures (800°C) affect the geopolymers and geopolymer composites was done by Kong et Sanjayan (2008) and another related study comparing fire-resistance (800-1000°C) of fly ash AAM and ordinary Portland cement was conducted by Sarker et al. (2014). The first mentioned study favors geopolymer in front of geopolymer/aggregate composite, the second concludes that geopolymers hold their mechanical properties far better than Portland cement based specimens after the elevated temperature exposure. There is also a study from Mill-Brown et al. (2013) concluding that geopolymers reinforced with silicon carbide exhibit hold stable thermal properties up to 1000°C, tensile properties highlight a significant reduction in stiffness at up to 760°C however showing sufficient retention of ultimate tensile strength to suggest potential for use in high temperature applications. The last to mention at the point is a study by Nikliоć et al (2016) researching thermal stability of blended binders on the basis of FA and electric arc furnace slag which claim that the addition of slag improves the strength of FA-based AAMs, however it also negatively affects the thermal stability above 600°C.

Adsorption as an integral part of separation techniques was already mentioned above. Porous geopolymers/AAMs have been researched and utilized in the field for more than two decades as they are capable of removing heavy metals, but this way they can be utilized also as a catalysts. In the study published by Zhang et Liu (2013) geopolymer adsorbent (with 17-700 nm pores) was used as a catalyst for degradation of dye from wastewater.

The field that already utilizes the advantages of AAMs made on the basis of secondary raw materials is building industry where the conventional concrete based on Portland cement can be partially or fully replaced by geopolymer concrete which pervious and mechanical properties are very similar to its conventional substitute (Tho-In et al., 2012). Due to a review on cement

production conducted by Schneider et al. (2011) Holcim company produced in total of annual production only 4% of ‘fly ash cement’ and 8% of ‘slag cement’ in 1995 whereas in 2009 it was 26% of fly ash cement and 9% of slag cement (there is also a ‘pozzolan cement’ produced which between the years stays at 9%).

In the field of ordinary metakaolin-based geopolymers Zhang et al. (2014B) found out that substitution of 10% of metakalolin by FA increases the reaction extent, 28-day compressive strength by 15%, and also increases the porosity of the resulting material with increasing level of fly ash replacement.

A porosity-related patent on geopolymers was published in 2010 in US by Frizon et al. named *Method of preparing a controlled porosity geopolymer, the resulting geopolymer and the various application thereof*. It is metakaolin-based material but the technology when further developed should be usable within the secondary raw sources based geopolymers as well.

The last studies to mention study the porosity/permeability of alkali-activated materials from the opposite point of view – to lower it as much as possible. A study aiming to develop new sealant material for carbon capture and storage wells used for the process of geological sequestration of CO_2 (Nasvi et al., 2013 and 2014) came up with a geopolymer material that has maximum permeability of 0.04μD which is 5000 times lower than the permeability value recommended by the American petroleum industry (API) which makes this geopolymer material potential primary sealant in a typical wellbore. On top of that Haider et al (2013) also studying the suitable materials for geo-sequestration of CO_2, only in saline aquifers, found that geopolymer materials cured in saline water show higher strength results than the ones cured in normal water. This discovery is very promising because Portland cements based oil well cements have unfavorable properties when cured in saline water.

Note: *This part had to be reworked due to the fact that the most relevant articles and papers on this theme were published very recently because this field of study is of growing interest. Because of this fact it may contain new information not known and thus not taken to account when the experimental part of the work was designed and performed.*

4 METHODS

4.1 SPIRAL JET MILL ALPINE AEROPLEX 100 AS

Spiral jet mill is a device for an ultrafine comminution of soft to medium hard materials which display brittle crystalline fracture behavior in the particle size range of 10 to 150 μm. The grinding process is very clean and possibly sterile because the mill has no rotating components, there are consequently no bearings and shaft seals, and thus no lubricants are present to contaminate material.

The feed product is conveyed to the mill via integrated injector charged with compressed air as well as the tangentially ordered Laval nozzle ring in the milling chamber. The grinding air causes a spiral jet of air to form in the grinding zone. The feed product circulates close to the nozzle ring and is thus intercepted repeatedly by the air jets exiting the nozzles. Comminution is the result of interparticle collisions caused by the particles flowing at different speeds in the nozzle jet (see Figure 10). The spiral flow and a special discharge-area geometry subjects the particles to a classification - only particles fine enough to lose the inertia of the stream are discharged, coarse particles remain in the mill. Common feed rate and air pressure settings at a maximum feed size of approximately 1.5 mm are capable of giving the end-product fineness values of d_{97} ranging between 5 and 30 μm. With finer feed, lower feed rate and higher jet air pressure the product particle size decrease. Dosing capacity of this particular mill is cca 150 -2 800 ml/h.

Figure 10: *Left – The overview of the spiral jet mill assembly (including vibratory dispenser, air pressure controller and collecting container); Right – Illustration of movement inside the milling chamber (Hosokawa, 2011).*

4.2 AIR JET SIEVE ALPINE E200 LS

The device (fulfilling DIN EN 9001 standard) is suitable for the analysis of any dry particulate matter with a sample size of 0.3 to 100 g. Material is set into motion only by air and therefore any of its qualities is not affected. The particles are blown upward by an airblade rotating arm (18 rpm) where the agglomerates should be broken when hitting the cover. Particles are then sucked by negative pressure (1 500 - 5 500 Pa according to settings) through the loosen sieve openings (see Figure 11).

Various sieves are available fulfilling DIN ISO 3310-1 with a mesh size of 20, 45, 63, 90, 125, 200, 500, 1 000, 1 500 and 2 000 μm. Parts of the air jet sieve assembly apart from the sieving unit are L-type industrial vacuum cleaner, Sartorius TE 802 laboratory scales, and GAZ 120 high performance cyclone for almost complete under-sieve fraction collection without any contamination.

Figure 11: *Air jet sieve assembly overview and sieving chamber air movement illustration above (Hosokawa, 2012).*

4.3 POWDER ULTRAFINE CLASSIFIER ALPINE 50 ATP TURBOPLEX

The classifying air flows into the machine, then through the classifying wheel in centripetal direction, extracts the fines and forwards them via cyclone to the container J. The coarse material rejected by the classifying wheel exits the machine through the coarse discharge. The air routing shown in the schematic below is simplified and doesn't show that before the coarse material exits the classifier, it is rinsed again intensively by air to remove the remaining fines. This results in very clean coarse fraction dispatched to container H.

The feedstock is fed from the side (in Figure 12 scheme from behind) via a rotary valve. The product fineness is controlled as a function of the classifying wheel speed using a frequency converter. (Hosokawa Alpine Turboplex Classifier ATP)

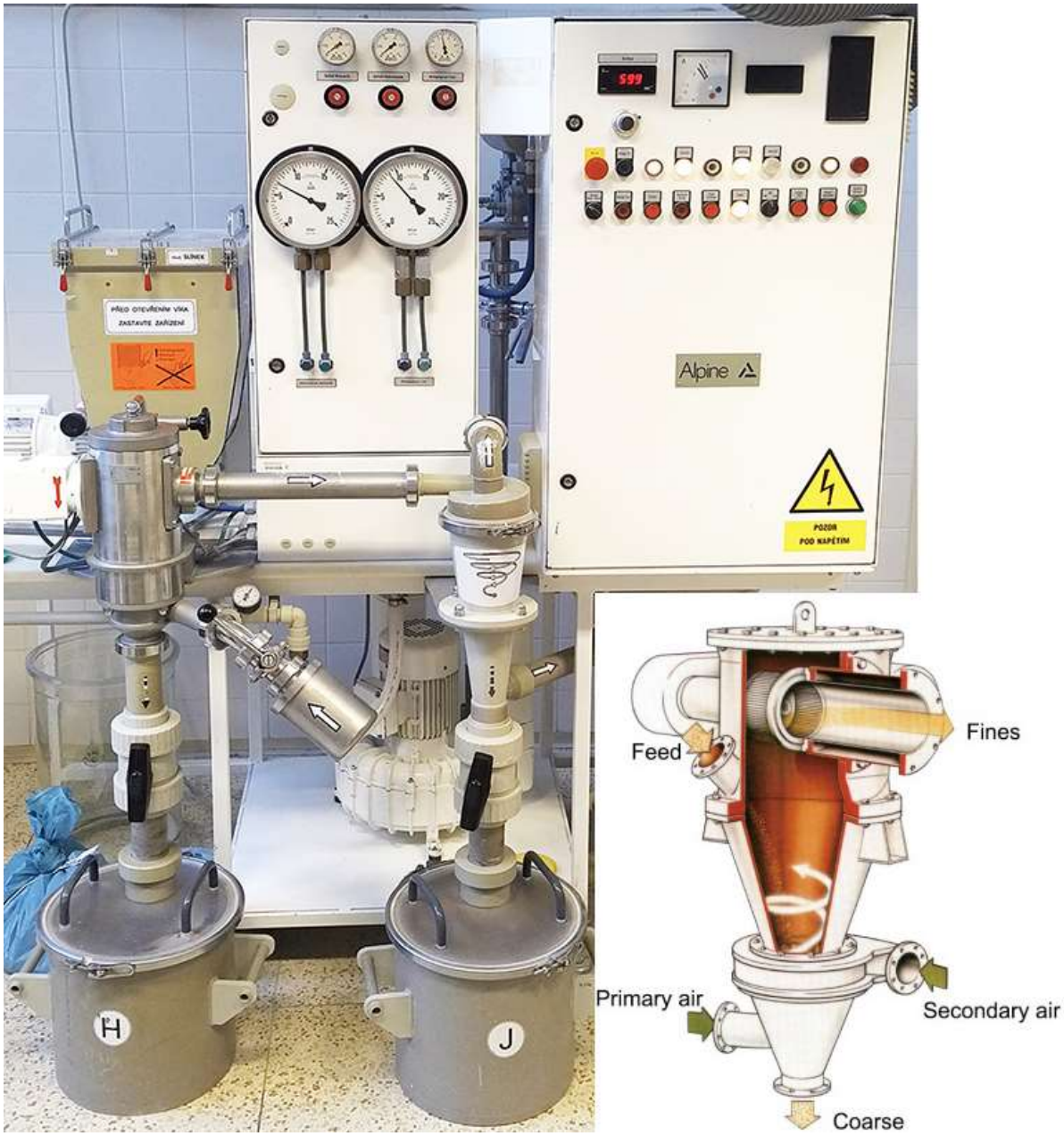

Figure 12: *ALPINE 50 ATP Turboplex and a scheme of the classifying chamber function. (Hosokawa Alpine Turboplex Classifier ATP)*

4.4 OPTICAL MICROSCOPE OLYMPUS BX41

The microscope in our laboratory is an ordinary optical binocular (see Figure 13) with maximum 500x magnification (ocular 10x, objective 50x). It contains a streaming camera connected to computer software. For the purpose of this work this type of microscope could be used only for cursory examination, detailed images of structures have to be taken by scanning electron microscope (SEM).

Figure 13: *Olympus BX41.*

4.5 SCANNING ELECTRONE MICROSCOPE

The Zeiss EVO LS10 (Figure 14) is a variable pressure scanning electron microscope (VP-SEM), commonly also called an Environmental SEM. It is capable of 6nm resolution in high vacuum mode and 1-30kV accelerating voltage. It produces high resolution images of traditional conductive SEM samples under high vacuum, but this type of SEM is particularly good also in the analysis of nonconductive, hydrated (it uses Deben coolstage II accessory to keep samples hydrated), oversize, or otherwise unusual samples. In extended pressure imaging mode (50-3000Pa using N_2 or water vapor), imaging can be done at set pressures up to 3000 Pa. It also has an elemental analysis using the Oxford Inca EDX accessory which is very helpful in exploration of heterogeneous structures. Available detectors include dual secondary electron detectors (high vacuum and variable pressure), retractable backscatter detector, and Oxford Inca EDX detector for elemental determination.

For the purpose of this work as in most cases the samples had to be polished to keep the things of interest in one plane and make the structure more visible - JEOL IB09010CP ionic polisher was used for the task. Then the samples had to be sputter coated with gold.

Figure 14: *Zeiss EVO scanning electron microscope with control and display components; measurement cell insight (A); revolving specimen holder (B). (Carl Zeiss AG, 2017)*

4.6 LASER GRANULOMETER MALVERN MASTERSIZER 2000

Particle size is important for understanding the properties and behavior of lots of different types of materials. Laser diffraction method for particle size measurement is in our laboratory performed on Malvern Mastersizer 2000. The measuring principle is based on Mie scattering-theory and Fraunhofer diffraction-theory principles. Measurement can be conducted in two ways. First way is simply called wet method – the sample is inserted into a solution (mostly distilled water), where it is dispersed by mixing and ultrasound (wet-measurement preparatory cell/dispenser is shown in Figure 15 on the bottom right). Then it is passed through the wet measuring cell. Second way is predictably called dry method, where the sample is inserted on a dispenser pan, from which it is sprinkled into the system and drifting into the dry measuring cell (the dry-measurement dispenser is shown in Figure 15 on the bottom left).

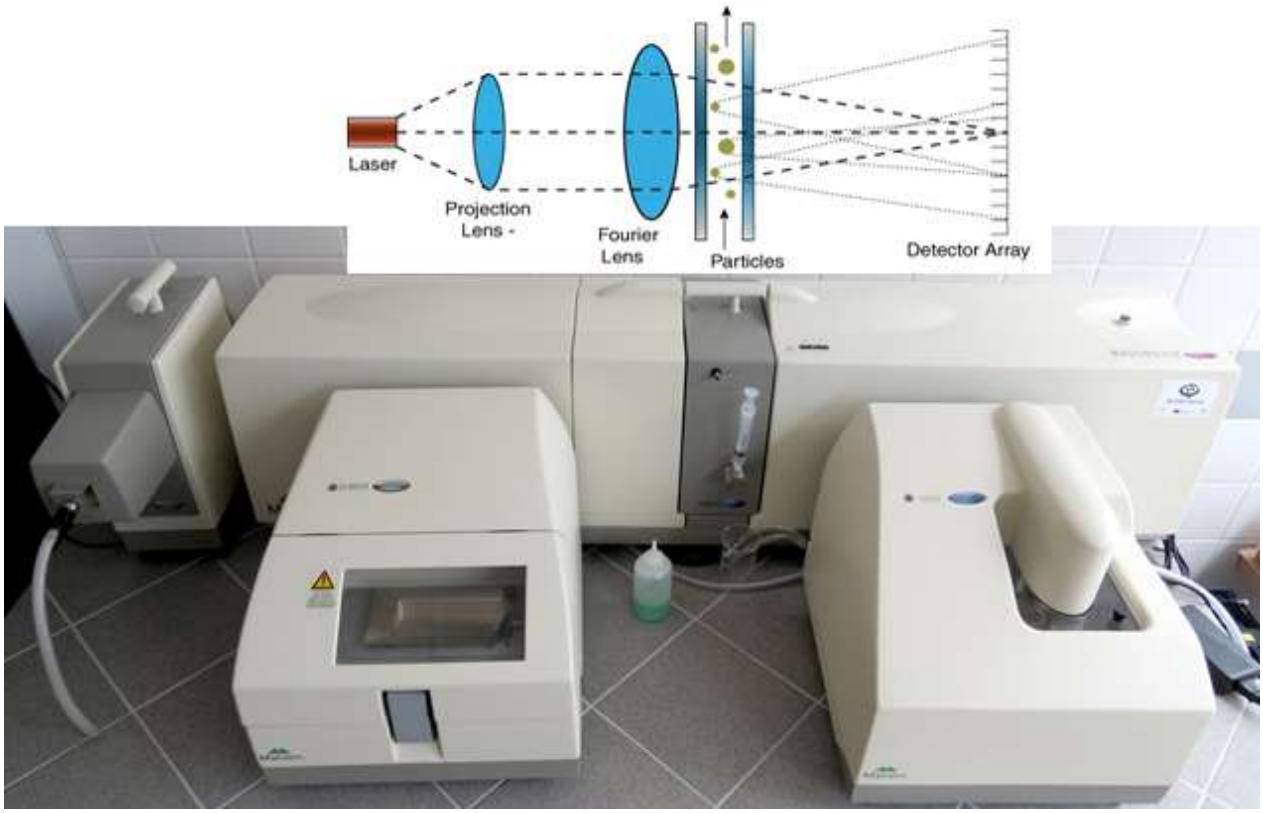

Figure 15: *Malvern Mastersizer 2000 with wet-measurement cell plugged in the middle and dry-measurement cell in the holder (left).*

The accuracy of measurement is influenced by several factors. Laser diffraction method assumes ideal spherical particle shape and the resultant distributions are converted to volume. This means that the distribution curve is shifted towards the larger particles if between small particles is included one bigger. The result can be thus distorted a lot in extremely non-ideal case but most samples are not of that nature and there is a simple way for the trained operator to identify the unreliable data. The next factor is the optimal setting of the measurement method for every particular material.

Bulk materials in particle size range of 0.02 to 2 000 microns are suitable for measurement by this device.

4.7 PLANETARY CENTRIFUGAL VACUUM MIXER THINKY ARV-310

The device shown in Figure 16 is used for mixing of water-like liquids, pastes, powders and various mixtures of low and high viscosity. It can mix e.g. adhesives, pigments, cosmetics, pharmaceuticals, nanoparticles, fillers etc.

Figure 16: *Planetary centrifugal vacuum mixer Thinky ARV-310 and a scheme of the mixing cell movement during operation.*

Combination of vacuum pressure reduction with rotation and planetary mixing enables efficient elimination of submicron-level air bubbles. With rotational and planetary movement under vacuum, deaeration of high-viscosity materials, which is normally considered difficult, can be performed with excellent quality. The processing time is reduced compared to the atmospheric mixer. In terms of operation, the centrifugal force of planetary movement during the mixing process suppresses the material within the container eliminating the need to keep an eye on the material as is needed with static vacuum chambers to not let the material overflow. The maximum weight of the mixed sample is 310 g in a standard container that can hold up to 300 cm^3.

4.8 POROMETER QUANTACHROME 3GZH

The Porometer 3Gzh is suitable for the analysis of gas permeability and pore size of a sample. Gas permeability is the measurement of the flow rate per unit area at one or more preset pressures through a known area and thickness of dry sample and for a selected data-acquisition time period.

For the pore size distribution measurement a liquid of low surface tension (Quantachrome POROFIL) is used in a displacement technique. By monitoring the pressure of gas applied to the sample and the flow of gas through the sample when liquid is being expelled a wet run is obtained. If the sample is then tested "dry" without the liquid in its pores a dry run is obtained. By comparing the flows of the wet run with those from the dry run the pore size distribution can be calculated. The number distributions are presented in the overall size range of approximately 500 μm diameter down to less than 0.05 μm. The overview of the machine assembly is shown in Figure 17.

Figure 17: *The control/CPU module (left) and the sample holder of the 3Gzh porometer.*

4.9 LABORTECH TENSILE TESTING MACHINE

The Labortech LabTest 6.0051 (Figure 18) machine for uniaxial tensile testing that is available in our associated laboratory at Netme Centre is used in this case for pressure test, namely four-point bending. It has exchangeable tensometers with different ranges up to 3kN. The clamping mechanism is used for ordinary tensile tests and has to be switched for the purpose of this work.

Figure 18: *LaborTech LabTest 6.0051 uniaxial testing machine.*

4.10 SIEMENS D5005 X-RAY POWDER DIFFRACTION ANALYSIS

X-ray powder diffraction analysis is the analytical method used to determine mineralogical (phase) composition of substances having a crystalline character. The measurement uses X-ray beams due to their ability to cause inter-atomic diffraction in the sample which then acts like a diffraction grating. Due to the periodicity of the crystal structure a radiation scattering and subsequent diffraction occurs on the crystal lattice and from its maxima a crystal lattice spacing of atoms can be determined (Figure 19). In a powder (polycrystalline) sample individual crystals directions are random, but due to their "infinite" number in the sample some of them are always oriented so that their set of planes meets the incident-radiation diffraction condition for angle θ from the Bragg equation:

$$n \cdot \lambda = 2d \cdot \sin\theta$$

where λ is the X-ray wavelength, n is an integer, d is a distance of two adjacent planes and θ is a diffraction angle.

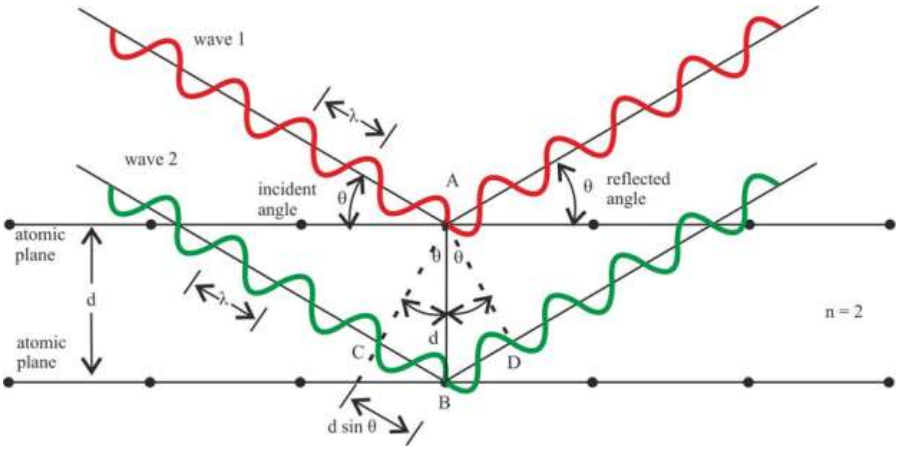

Figure 19: *Schematic representation of Braggs law (Waeselmann, 2012).*

Figure 20: *XRD goniometer of Siemens D5005 set accordingly to the scheme of the function.*

4.11 EXPERIMENTAL FILTRATION POST

Our filtration post, shown in Figure 21 was designed and custom-built in cooperation with MVB Opava s.r.o. for testing the filtration properties of completed filtering media in the form of plane discs or cylindrical barriers, and there is also a compartment for testing of hollow fibers. It is a device containing basically 4 interswitchable circuits with flow meter/controller, pressure meter/controller and turbidimeter, all connected to Memograph M data logger. Maximum pressure of the installed air-operated diphragm pump is 5 bars with a flow rate of 24 l/s. Desirable accessory for the case is also a pulsation damper installed in the circuit.

Figure 21: *Experimental filtration post.*

5 EXPERIMENTAL PART

5.1 MATERIALS

5.1.1 Particular materials

Fly ash is an industrial by-product from pulverized coal combustion. This material is collected using electrostatic separators which prevent it from releasing into the atmosphere. It mostly consists of aluminosilicate particles with pozzolanic properties, with mineral constituents including a glassy phase and minor crystalline phases such as quartz, mullite or hematite.

It is generally considered that this material has a significant potential for utilization in various applications when activated using an alkaline solution. Thus far, the most studied applications have been preparation of alkali-activated fly ash (AAFA) based concrete for construction and building purposes. Other applications of fly ash such as concrete admixtures or production of blended cement were of general importance for long time (Collepardi, 2010). More recently, a lot of high-tech applications of alkali-activate materials has been studied. These materials were used in many chemical-engineering processes including adsorption (Runtti et al, 2016; Lee et al, 2017), hot gas cleaning (Jo et al, 2016) and membranes separation (Liu et al, 2014; Bulejko et al, 2014) the latter of which is of growing interest in recent years.

In this work fly ash from Prunéřov II high temperature combustion power plant was used. The type was chosen due to its relatively low level of free lime (see Table 5 on page 21) which could otherwise introduce hydraulic properties (CASH gel generation) into pure AAFA samples and influence the results. If too much lime is present it would have to be acid treated prior to alkali activation to increase its activity by removing the 'impurities' (such as CaO and Fe_2O_3, bound organic molecules) that can compete with alumina in the formation of zeolite framework. In this case the low lime fly ash was chosen and the acid treatment was omitted because the procedure is intricate and also includes energy-intensive stage of calcination (700°C for 3h) which is consequently also cost demanding (Lee et al, 2017B).

Table 6: Prunéřov II fly ash oxide composition.

Main oxides (%wt.)

SiO_2	Al_2O_3	CaO	Na_2O	K_2O	MgO	SO_3	Fe_2O_3	TiO_2	P_2O_5
47.3	23.2	6.0	0.6	1.6	1.2	2.3	15.5	1.3	0.2

Supplementary oxides (%wt.)

Cr_2O_3	MnO	V_2O_5	NiO	CuO	ZnO	As_2O_3	Rb_2O	ZrO_2	SrO
0.04	0.15	0.06	0.02	0.02	0.04	0.02	0.02	0.03	0.05

BaO	CeO_2	Sm_2O_3	Tb_4O_7	Ho_2O_3
0.1	0.03	0.01	0.02	0.01

The fly ash granulometry had to be optimized prior to the work. The classification was done using combination of sieving and air fractionation using an Alpine Windsichter ATP50 cyclone classifier. Particle size distributions of unclassified and classified fly ash that were determined by laser diffraction method are given below in Figures 26 and 27. The size and morphology of particles was also observed using SEM and the micrographs are in Figures 22 and 23 that clearly show that the finest portions of the material were separated. The oxide composition of the Prunéřov fly ash is listed above in Table 6. In order to know the phase composition an X-ray diffraction (XRD) analysis was also performed. According to that an amorphous phase content of the used fly ash fraction is about 60%. Mullite is predominant from crystalline phases (about 25%), but also quartz, hematite and magnetite were detected in noticeable amounts.

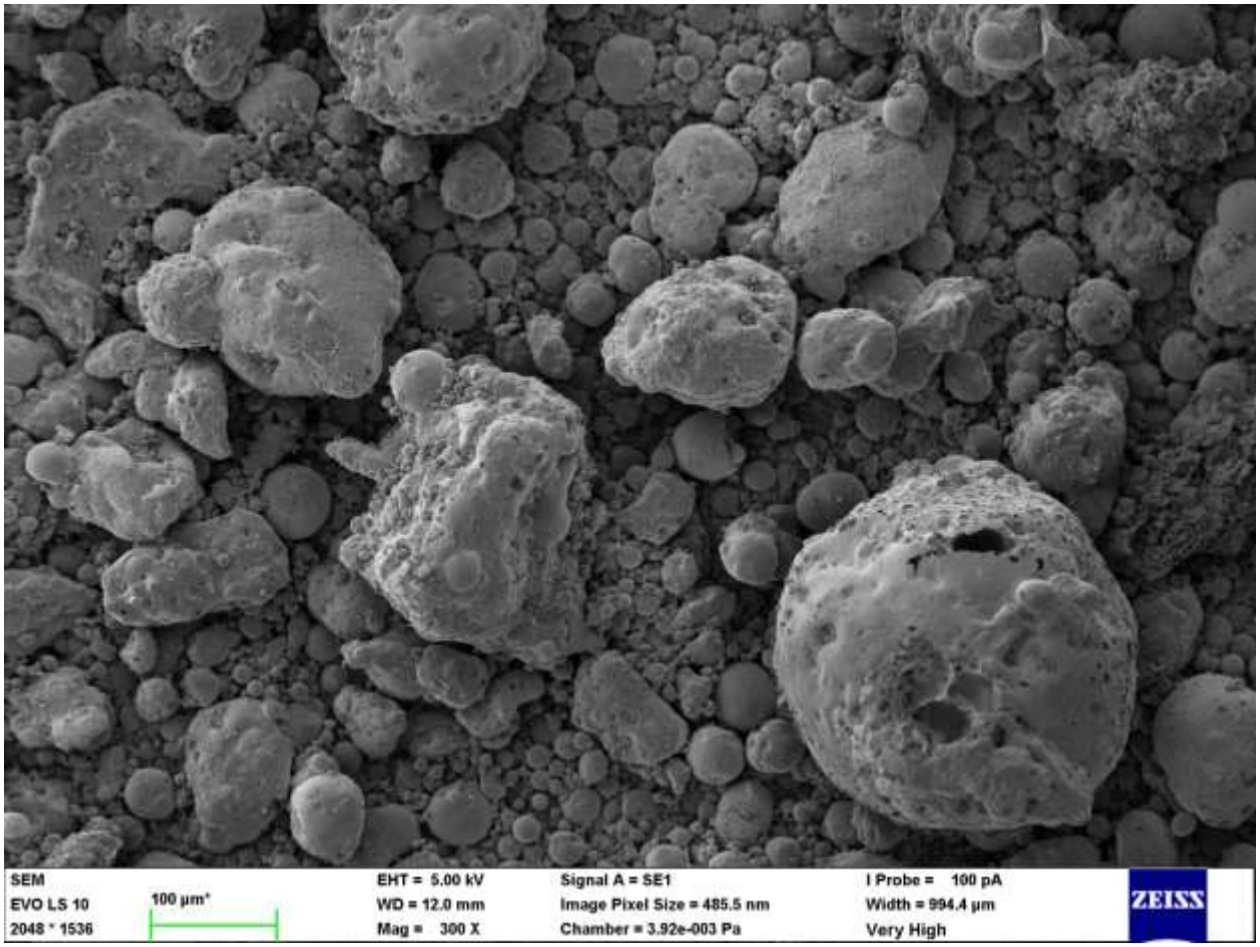

Figure 22: *Prunéřov II fly ash after removal of the fraction above 500µm.*

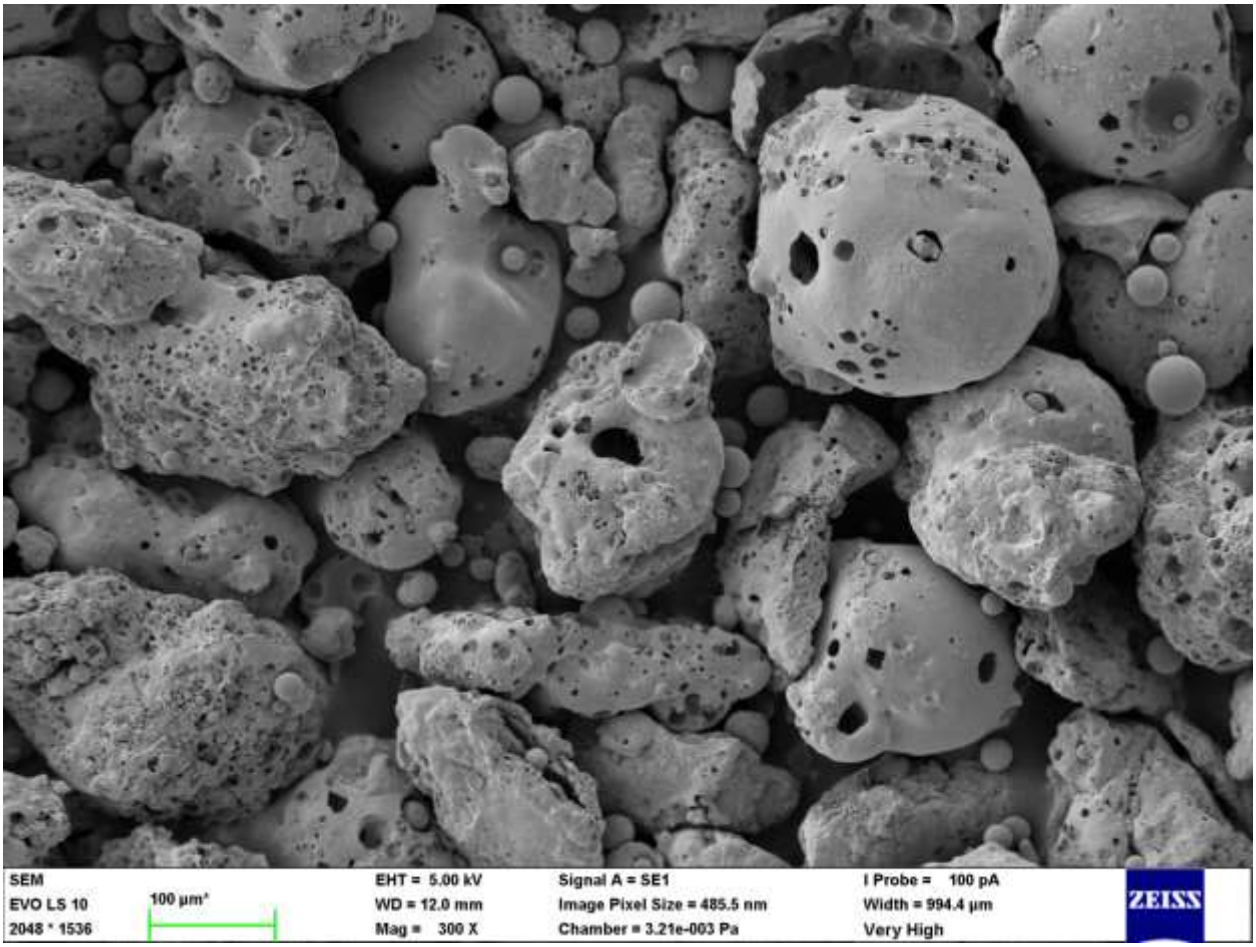

Figure 23: *Prunéřov II fly ash after second fractionation to remove the finer fractions.*

The finely ground granulated blast furnace slag (GGBFS) used for the work origins from Kotouč Štramberk company. It also had to be classified to exclude the finest portion of the particles that could fit into the pores and block them. The oxide composition is shown in Table 7.

In concrete practise (which as sole industry utilize it nowadays on daily basis) the quality of blast furnace slag is given by Keil's index *F (Péra et al., 1999)*:

$$F = \frac{CaO + CaS + 0.5 \cdot MgO + Al_2O_3}{SiO_2 + MnO}$$

When $F<1$ the slag is not suitable for further use in binders, $F>1.5$ is taken as good quality and $F>1.9$ an excellent quality. This particular GGBFS has $F=1.57$ and therefore is of good quality.

Particle size distributions of both unclassified and classified GGBFS were determined using Malvern Mastersizer 2000 (see Figures 26 and 27) laser diffraction analyzer and for morphology exploration ZEISS EVO LS 10 scanning electron microscope was used (see Figures 24 and 25). Blaine fineness of unclassified GGBFS was about 400 m^2/kg while its selected fraction had Blaine fineness of about 250 m^2/kg.

The composition is listed in Table 7 where can be seen that it contains over forty percent of CaO. Phase composition was characterized using the X-ray diffraction method (XRD). Both types of GGBFS had the same phase composition containing about 88% of amorphous phase, 9% of akermanite and 3% of calcite.

Table 7: Kotouč Štramberk slag oxide composition.

Oxides (%wt.)									
SiO_2	Al_2O_3	CaO	Na_2O	K_2O	MgO	SO_3	Fe_2O_3	TiO_2	MnO
34.7	9.1	41.1	0.4	0.9	10.5	1.4	0.3	1.0	0.6

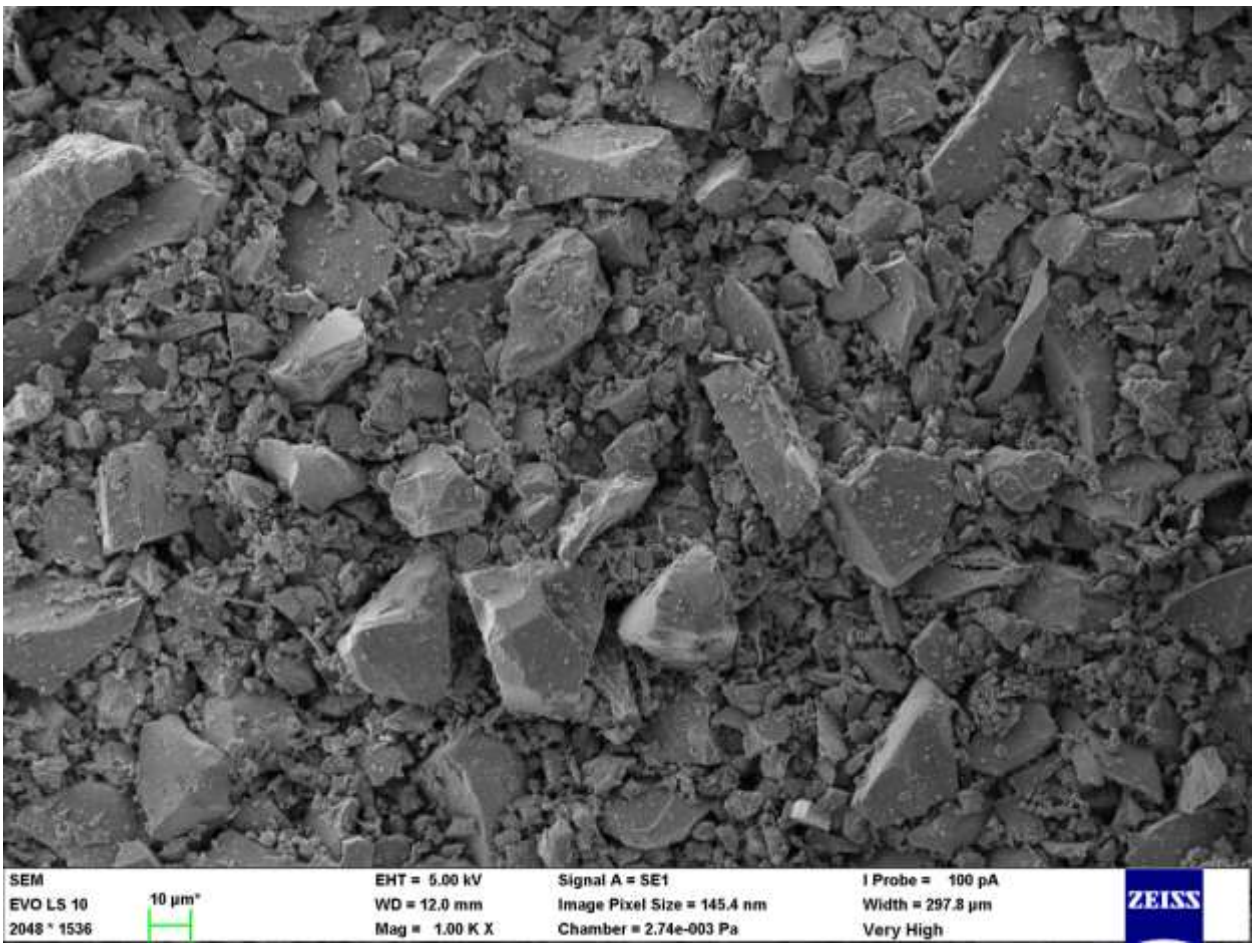

Figure 24: *Non-fractionated GGBFS.*

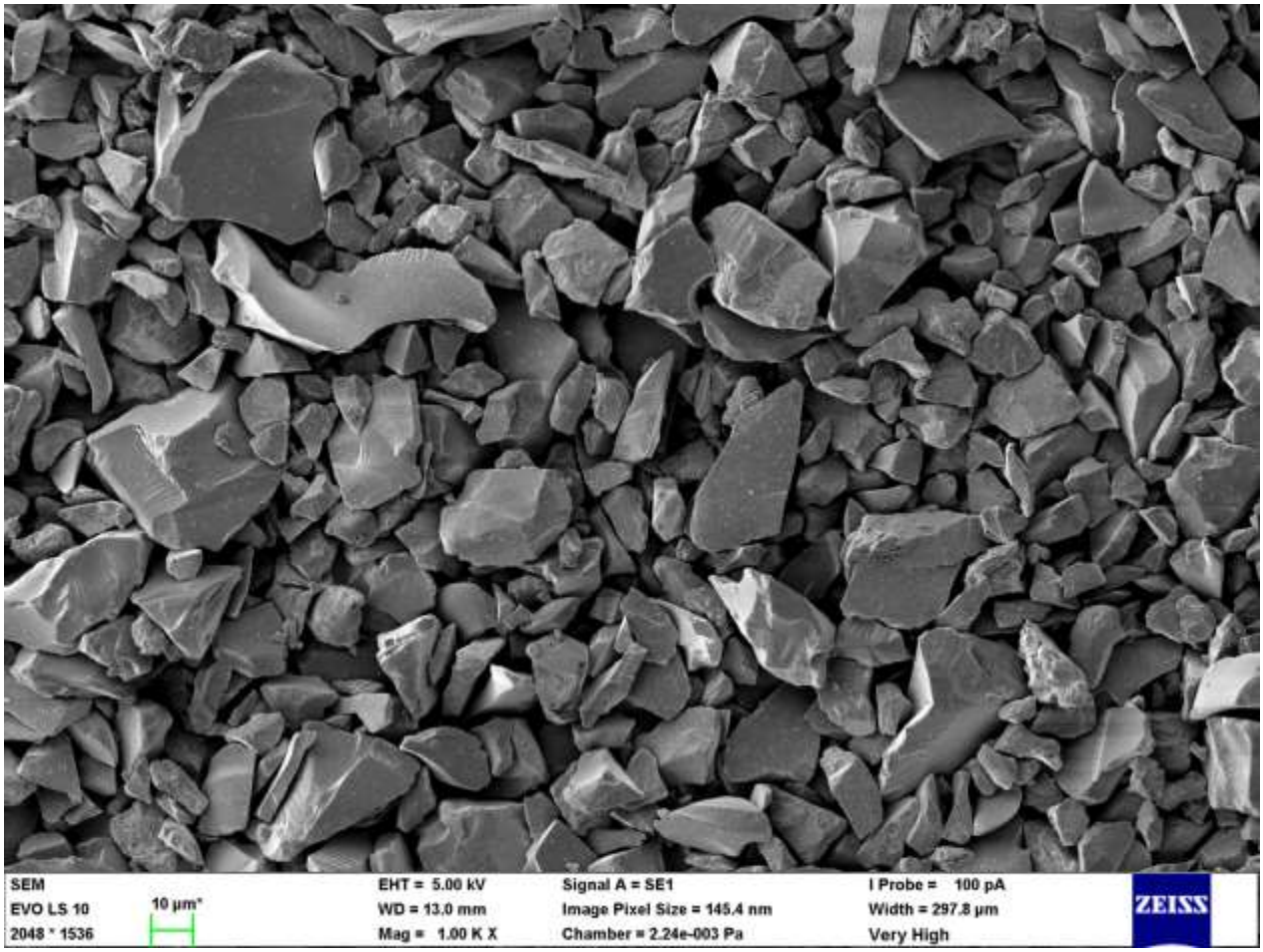

Figure 25: *GGBFS after fractionation*

The last of the particulate materials used for the preparation of alkali activated mixtures was bauxite. It was used only to supply the aluminum oxide to the mixtures to fit the composition requirements. The maximum limit of bauxite in the mixture was set down to 10%. Bauxite also had to be classified (see Figure 26), this time by sieving out the coarser part on 90µm sieve. The fine portion under 10µm that left after the fractionation (see Figure 27) was in this amount considered negligible or even beneficial for the formation of NASH gel. The bauxite used for this work has predominance of boehmite, diaspore and gibbsite and the oxide composition is listed in Table 8.

Table 8: Bauxite oxide composition.

Composition (%wt.)			
Al_2O_3	Fe_2O_3	SiO_2	TiO_2
86.0	2.0	8.0	4.0

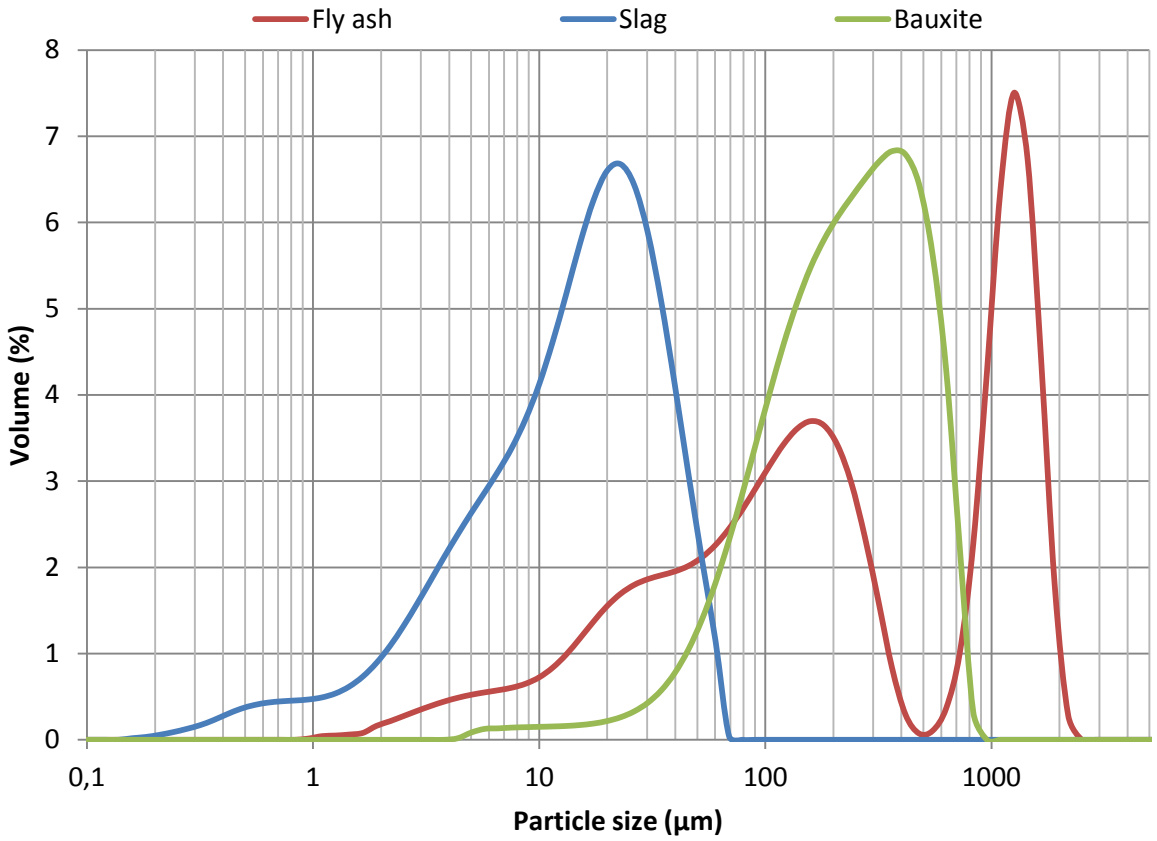

Figure 26: *Particular materials granulometries before classification.*

The above listed particular materials were investigated in terms of granulometry and the result is shown in the Figure 26. It can be clearly seen that bauxite was too coarse for the purpose and only the finest portions of it could be used. On the other hand the blast furnace slag had to be classified to remove the smallest particles which would otherwise block the space between bigger particles and result in lesser to no through-pores. Fly ash had to be classified both from the fine and the coarse end to match the required granulometry.

Figure 27 shows the bulk materials after the classification processes that were subsequently used for the experimental work. Significantly more uniform granulometries are obvious. The target to obtain the fractions between tens and lower hundreds of microns was achieved, only bauxite contained a small amount (up to 10%) of the finest portion. Therefore, it was neglected.

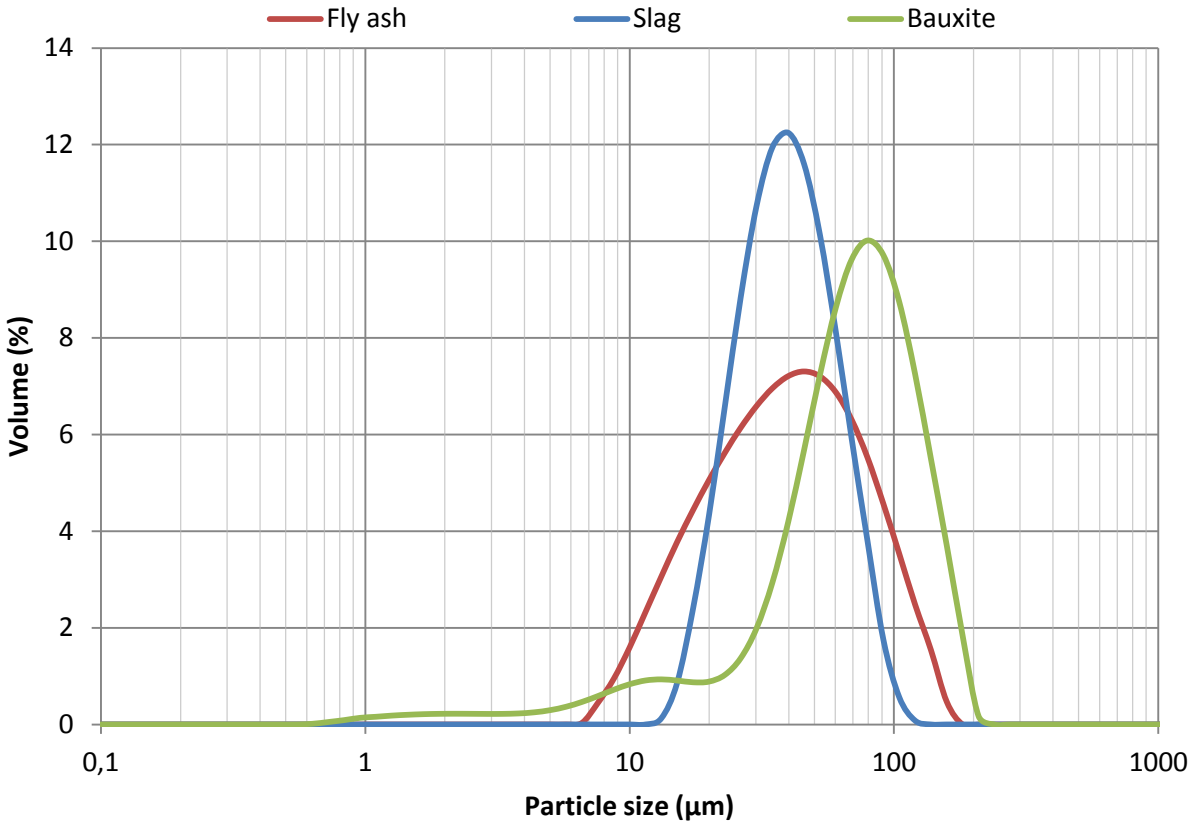

Figure 27: *Particular materials granulometries after classification.*

5.1.2 Activators

The liquid activators were selected on the basis of their suitability and their price. The first to mention is simple sodium hydroxide 50%wt. aqueous solution. In the composition listed in Table 9 the NaOH internal water (NaOH ~ 77.5% Na_2O + 22.5% H_2O) is taken to account. The second alkali activator was concentrated sodium silicate water glass, with the exact composition listed also in Table 9.

Table 9: Sodium hydroxide 50%wt. (left) and water glass (right) activators oxide compositions.

Composition (%wt.)	
Na_2O	H_2O
38.75	61.25

Composition (%wt.)		
Na_2O	SiO_2	H_2O
17.1	38.8	44.1

5.1.3 Material costs

It is not possible to calculate the direct unit price of the potential filtration barriers industrially manufactured with this kind of alkali activation method because there are too many variables that has to be taken to account: cost of labor and its amount per unit, machines used for pretreatment of the input materials and for the production process itself, dissolution of their cost in the product costs and power consumption projection into production price etc. Therefore this chapter only summarizes the place- and time-usual costs of raw materials used for the work and repeats the main idea that the advantage of the process is the bypassing of high energy-intensive processes of sintering or calcination during the production process and/or its replacement with only slightly elevated temperature curing.

Table 10: Material costs.

Material	Price per unit (excl.VAT)
Water glass (conc.)	0.45 USD/kg
NaOH 50% aq.	1.35 USD/liter
Fly ash	7.42 USD/ton
Slag	58.48 USD/ton
Bauxite	0.67 USD/kg

The material costs for such barriers are very low (see Table 10) considering the amount needed for fabrication of one unit comparing to the trivial prices per ton of GGBFS and FA which are the main entry items. The majority of the final price would therefore constitute the production process and its overall volume that further reduces the price of anything due to the dilution of the production technologies costs into the final price of the product.

5.2 COMPOSITION CALCULATION PARAMETERS

Even after detailed exploration, it was not very clear what most of the experimental compositions listed in the literature are based on. Most authors state the parameters of the mixtures they tested but do not clarify why (Jedidi et al, 2011, Kim et al. 2013). To make this work more robust, it was necessary to make a solid basis. This had led the author to design a mathematical tool to calculate the mixture compositions based on basic variables used in preparation of ordinary geopolymers. This approach had never been used in this field.

After reviewing composition variables influencing the strength and stability of different alkali activated materials, three mentioned below were found to play a crucial role.

5.2.1 SiO_2:Al_2O_3

The first parameter of the geopolymer composition, often also reported as Si/Al ratio, determines the microstructure of the material. It simply originates from the alkali-aluminosilicate-hydrate (N-A-S-H) gel structure formation during the alkali activation of various aluminosilicates. The Si/Al ratio in N-A-S-H ranges generally approx. from 2.8 to 3.6. According to J. Davidovits 1991 work *Geopolymers: Inorganic Polymeric New Materials* activated materials are best formed with an Si:Al ratio in the range of 1 to 3. It has to be noted here that his work targeted the mechanical strength alone, not on the porosity development. Duxson et al in their later work from 2005 titled *Understanding the relationship between geopolymer composition, microstructure and mechanical properties* stated that the materials tend to be highly porous for Si/Al ratios ≤ 1.40 but largely homogenous for Si/Al ≥ 1.65. That means our first parameter in the oxide form SiO_2:Al_2O_3 (where there is one Si atom to two Al atoms) has to be in the range of 2.80 to 3.30 to obtain a desired porous structure.

5.2.2 M_2O:Al_2O_3

The second parameter was used for monitoring the charge balance in the bonding network. The activation process of aluminosilicate precursor initiates a polycondensation reaction leading to short-range ordered molecular network of SiO_4 and AlO_4 tetrahedrons joined by oxygen bridges. In this configuration, the AlO_4 tetrahedron introduces a negative charge, which the alkali metal balances by 'incorporation into the structure' or more precisely locating itself into the gaps between the tetrahedron structures (see chapter 2.5.3). Therefore it is clear that the ideal M:Al ratio is best to be a unity. Rowles and O'Connor concluded in their work *Chemical Optimisation of the Compressive Strength of Aluminosilicate Geopolymers Sythetized by Sodium Silicate Activation of Metakaolinite* in 2003 that compressive strength of the material maximizes when there is a slight excess of Na (M) beyond the unity, amounting up to 1.25. Their later work *Chemical and Structural Microanalysis of Aluminosilicate Geopolymers Sythetized by Sodium Silicate Activation of Metakaolinite* states that the charge balance of around unity is sufficient and a lot of excessive Na could even damage the emerging polymer network by terminating Si–O–Na chains and of course causing more efflorescence.

For the purpose of this work and its experimental task this variable was set down to 0.9–1.1 with experimental overlap up to 1.3 in some cases.

5.2.3 H_2O:M_2O

The third parameter was chosen to control the amount of water and this way the consistency and workability of the mixtures based on the work of Yusuf et al.: *Effects of H_2O/Na_2O molar ratio on the strength of alkaline activated ground blast furnace slag-ultrafine palm oil fuel ash based concrete, published in 2014*. Increase in this ratio negatively affects the final strength (Xie et Kayali,2016), but positively impact the mixture workability (Yusuf et al. 2014; Puertas et al. 2014). This parameter therefore does not have its optimum value set due to the chemical point of view but it is more intended for an optimization of the consistency for further processing.

For press-molding of the barriers, it was targeted to have the mixture as dry as possible, yet still capable of holding together after pressing because this way corresponds with the presumption that less water, in this case meaning more concentrated activator, increases the strength of the product (Singh et al, 2016; Kaur et al, 2018). The same conclusion comes out of the basic microscale conception that the best way to obtain the continuous microporous structure is to only wet the surface of the particles and to let the activator to dissolve the outer layer of the material and consequently create necks between them. It has to be mentioned though that this optimum consistency bound (dry part to liquid part ratio) is always applicable to certain particles granulometry and even their morphology and is obviously never sharp. On top of that the miscibility of the mixture even with the planetary-mixing machine is limited. The dryer the mixture the more difficult is to preserve good and even mixing in terms of necessary forces and related considerable heating – causing some part of already small amount of water to evaporate during the mixing process.

This variable had to be therefore empirically optimized from all perspectives mentioned above and is applicable only for used ingredients granulometry and even morphology as the rheology varies significantly with the particle shapes and is of greater importance the less of the fluid ingredient is in the system as it increases the interparticle hydrodynamic interactions.

This variable had to be later supplied or in some cases completely replace by simple water to solid ratio abbreviated in tables and text below as ‘w/s’ to correctly fulfill its role of consistency controlling parameter.

Note: *In this case focusing on low cost filtration materials sodium based alkali activators were used due to their price which is far much lower than the price of the second most common potassium-based ones. The true formulas of the 5.2.2 and 5.2.3 titles can be therefore written as $Na_2O:Al_2O_3$ and $H_2O:Na_2O$ but because the variables are valid for any alkali activator, the general formula was used in the titles.*

5.3 COMPOSITION CALCULATION METHODS

Two mathematical methods were designed for the computation of the AAM mixture compositions. The first and simpler method was programmed via the Solver in MS Excel, to verify the idea and test the results. The second more complex solution was developed and programmed afterwards using MATLAB.

5.3.1 MS Excel Solver

This first computational method was created to verify the possibility of mathematical calculation of the composition in conjunction with simultaneous practical tests of the resulting mixture compositions. After series of experimental mixtures preparation and molding tests the P3 parameter was set to be around 5 to obtain mixtures with ideal consistency.

In the first step it was necessary to know the oxide content of each ingredient and formulate it to a shape that the Solver could use. Therefore the relevant oxides compositions of ingredients were formed to a first matrix shown below. Then a complementary matrix was prepared where fractional multiples of each field from the first matrix were filled in by Solver due to given criteria.

Note: *Liquid ingredients are highlighted in blue. Bauxite is also marked with different color because it had to be added beyond the intended composition just to supply the aluminum oxide to the mixture and obtain suitable results following the set parameters. Otherwise it was not possible to achieve the ideal oxide ratios and the computation returned errors. The Solver was given a condition of 10% maximal content of bauxite in the mixture.*

Composition (mol/100g)	H_2O	Sio_2	Na_2O	Al_2O_3
Water glass	2.447	0.646	0.276	0
NaOH 50% aq.	3.399	0	0.625	0
Fly ash	0	0.787	0.027	0.227
Slag	0	0.578	0.016	0.089
Bauxite	0	0.133	0	0.883

Then the MS Solver was programmed in the manner that will be explained on the following example to calculate the composition of mixture as close to the given ideal ratios as possible.

X	H_2O	Sio_2	Na_2O	Al_2O_3
0	0	0	0	0
19.151	65.095	0	11.973	0
42.529	0	33.482	1.159	9.677
35.095	0	20.270	0.562	3.132
3.211	0	0.428	0	2.835

The Xs (marked red in the previous matrix) are variable cells – multipliers (each multiplying its line from the previous matrix) that solver changes during the computation. In the final consequence for the particular mixture Xs represent the amount of ingredient on the same line of the initial table.

	P1 (SiO_2/Al_2O_3)	**P2** (Na_2O/Al_2O_3)	**P3** (H_2O/Na_2O)	Sum	
Y	3.463	0.875	4.753	99,986	
Ideal	3.0	1.0	5.0	100	**Solver (Min)**
D2	0.003712	0.000195	0.042896	27.562	**8.030**

The Ys are simple ratios of sums of the X-multiplied amount of oxides in all ingredients in multiplication table (P1 = Parameter 1 etc.). They are changed according to values multiplied by Xs so they are also variables. The line bellow the Ys titled Ideal are variables changed manually due to operator's needs outgoing from literature based ratios and the experimental tests. 'Ideal' values are subtracted from the Ys under second power to form a D2 (absolute value).

The last computational box was added to control the number of parts (set by 'Ideal' to 100). The first line of the box under the 'Sum' title is actually sum of Xs and the second is again Ideal (manually changed value giving the overall intended number of parts) and those two are subtracted to form a D2 as in the case of the left adjacent matrix.

The very last bounded value 'Solver (Min)' is the actual Solver result under searching the minimum of the function while giving him the sum of all D2 values.

So if we go retrospectively the solver tries to find minimum of the absolute value of difference between Ys and Ideals by randomly changing the Xs values.

On top of that any D2 formula can be manually multiplied by selected number prior to the calculation to assign it a greater level of importance and this way it is possible to force the Solver to focus more on one variable than the other.

Due to the subsequent finding that one task can return many different results it was clear that there are multiple results for the given conditions. The method was therefore upgraded and transferred to MATLAB to show the whole set of results.

5.3.2 MATLAB

MATLAB source files below show the same composition matrix and the same P1, P2, P3 parameters used in the MS Excel Solver. On top of that MATLAB gave us the option of setting the Ps in intervals and searching $1 \cdot 10^7$ values in one round (it could be set higher but this amount already takes gigabytes of operation memory). There was also added an extra water filter parameter that controls the total amount of water, because the ratio alone is insufficiently determinant factor for the mixture consistency and subsequent workability.

```
clear;clc;
pnts = 1e7;

indxs = [5];
rest_indxs = setdiff([1:5],indxs);
l_indxs = length(indxs);
min_indxs = 0;
max_indxs = 10;

sum_indxs = min_indxs+(max_indxs-min_indxs)*rand(pnts,1);
sum_rest = 100-sum_indxs;

WTS = 1./rand(pnts,5);
if l_indxs>1
WTS_indxs = sum(WTS(:,indxs)');
WTS_rest = sum(WTS(:,rest_indxs)');
else
WTS_indxs = WTS(:,indxs)';
WTS_rest = sum(WTS(:,rest_indxs)');
end

DIVS = zeros(pnts,5);
Xs = zeros(pnts,5);

for i = indxs
DIVS(:,i) = WTS_indxs';
Xs(:,i) = sum_indxs.*WTS(:,i)./DIVS(:,i);
end
for i = rest_indxs
DIVS(:,i) = WTS_rest';
Xs(:,i) = sum_rest.*WTS(:,i)./DIVS(:,i);
end

M = [2.447      0.646       0.276       0
    3.39900111  0           0.625201678 0
    0           0.787283622 0.027251651 0.227540212
    0           0.133156    0           0.882699
    0           0.577563249 0.016007835 0.089250687];
%   H2O           SiO2        Na2O        Al2O3

Parts = Xs*M;
Ps = [Parts(:,2)./Parts(:,4) Parts(:,3)./Parts(:,4) Parts(:,1)./Parts(:,3)];

%Water filter
water_low = 50;
water_high = 95;
Q = find(Parts(:,1)<water_high & Parts(:,1)>water_low);
```

```
%P filters
P1_low = 2.30;
P1_high = 3.20;
P2_low = 0.90;
P2_high = 1.30;
P3_low = 0.0;
P3_high = 10.0;

% Qs
Q1 = find(Ps(Q,1)>P1_low & Ps(Q,1)<P1_high & Ps(Q,2)>P2_low & Ps(Q,2)<P2_high &
Ps(Q,3)>P3_low & Ps(Q,3)<P3_high);
Q2 = Q(Q1);
X = Ps(Q2,1);
Y = Ps(Q2,2);
Z = Ps(Q2,3);
```

The calculation is repeated and the results stored by the following command.

```
fileName = 'results.txt';
repetitions_nr = 10;
fileID = fopen(fileName,'at');
fprintf(fileID,'%6s %12s %12s %12s %12s %12s %12s %12s %12s %12s %12s
%12s\n','P1','P2','P3','waterglass','NaOH50','ash','bauxite','slag','H2O','SiO2
','Na2O','Al2O3');
fclose(fileID);
for j=1:repetitions_nr
Composition_calculation_loop
fileID = fopen(fileName,'at');
for i=1:length(Q2)
fprintf(fileID,'%6.2f %12.2f %12.2f %12.2f %12.2f %12.2f %12.2f %12.2f %12.2f
%12.2f %12.2f %12.2f\n',interiorPoints(i,:),Xs(Q2(i),:),Parts(Q2(i),:));
end
fclose(fileID);
end
```

The result of the calculations can be also transferred into various figures to visualize the data (see Figures 28 to 33). The source files for creating diagrams representing the ratio of solid components in the coordinate system are shown below.

```
load results.txt;
x=results (:,6);
y= results (:,7);
z= results (:,8);

figure;
scatter3(x, y, z, 2, x, 'filled');
xlabel('Ash');ylabel('Bauxite');zlabel('Slag');

figure;
trisurf(hullFacets,DT.X(:,1),DT.X(:,2),DT.X(:,3),'FaceColor','b')
xlabel('Ash');ylabel('Bauxite');zlabel('Slag');
title('Convex hull');
```

The Convex hulls in Figures 29, 31 and 33 were created by overlapping the spaces bounded by marginal points by flat planes to better show the 3D space shape of the data set and its boundaries in planar pictures as it is otherwise not very clear without rotating the structure.

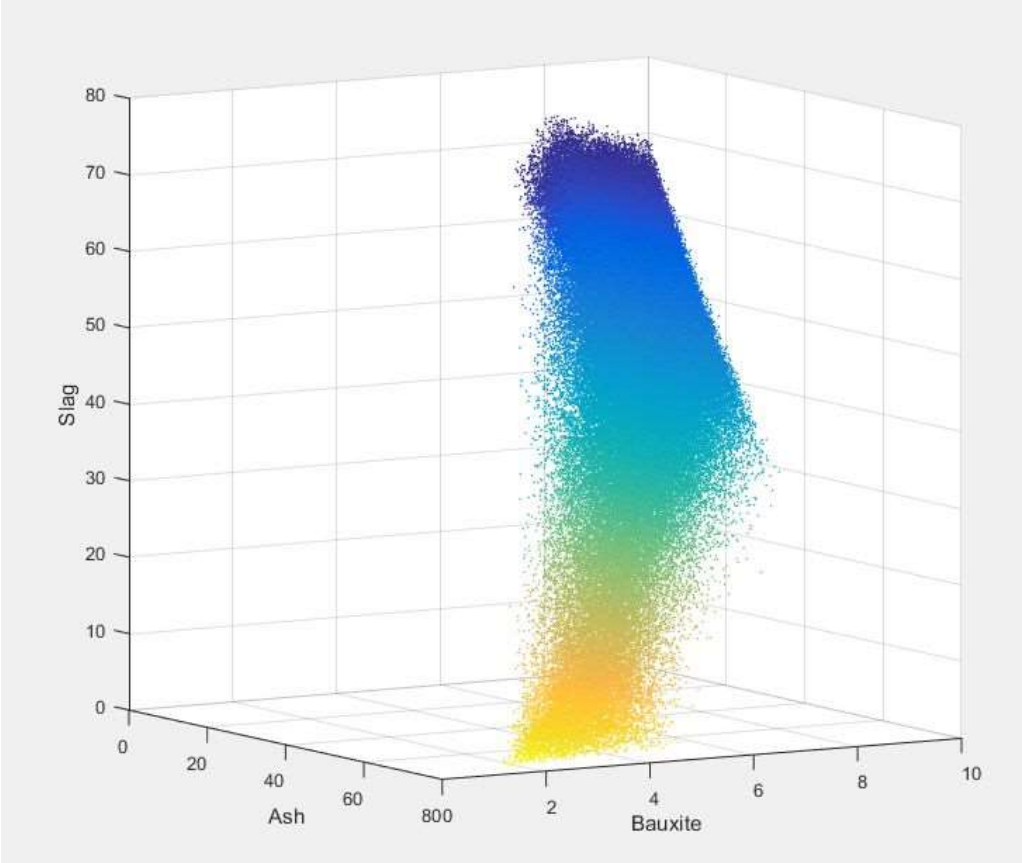

Figure 28: *The MATLAB-based compositions illustrated in 3D coordinate system.*

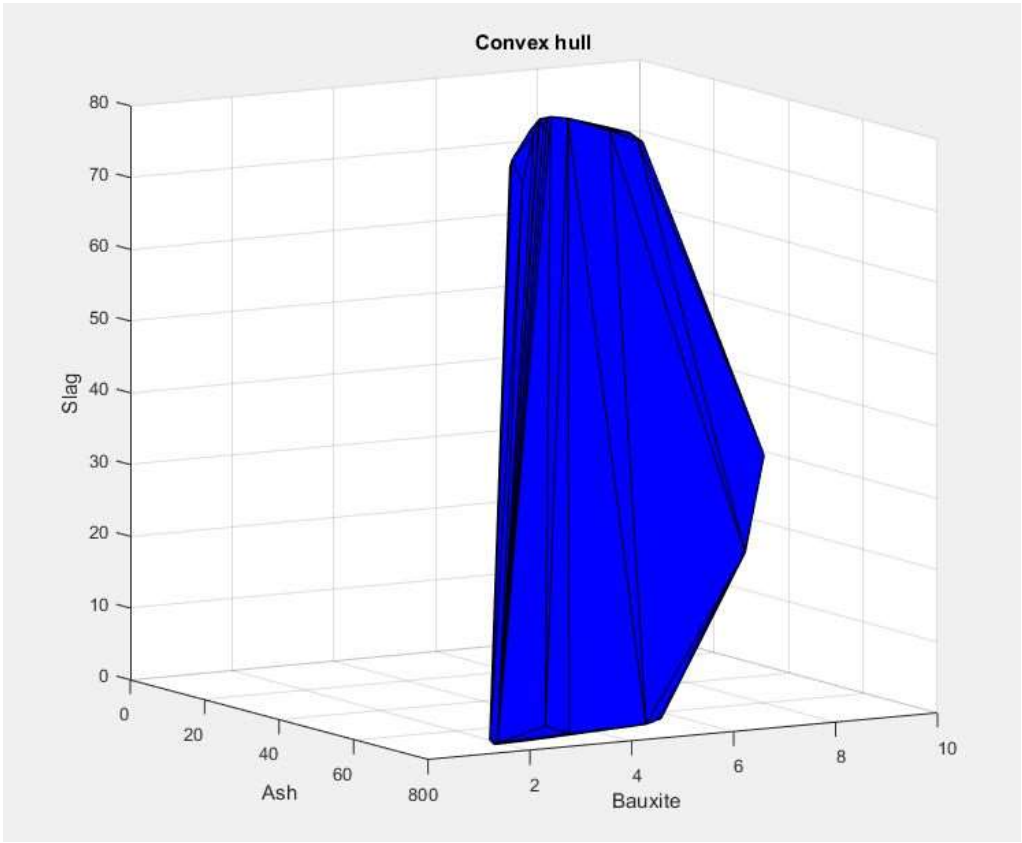

Figure 29: *Convex hull of the set in Fig.28 view on the coordinate system.*

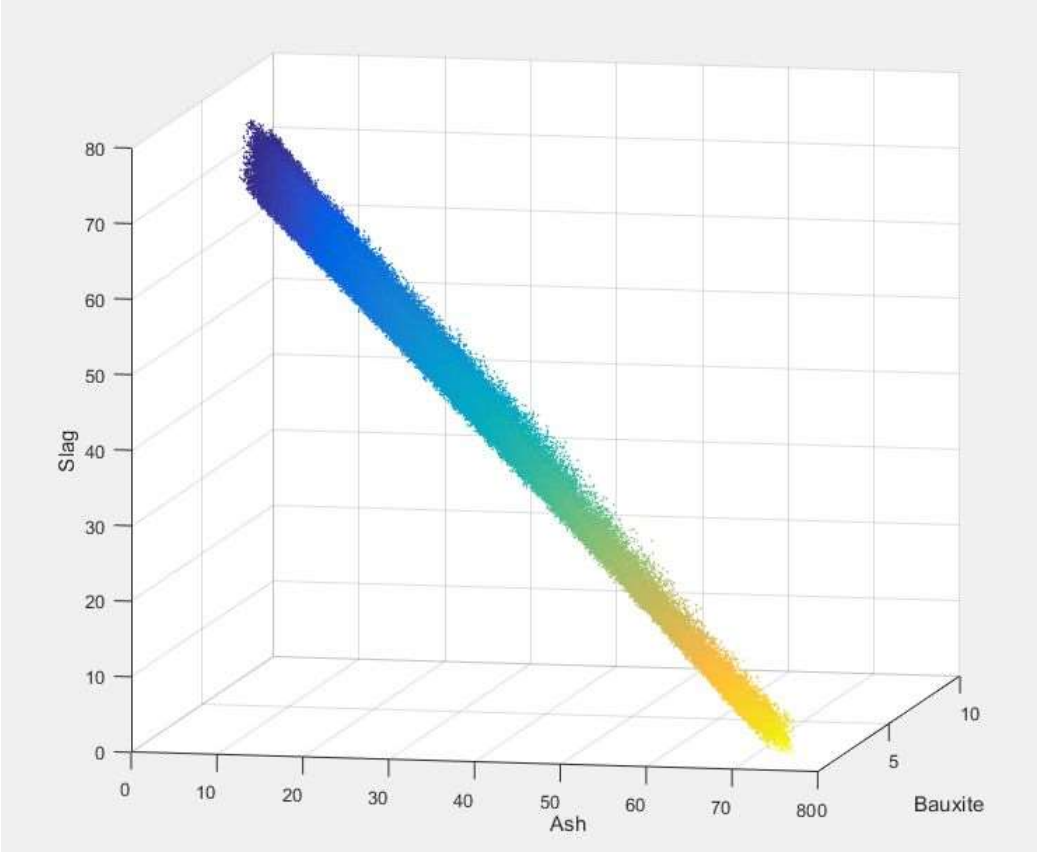

Figure 30: *The MATLAB-based compositions illustrated in 3D coordinate system.*

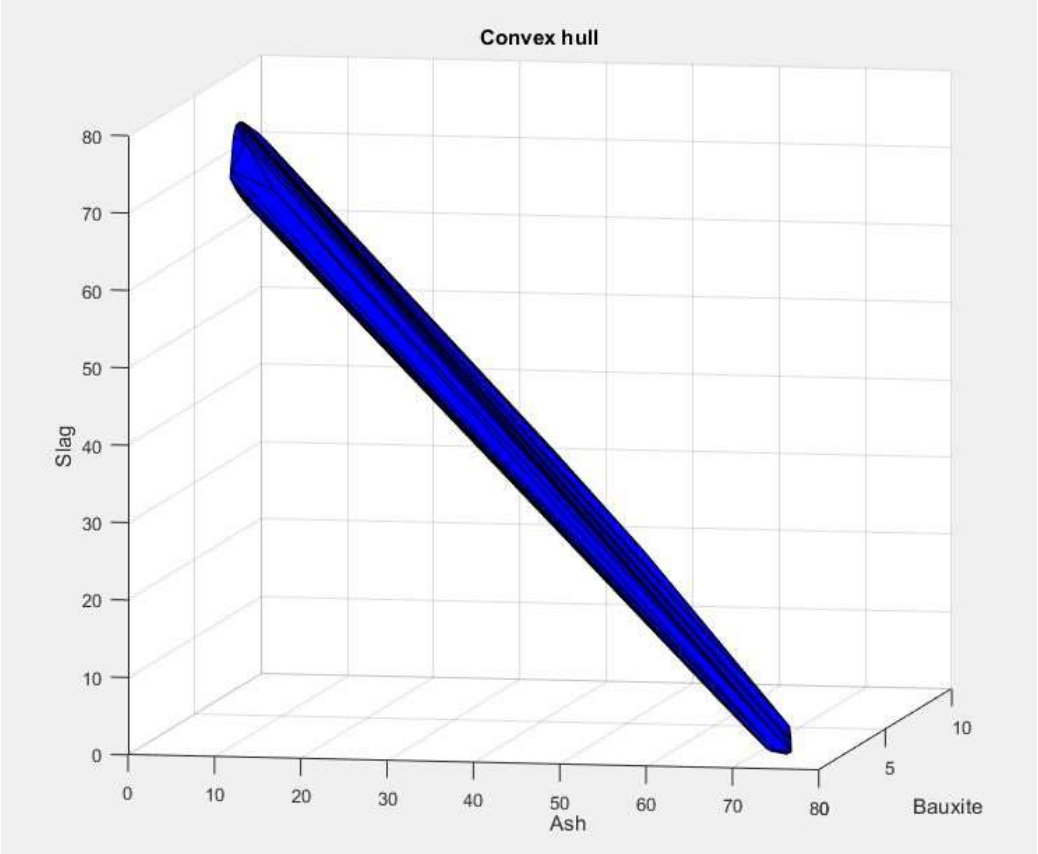

Figure 31: *Convex hull of the set in Fig.30 view on the coordinate system.*

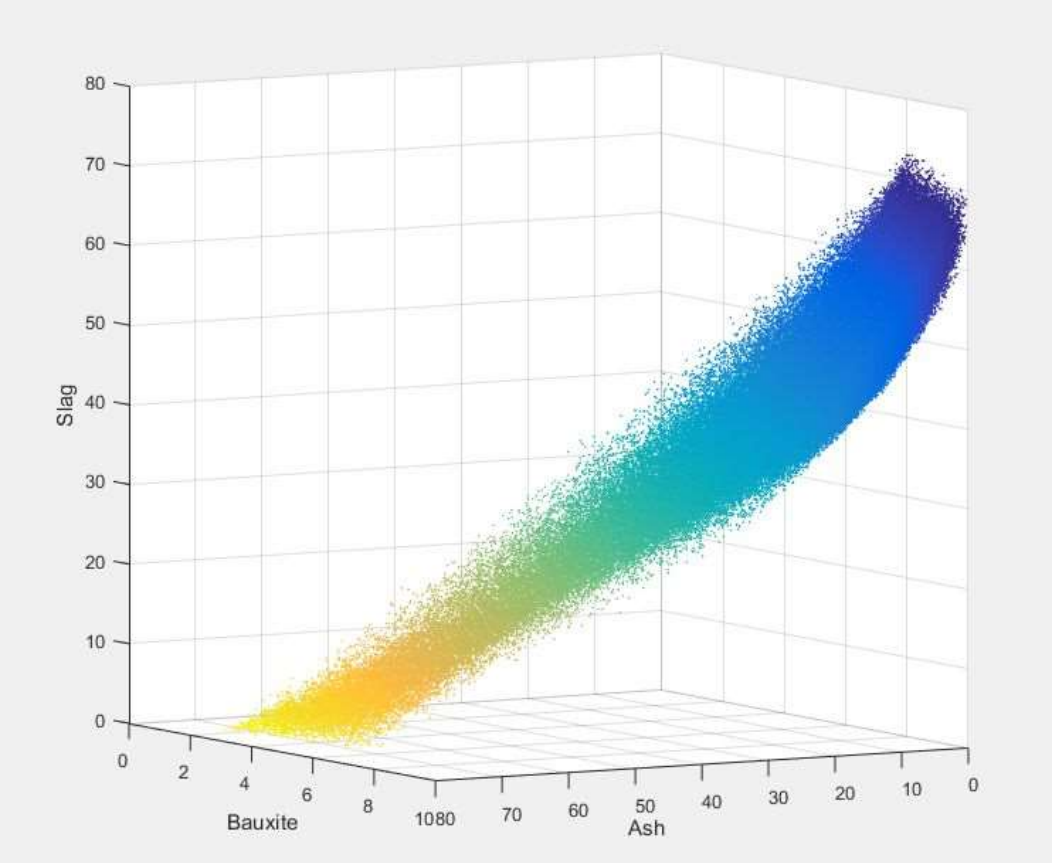

Figure 32: *The MATLAB-based compositions illustrated in 3D coordinate system.*

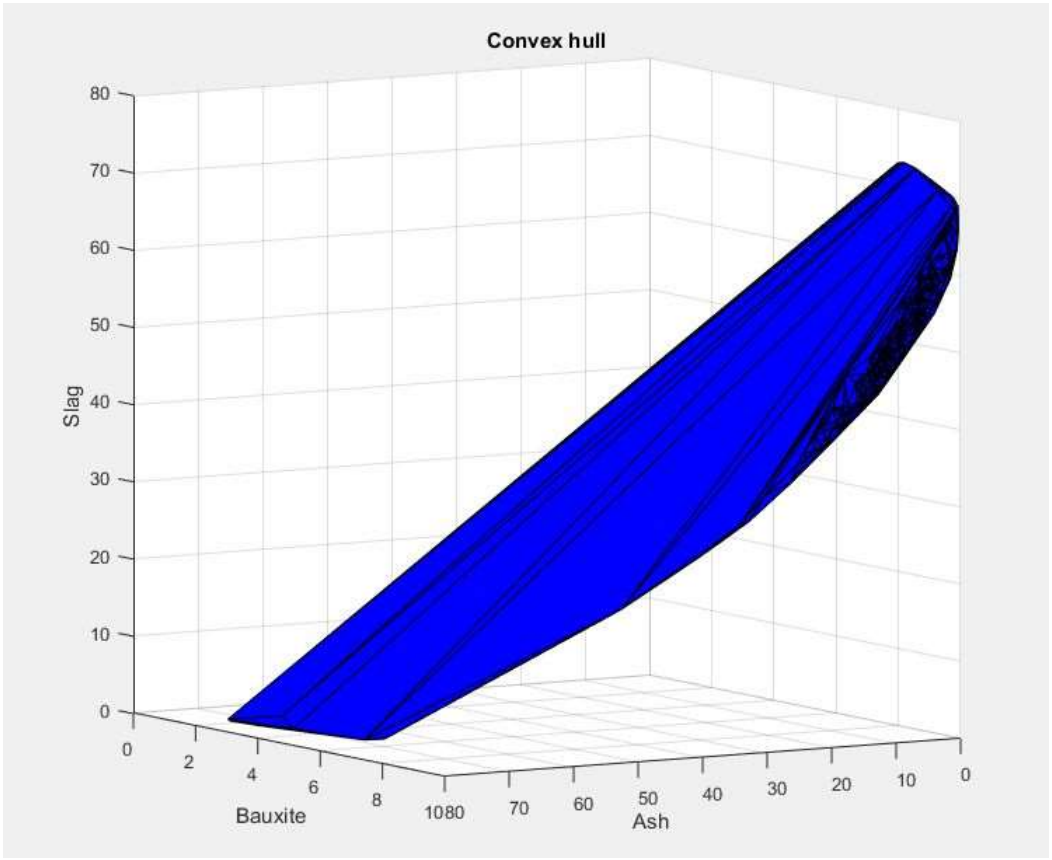

Figure 33: *Convex hull of the set in Fig.32 view on the coordinate system.*

5.4 MIXTURES COMPOSITIONS

The MATLAB raw data containing over 70,000 results was gradually eliminated (mostly for near-duplicity or too high water content) and cropped but what remained was still slightly below half of the original dataset. Because the parameter P3 alone (as only an oxides ratio) did not sufficiently characterized the amount of water in terms of mixture consistency, water to solid ingredients ratio (equivalent to water/cement 'w/c' ratio in the concrete practice; labelled w/s in the tables and diagrams) had to be taken into account as well. During the subsequent searching 23 compositions were chosen that has the P1 and P2 values located across the whole intended ranges and at the same time differ in composition one from another. This way it was ensured that the following Table 11 sorted by any P parameter or any mixture component will cover the whole range of possible values of that particular parameter/component with certain distances although some of them in particular order may seem too close to each other. For example in the order below the table is sorted by fly ash content and it can be seen that the first two values are a bit too close, but the composition 1 and 2 have the ideal spacing in terms of sorting by blast furnace slag and also differ largely in P1 where they are located nearly on the opposite sides of the range. This way the required amount of mixtures was minimized yet any trend in results should be traceable and recognizable simply by sorting the results in the order corresponding to order of the desired parameter or component quantity.

Table 11: MATLAB-based compositions chosen for experiments.

#	P1 (SiO_2/Al_2O_3)	P2 (Na_2O/Al_2O_3)	P3 (H_2O/Na_2O)	Glass	NaOH	Ash	Baux.	Slag	w/s
1	2.70	1.09	5.11	0.48	23.73	0.25	9.98	65.56	0.195
2	3.17	0.92	4.95	0.28	18.24	0.34	8.14	73.00	0.139
3	3.18	1.31	5.15	1.38	24.99	6.14	7.13	60.35	0.216
4	3.04	0.98	5.50	7.57	18.33	9.79	8.95	55.35	0.197
5	2.56	1.00	5.12	1.27	24.04	14.81	9.99	49.89	0.205
6	3.07	1.00	5.42	7.00	19.72	20.13	7.80	45.35	0.207
7	3.17	1.31	5.14	1.69	26.44	20.37	5.96	45.54	0.236
8	2.68	0.91	5.54	9.03	19.91	26.31	10.00	34.75	0.228
9	2.52	0.98	5.29	4.69	24.19	26.68	10.00	34.44	0.237
10	3.16	1.12	5.17	3.22	23.32	26.77	6.02	40.68	0.214
11	3.08	1.06	5.21	4.30	22.86	33.27	6.10	33.47	0.218
12	3.19	0.96	5.12	3.55	20.46	33.53	5.62	36.83	0.186
13	3.20	1.08	5.01	1.43	23.94	39.16	4.58	30.90	0.205
14	2.90	0.95	5.36	7.21	21.10	39.55	7.25	24.89	0225
15	2.35	0.90	5.15	2.94	25.79	44.54	9.96	16.77	0.240
16	3.10	0.90	5.62	11.95	17.81	45.38	6.49	18.36	0.230
17	3.16	1.05	5.09	3.16	23.86	48.72	4.24	20.02	0.219
18	3.18	1.07	4.98	1.30	25.48	56.54	3.12	13.57	0.221
19	2.99	0.90	5.31	7.57	21.01	59.05	5.34	7.04	0.227
20	2.76	0.95	5.12	3.67	24.99	59.65	6.01	5.68	0.237
21	2.44	0.90	5.01	1.23	27.06	60.64	7.89	3.18	0.239
22	2.79	0.90	5.05	3.13	24.17	63.95	5.52	3.24	0.223
23	3.20	0.93	4.83	0.61	23.72	73.24	1.84	0.60	0.196

Note: *The blue lines were added later as complementary values of parameters as close as possible to the lines with highlighted w/s which were still overly wet for the mold pressing and displaced liquids under the pressure. The line with red highlighted w/s does not have a suitable dryer substitute in the dataset.*

Besides the mixtures obtained by MATLAB calculations also pure FA and BFS mixture series were prepared using only sodium hydroxide as an activator (see Table 12). Constitution of these mixtures was designed by empirical knowledge obtained until during the experimental work. The doses of activator were set to 6% and 12% of Na_2O with respect to the powder weight. The water to particulate w/s ratio, taking the NaOH inner water (NaOH ~ Na_2O + H_2O) into account, was 0.095 for 6% mixtures and 0.190 for 12% mixtures.

Table 12: Pure two-component fly ash (FA) and slag (S) mixtures compositions.

#	P1 (SiO_2/Al_2O_3)	P2 (Na_2O/Al_2O_3)	P3 (H_2O/Na_2O)	NaOH	Ash	Slag
FA-6	3.46	0.55	4.24	7.74	50	0
FA-12	3.46	0.92	4.73	15.48	50	0
S-6	6.47	1.26	4.67	7.74	0	50
S-12	6.47	2.35	5.02	15.48	0	50

The other question examined in connection with the previous one was the extent of activator concentration influence on the resulting strength of the AAM. It was examined due to observation of increased friability of prepared FA-6 samples. For the purpose the calibration-like set of mixtures was designed with 1% to 6% dose of Na_2O. The water to particulate ratio was set to 0.095 for all the following mixtures (see Table 13).

Table 13: FA and S compositions for investigation of the activator concentration influences.

#	P1 (SiO_2/Al_2O_3)	P2 (Na_2O/Al_2O_3)	P3 (H_2O/Na_2O)	NaOH	Water	Ash	Slag
FA-1	3.46	0.19	12.15	1.29	3.96	50	0
FA-2	3.46	0.26	8.86	2.58	3.17	50	0
FA-3	3.46	0.33	6.97	3.87	2.38	50	0
FA-4	3.46	0.40	5.75	5.16	1.59	50	0
FA-5	3.46	0.47	4.89	6.45	0.80	50	0
FA-6	3.46	0.55	4.24	7.74	0	50	0
S-1	6.47	0.36	16.40	1.29	3.96	0	50
S-2	6.47	0.54	10.92	2.58	3.17	0	50
S-3	6.47	0.72	8.19	3.87	2.38	0	50
S-4	6.47	0.90	6.55	5.16	1.59	0	50
S-5	6.47	1.08	5.45	6.45	0.80	0	50
S-6	6.47	1.26	4.67	7.74	0	0	50

5.5 PREPARATION PROCEDURE

Due to very high viscosity of the mixture the mixing had to be done by planetary centrifugal mixer described above where the solid ingredients (already mixed together in ratio corresponding to the particular composition) were admixed by parts. The mixer was set to 2000 rpm for 3 times 20 seconds with manual mixing between runs. The time may appear too short but the 2000 rpm mix rapidly and first of all further mixing overheats the mixtures so they tend to compact and they also lose part of their workability due to loss of water by evaporation.

The mixture had to be then scattered manually and after weighting the intended amounts were transferred into molds already lined with support pad and flexible washer (described below). The mixtures had to be evenly spread across the mold before the pressing itself was executed on the pressing device with pressure gauge (shown in Figure 34) to achieve the pressure as uniform over the area as possible. The pressing was performed at 1 ton for the barriers 25 mm in diameter which equals to approx. 1.99 kg/mm^2 ~ 19.5 MPa.

Figure 34: *Hydraulic manual press with pressure gauge.*

During the development of this method the flexible washers and pressing support pads were added to improve the mold emptying (see Picture 35). The flexible washers made out of paper also

helped in the removing process because the molding do not stick to the support pads and the washers themselves can be removed without damaging the product or in most cases peel off spontaneously by contortion under the effect of strong alkali on one side and dryer unaffected surface on the other.

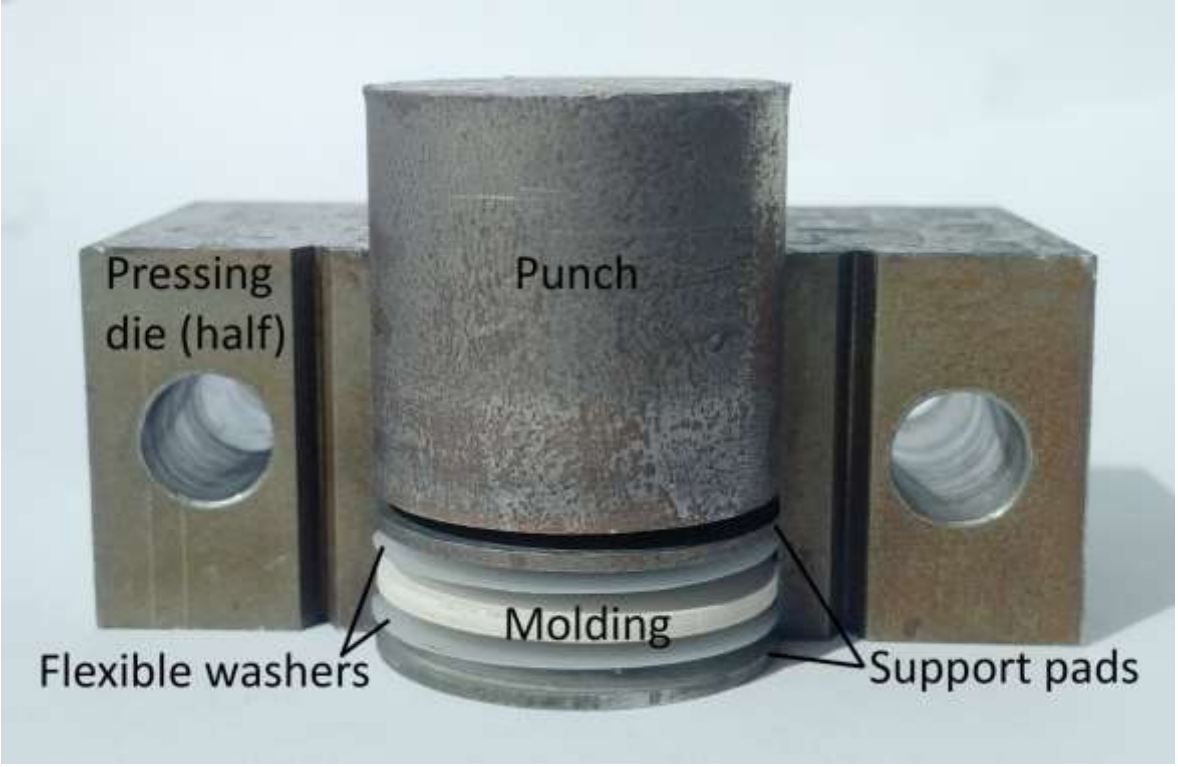

Figure 35: *The exhibition of the molding layout during the 25mm barriers preparation.*

After demolding the barriers were moist cured (closed in a tight box with wet sponge) under 70 °C for 24 hours. Due to research already done on the curing procedure of materials containing alkali activated materials 60-70 °C seem to be optimal temperature (Hardjito et al, 2009). Longer period of time (48h+) was concluded a bit better for the strength of the alkali activated materials, the difference in strength against the 24 hours cured materials was however not striking so it did not justified the increased energy consumption. Therefore for the purpose of this work (trying to keep the consumption of production energy as low as possible) the shortest verified curing time was preferred (Memon et al, 2011; Bakharev, 2005; Van Jaarsveld et al, 2002; Rovnaník, 2010; Hardjito et al, 2004 and 2009).

Some of the bodies made of mixtures containing mostly GGBFS tended to bend or crack during the storage under laboratory conditions which is known phenomenon that happens due to considerable shrinkage of alkali activated slag-based materials (Bilim et Karahan, 2015; Bilim et al., 2013; Sakulich et Bentz, 2013). Therefore, the cured bodies were then stored in a box with increased humidity to maintain the moisture after the curing process which helped to eliminate the issue.

Figure 36: *Examples of 25mm and 50mm barriers, ordinary (left) and experimentally reinforced with short-chopped silanized E-glass fiber roving (right).*

Picture 36 shows examples of ordinary filtration barriers and barriers from the same mixture experimentally reinforced by silanized E-glass fiber roving chopped to 17μm x 3mm. That was hoped to be one of the directions this study was intended to go further and try to improve the strength of the barriers through the reinforcement with glass fibers. The ordinary unsilanized fibers proved to have no adhesion to the alkali activated material so the fibers with silanized surface were hoped to improve the interphase joint. Unfortunately the silanization also sticks the fibers together and they cannot be satisfactorily separated and spread in the mixture evenly even in the planetary mixer. Therefore this branch of the study was abandoned. It cannot be satisfactorily said if the fibers increase the strength but it can be concluded that when used in the order of units of percent they do not influence the porosity of the material.

Figure 37: *Molds and punches manufactured for 25mm and 50mm barriers production and an experimental mold with built-in support for filtration testing post.*

All the molds, punches and supports (Figure 37, 38 and 39) needed for the purpose of this work were designed by the author and produced with his contribution mostly from stainless steel (within the Heat Transfer and Fluid Flow Laboratory) during the work to correspond the porometer and filtration testing panel cell diameters in case of barriers and the regulations of ČSN EN 12390-5 in case of strength testing columns. As well was made the uniaxial tensile strength measuring clamping bracket depicted in Figure 45 that follows the ČSN EN 12390-5 for the 10x10 mm testing columns as the clearance between the lower support is 30 mm, the supports rotate freely and there was also a centering guide included to the design to assure the proper alignment of the elements.

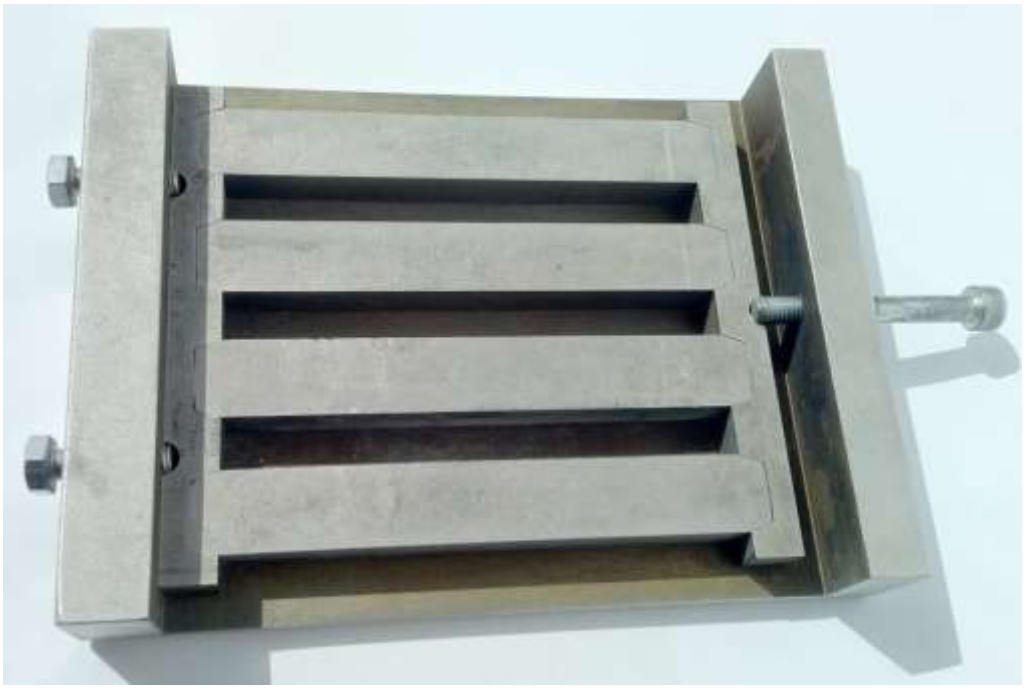

Figure 38: *Horizontal mold manufactured for uniaxial strength testing columns production (column size lxhxw = 100x10x10mm).*

Figure 39: *Experimental vertical mold and punch manufactured for uniaxial strength testing columns production by pressing column size lxhxw = 100x10x10mm.*

There was also a vertical mold manufactured to be tested during the experimental work in order to obtain the testing columns of defined cross-section dimensions prepared under the same pressure as the filter barriers. However, this method was found unsuitable due to dissipation of the pressure by transferring it to the walls of the mold via particles of the mixture. The pressure is gradually dissipated and lower layers of the material in the pressing direction are less and less compressed with the increasing distance from the punch. The outcome is therefore unequally made, even when the walls were treated with various separation coatings, it was almost impossible to demold the columns without damage.

Figure 40: *Example of unsuccessfully made testing columns with pressure dissipation between layers pressed at each other visible due to color-changing phenomena.*

As can be seen in Picture 40 some of the mixtures showed an interesting phenomenon of turning dark green sometimes getting to shades of blue or violet (Figures 41 and 42). Some of them spontaneously but in most cases it was observed only on the pressed bodies particularly in the places exposedto highest pressures (in case of planar barriers spots appeared where lumps of the material were left before the pressing). This phenomenon emerged during first few days or up to 3 weeks from the preparation. The origin of this phenomenon is due to literature connected with the occurrence of S_3^- (trisulphur radical anion) which is a blue chromophore known to be an origin of the blue colour of ultramarine pigment. The green then supposed to be the disulphur radical which is a green chromophore, but also other possibilities cannot be excluded, e.g. transition metals present in slag may associate with ligands from the alkaline solution to form various chromophore complexes (Chaouche et al, 2017). Due to other source the green color may also be caused by sulphide-containing AFm phase which has also intensive green colour (Lothenbach et Gruskovnjak, 2007). The production of these chromophores has to be affected by ambient atmosphere reaction and/or also connected with loss of moisture because the phenomenon never

occurred on the bodies stored in the high humidity boxes and the experimental barrier left to cure in laboratory conditions shown in Figure 43 proves the process was delayed on the bottom surface which is not exposed to drying and ambient atmosphere as much as the top surface which has the coloration in multiple spots. The figure shows that after a week only the side exposed to air shows the signs of blue-green coloration (as well as fading to white in unaffected areas by losing the moisture and efflorescence). The most colored spots formed in the areas where there were lumps of material before pressing. These areas have higher level of compaction and turn green first or as sole like in this case where the coloration did not spread much further with time.

Figure 41: *A spread of mixture extremely manifesting the color-changing phenomena after leaving it for 5 weeks in laboratory conditions.*

Figure 42: *A barrier and a leftover material showing the color-changing phenomena after leaving it for 3 weeks in laboratory conditions.*

Samples of the material from Figure 42 were subjected to XRD analysis and compared to XRD results of the same material taken from the interior of the body that did not colored yet. The analysis had shown no differences. It can be therefore concluded that the color is not cause by occurrence of different mineralogical phases and the explanation most likely correlate with the literature based conclusions listed above.

Figure 43: *Two identical mixture filtration barriers after 1 week in laboratory conditions, bottom surface (left) to top surface (right) comparison.*

5.6 MECHANICAL TESTING

Geopolymers/AAMs are often mechanically tested by penetration tests. However mostly the materials are produced for utilization in construction applications so the hardness is of interest. Because this work deals with these materials as filtering media the product requirements are different and therefore the usual approach was abandoned and the bending strength testing was used instead. The strength of the materials was tested in four-point bending test on testing columns 10x10 mm in cross section. This test was preferred over the three-point bending because it is more appropriate for non-homogenous materials as it spreads the stress to a larger region of the testing body. Because there are no official standard testing methods for geopolymers/AAMs available the methodology used in this work is based on ČSN EN 12390-5 which is the Czech version of the European concrete testing standard EN 12390-5:2009 "*Testing hardened concrete. Flexural strength of test specimens"* (testing scheme – Figure 44).

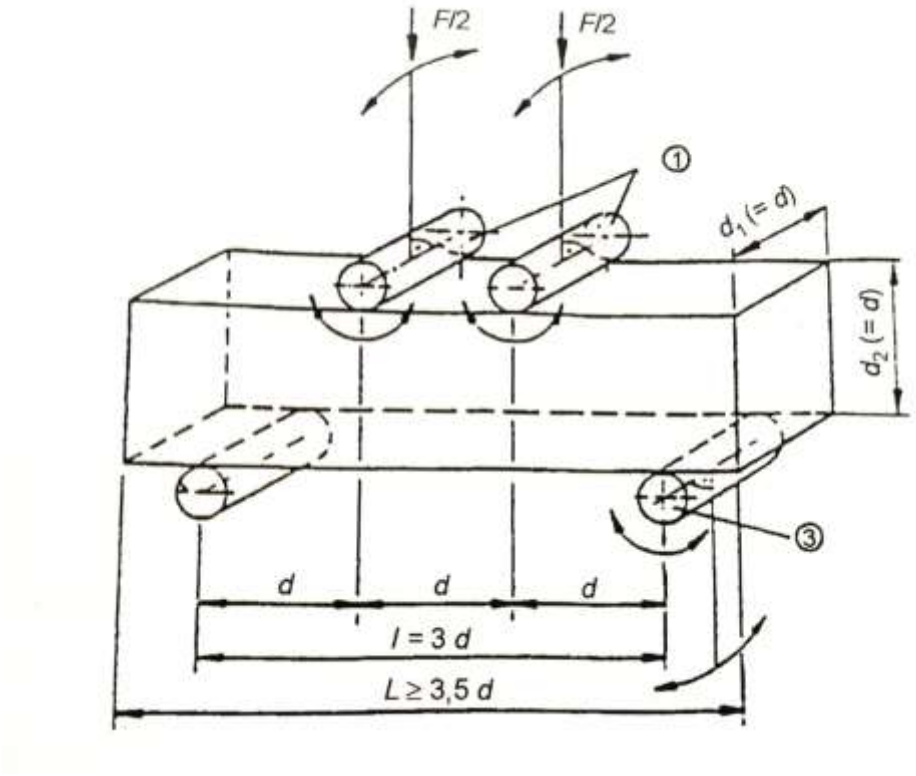

Figure 44: *Uniaxial tensile strength testing layout scheme with two bodies loading (ČSN EN 12390-5).*

The uniaxial tensile strength is defines as: $f_{ct} = \dfrac{F \cdot l}{d_1 \cdot d_2^2}$

where f_{ct} is the uniaxial tensile strength, in MPa (N/mm^2);
F maximal loading strain, in N;
l distance between supporting rollers, in mm;
d_1 and d_2 dimensions of the cross section of the testing column, in mm.

Due to the requirements of the technical standard new testing assembly (Figure 45) was a designed and produced to fit our LaborTech tensile testing machine (Figure 46).

Figure 45: *Uniaxial tensile strength measuring clamping bracket designed and manufactured to follow the ČSN EN 12390-5 rules.*

Figure 46: *Strength-testing of the prepared AAM columns prepared 100 mm in length to assure 3 measurements from each body (broken in halves and those tested separately).*

Table 14: Uniaxial tensile strength measurements results in context with mixtures compositions and parameters, each result averaged from 4 measurements.

#	f_{ct} (MPa)	Standard deviation	P1 (SiO_2/Al_2O_3)	P2 (Na_2O/Al_2O_3)	P3 (H_2O/Na_2O)	Ash	Baux.	Slag	w/s
1	**4.84**	**0.39**	2.70	1.09	5.11	0.25	9.98	65.56	0.195
2	**6.88**	**0.41**	3.17	0.92	4.95	0.34	8.14	73.00	0.139
3	**7.31**	**0.40**	3.18	1.31	5.15	6.14	7.13	60.35	0.216
4	**6.95**	**0.35**	3.04	0.98	5.50	9.79	8.95	55.35	0.197
5	**4.92**	**0.28**	2.56	1.00	5.12	14.81	9.99	49.89	0.205
6	**5.59**	**0.28**	3.07	1.00	5.42	20.13	7.80	45.35	0.207
7	**3.49**	**0.26**	3.17	1.31	5.14	20.37	5.96	45.54	0.236
8	**4.26**	**0.17**	2.68	0.91	5.54	26.31	10.00	34.75	0.228
9	**5.30**	**0.36**	2.52	0.98	5.29	26.68	10.00	34.44	0.237
10	**6.02**	**0.23**	3.16	1.12	5.17	26.77	6.02	40.68	0.214
11	**4.86**	**0.49**	3.08	1.06	5.21	33.27	6.10	33.47	0.218
12	**7.69**	**0.57**	3.19	0.96	5.12	33.53	5.62	36.83	0.186
13	**6.34**	**0.22**	3.20	1.08	5.01	39.16	4.58	30.90	0.205
14	**5.72**	**0.11**	2.90	0.95	5.36	39.55	7.25	24.89	0225
15	**3.67**	**0.41**	2.35	0.90	5.15	44.54	9.96	16.77	0.240
16	**6.23**	**0.10**	3.10	0.90	5.62	45.38	6.49	18.36	0.230
17	**6.00**	**0.25**	3.16	1.05	5.09	48.72	4.24	20.02	0.219
18	**6.61**	**0.39**	3.18	1.07	4.98	56.54	3.12	13.57	0.221
19	**6.47**	**0.20**	2.99	0.90	5.31	59.05	5.34	7.04	0.227
20	**4.41**	**0.46**	2.76	0.95	5.12	59.65	6.01	5.68	0.237
21	**2.53**	**0.33**	2.44	0.90	5.01	60.64	7.89	3.18	0.239
22	**5.48**	**0.24**	2.79	0.90	5.05	63.95	5.52	3.24	0.223
23	**5.64**	**0.38**	3.20	0.93	4.83	73.24	1.84	0.60	0.196

Table 14 shows all the MATLAB based mixtures' uniaxial tensile strength measurement results and their standard deviations altogether with the mixture parameters and compositions. Mixture 12 which is one of the driest (lowest w/s parameter) had achieved a maximal strength, namely 7.69 ± 0.57 MPa and mixture 21, which is the overall wettest one (highest w/s parameter), had the lowest overall strength of 2.53 ± 0.33 MPa. Composition number 3 that also exceeded 7 Mpa in uniaxial tensile strength testing has a majority of BFS in composition and contains more liquids than number 12.

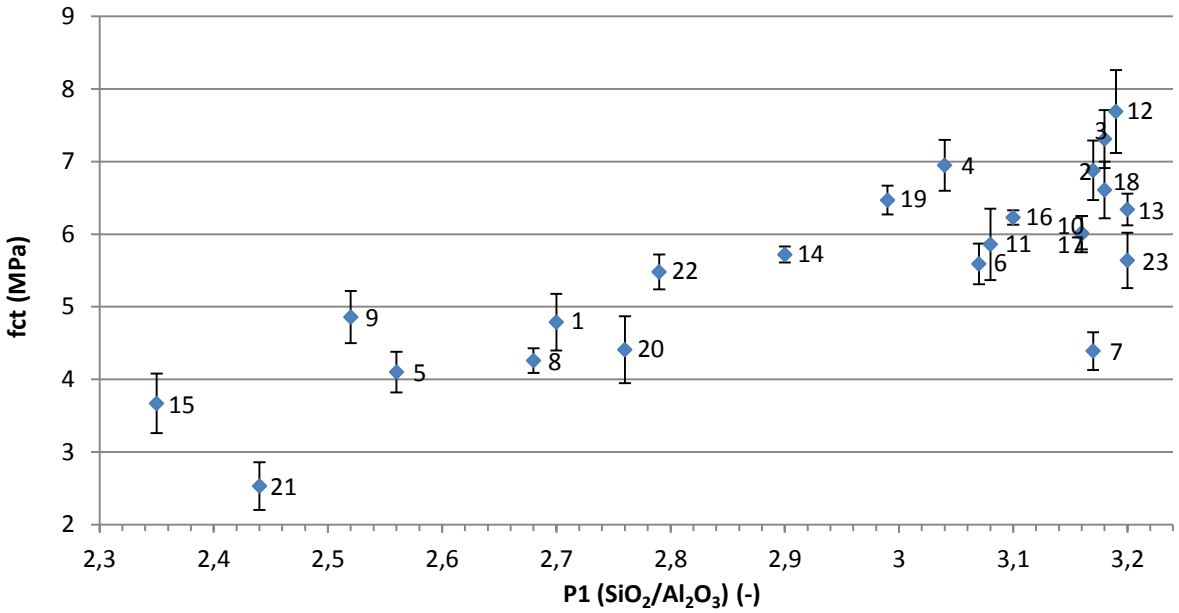

Figure 47: *Parameter P1 to uniaxial tensile strength dependence diagram.*

The tensile strength on P1 dependence in Figure 47 confirms the premise that within the given range the strength of mixtures increases with increasing P1. Mixture 7 shows the biggest deviation from the main trend, but the P2 to *fct* dependence diagram offers an explanation in very high P2 ratio where sodium can break down the polymer network by terminating Si–O–Na chains. This phenomenon is most likely influenced by water content because mixture 3 that has analogical values in all parameters but a different components ratio and much lower w/s ratio achieved very good strength. The lowest strength of the mixture 21 had to be caused by low P1 in combination with very high water content.

P2 to tensile strength dependence in Figure 48 does seem to show trend only in the lower bound of the cluster of values which tend to increase with P2.

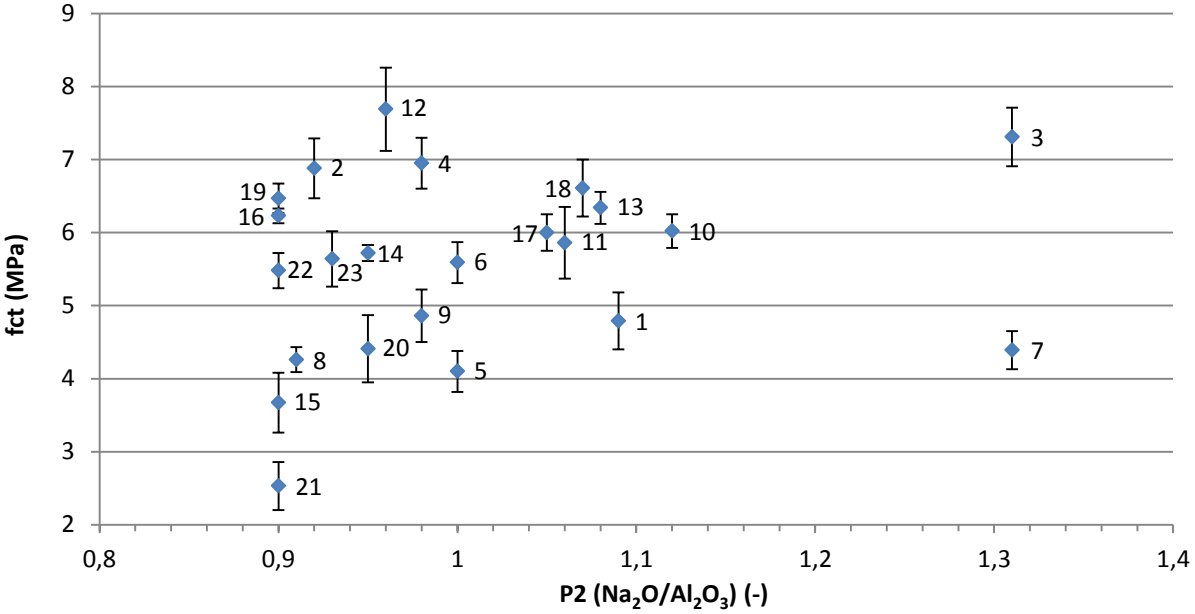

Figure 48: *Parameter P2 to uniaxial tensile strength dependence diagram.*

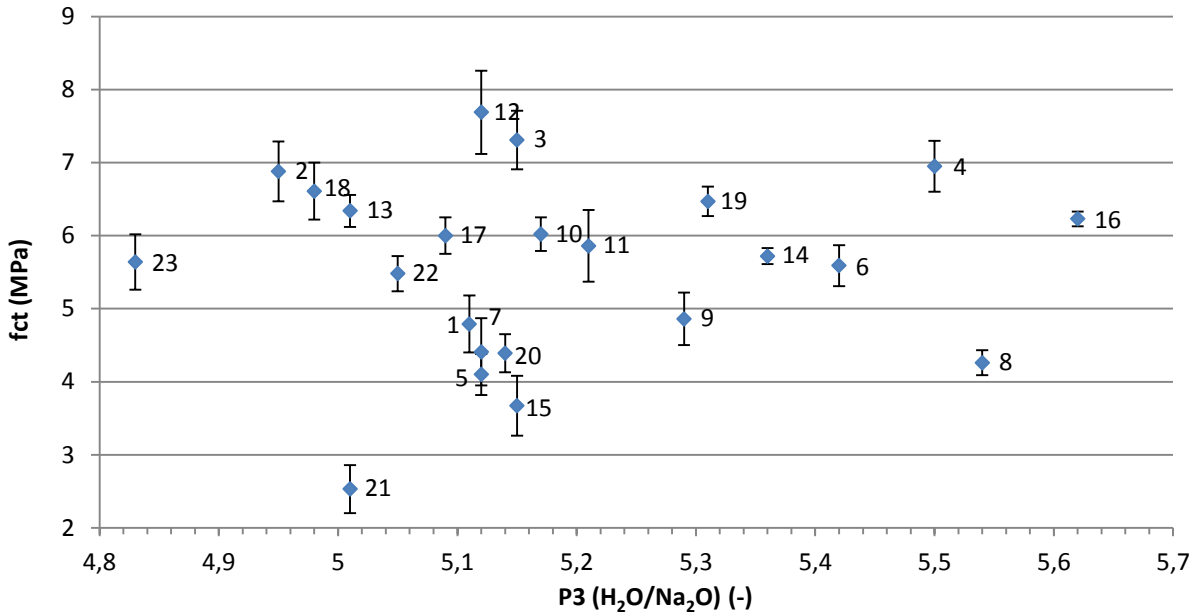

Figure 49: *Parameter P3 to uniaxial tensile strength dependence diagram.*

Because the P3 was found insufficient during the preparation process to characterize the consistency of the mixtures it was supplied by w/s coefficient, here are both of them in diagrams dependent to the uniaxial tensile strength (Figure 49 and 50). Diagram above this paragraph shows the decrease of the strength to the H_2O/Na_2O ratio of approximately 5.15 and then the *fct* increases from this minimum.

In the diagram below (Figure 50) the strength is slightly decreasing with increasing w/s. The greatest deviation of mixtures 1 and 5 can be explained by their very low P1 (slightly over 2.5) that makes them less compact.

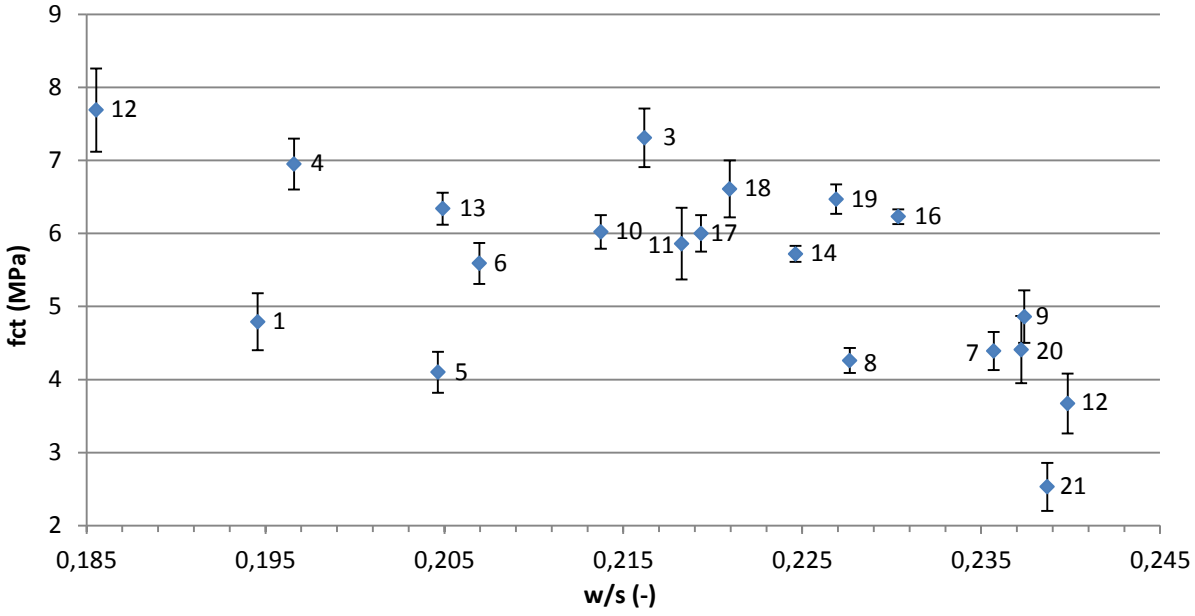

Figure 50: *Water to solid ratio to uniaxial tensile strength dependence diagram.*

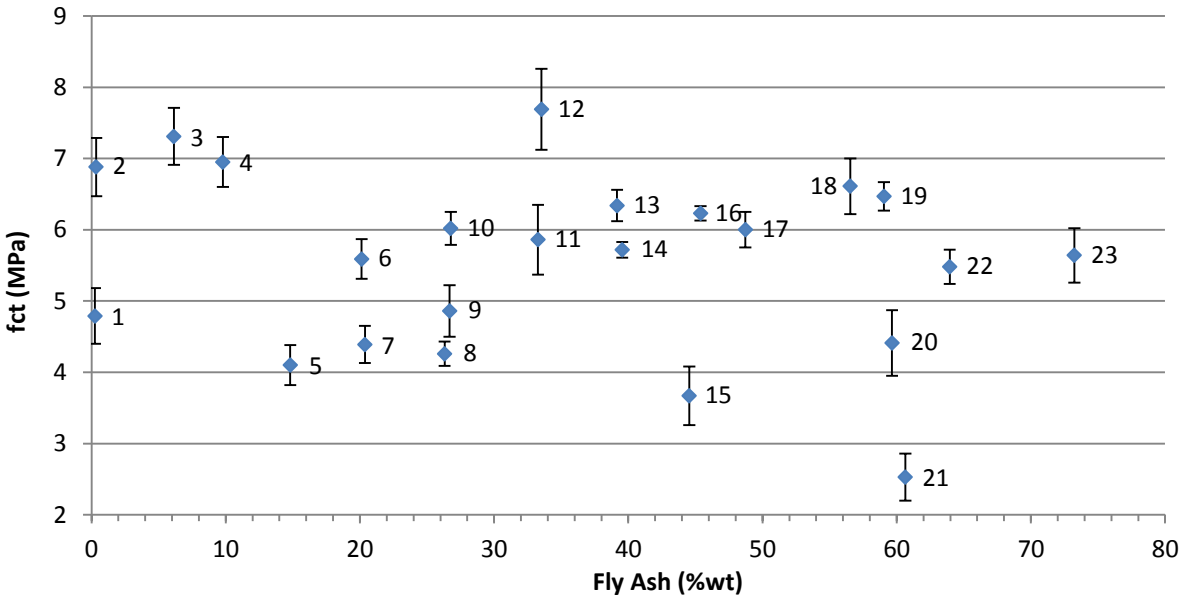

Figure 51: *Fly ash content to uniaxial tensile strength dependence diagram.*

Fly ash and slag content to tensile strength dependencies (Figure 51 and 52) do not show any trend whatsoever if we do not take into account that mixtures 15, 20 and 21 has the highest water content – after these are neglected it can be seen a slight tendency of the tensile strength to increase with increasing fly ash content and decrease with increasing slag content. However, this appearance does not match the tensile strength results of the two-component mixtures that are show in the Figure 53. Pure activated slag clearly achieved greater uniaxial tensile strengths in all mixtures of the testing series although for pure 50% NaOH utilization it greatly depends on the P2 value. In Table 15 parameter P2 increases to 0.92 for FA-12 and the strength increases in the same manner. For the slag series however, the strength maximum belongs to mixture S-5 which only slightly exceeds unity, but from there on it decreases as the Na_2O/Al_2O_3 ratio significantly increases.

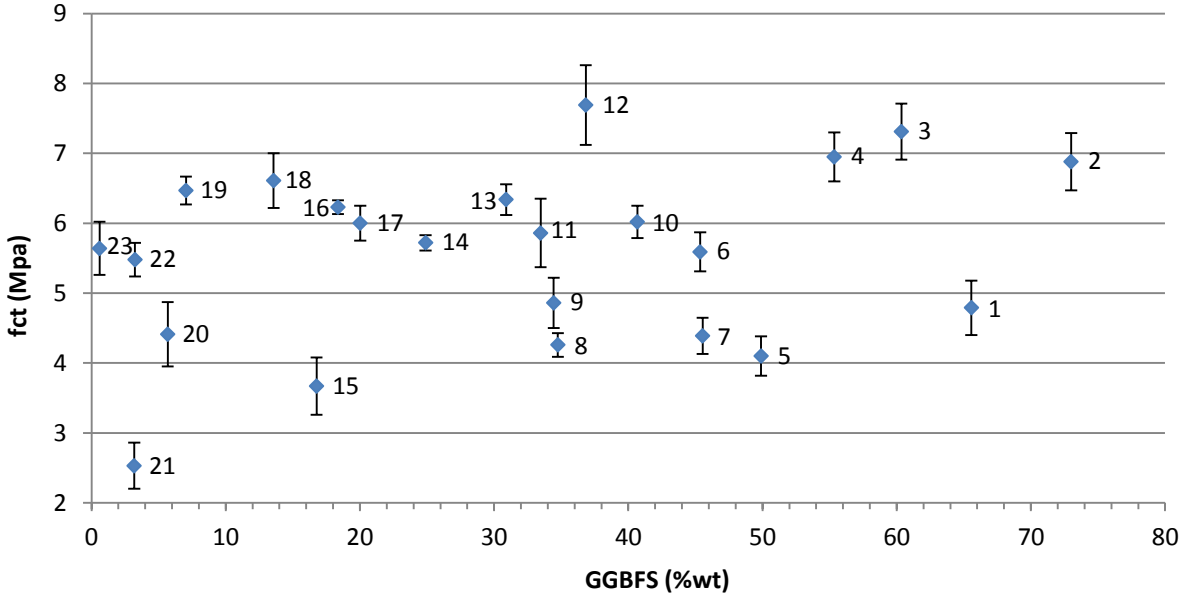

Figure 52: *Blast furnace slag content to uniaxial tensile strength dependence diagram.*

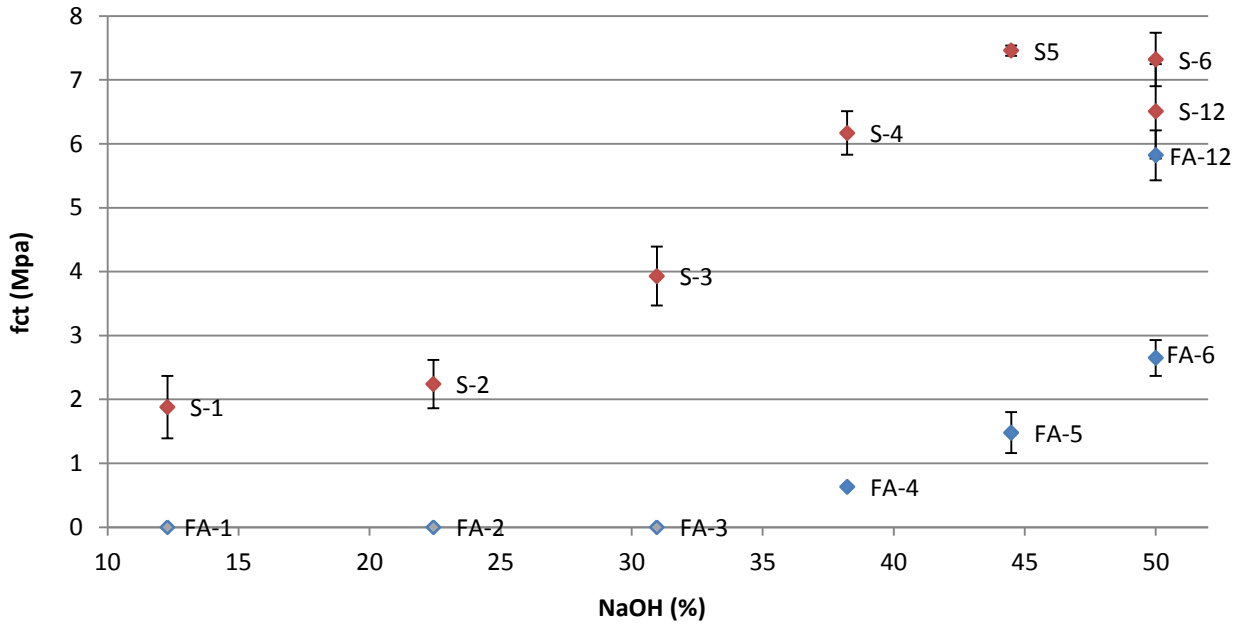

Figure 53: *Alkali activator (sodium hydroxide) concentration to uniaxial tensile strength dependence diagram of the fly ash and GGBFS based mixtures series.*

The FA-1, FA-2 and FA-3 mixtures in figure above were marked grey because they were not measured for uniaxial tensile strength as they could not be demolded without breakage.

In general it can be concluded that the strength parameters favor more GGBFS for the production of porous media. It is, however, questionable how much the particle morphology does influence the strength of the samples. GGBFS particles are angular compared to round shaped FA particles. If the GGBFS particles are in contact with each other along their edges or walls they have of course greater contact area although continuous porosity can be reduced.

Table 15: Uniaxial tensile strength results of the fly ash and GGBFS based mixtures in context with compositions and parameters, each result averaged from 4 measurements.

#	Fct (MPa)	stand. deviation	P1 (SiO_2/Al_2O_3)	P2 (Na_2O/Al_2O_3)	P3 (H_2O/Na_2O)	NaOH	H_2O
FA-1	**0.00**	**0.00**	3.46	0.19	12.15	1.29	3.96
FA-2	**0.49**	**0.17**	3.46	0.26	8.86	2.58	3.17
FA-3	**0.81**	**0.35**	3.46	0.33	6.97	3.87	2.38
FA-4	**1.45**	**0.56**	3.46	0.40	5.75	5.16	1.59
FA-5	**2.97**	**0.32**	3.46	0.47	4.89	6.45	0.80
FA-6	**3.65**	**0.28**	3.46	0.55	4.24	7.74	0
FA-12	**6.82**	**0.39**	3,46	0,92	4,73	15.48	0
S-1	**1.88**	**0.49**	6.47	0.36	16.40	1.29	3.96
S-2	**2.24**	**0.38**	6.47	0.54	10.92	2.58	3.17
S-3	**3.93**	**0.46**	6.47	0.72	8.19	3.87	2.38
S-4	**5.37**	**0.34**	6.47	0.90	6.55	5.16	1.59
S-5	**7.46**	**0.08**	6.47	1.08	5.45	6.45	0.80
S-6	**7.32**	**0.42**	6.47	1.26	4.67	7.74	0
S-12	**4.51**	**0.54**	6,47	2,35	5,02	15.48	0

Note 1: *The bending strength measurements presented above were performed after 7 days. Few samples were however tested in another laboratory on 3-point bending after approximately 3 months after production and the highest result which was of S-6 mixture was 21.72 ± 2.45 MPa.*

Note 2: *The attempts to prepare pressed testing columns of defined cross-section by vertical pressing lead the author to another idea. To compare how pressing influences the strength of the AAM bodies 50mm barriers were pressed out under 4tons pressure ~ 78MPa (multiplying the pressure to apply by the difference in area compared to 25mm barriers). Those were after curing grinded and sanded to the shape of testing columns. Due to trimming them manually each column was of course a bit different and due to pressing process their width was not equal to their height (as instructed in ČSN EN 12390-5), but each of them was measured and the size added to the software of the testing machine which can relate the measured values to the specimen dimensions and adjust the results accordingly. The results were although not very convincing and therefore are not reported in this work. The overall summary of the obtained results would be that pressing affects the strength of these materials by -14% to +25% compared to the results of the testing columns prepared by manual compaction taken as a 100% standard. The negative values could be caused by structural defects as well as local disruptions cause by manual trimming of the samples.*

Note 3: *There was also another experimental strength tests carried out with five samples of AAM testing columns left for one year under demineralized water which was regularly replaced in order remove alkaline residues. The pH controlled by the litmus papers showed alkalinity even after a year of leaching. The explanation was found in literature after further investigation – see Figure 54.*

The uniaxial tensile strength tests revealed that the columns exposed to water leaching lost 26-52% of the strength compared to those left for one year in laboratory conditions (approx. 35% relative humidity and 25°C) taken as a 100% standard. This decrease in strength results could be most likely caused by the fact that excessive NaOH or its carbonation products in the unleached samples are present in a solid form and fill some of the pores so they inevitably has to influence the overall strength of the material.

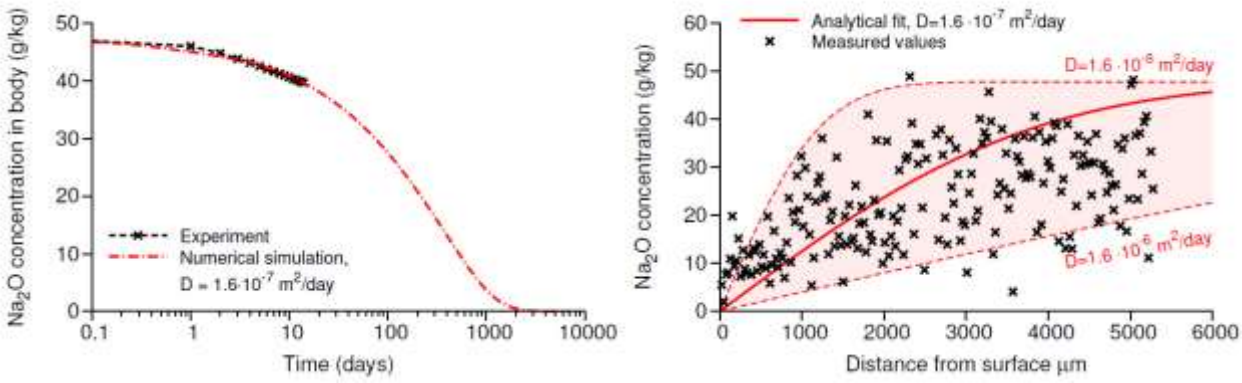

Figure 54: *Concentrations of Na_2O in the alkali-activated fly ash paste specimens. The prism 40x40x160mm was leached in regularly replaced deionized water.(Hlaváček, 2014)*

5.7 POROSITY

The figures below show CFP (Capillary Flow Porosimetry) measurements with different ranges of pores contained in the filter barriers. The premise was that because the granulometry of the input ingredients is always the same, only in different ratios, the porosity results should depend greatly on the content of alkali activator that dissolves matter and then the resulting amount of forming N-A-S-H gel creates necks of various thicknesses between the particles. This assumption was to certain extent verified.

Impact of GGBFS classification on pore structure of the prepared membranes studied using MIP is shown in Figure 55. Both unclassified and classified GGBFS had significant intrusions in the range of pore diameter between 0.2 and 5–10 μm. While the curves of unclassified GGBFS were flat with very diffuse maximum in the range of 0.6–3 μm, for classified GGBFS new very intense sharp peak appeared, whose maximum corresponded to the pore diameter of 6 μm. Classification of GGBFS also resulted in significant total porosity increase from 23.8 ± 0.4% for unclassified slag to 37.8 ± 2.0% for the selected coarser fraction.

The explanation of such observations is the prime assumption that unclassified GGBFS contains particles of various sizes and thus finer particles can fill the free spaces between the coarser ones (also confirmed by SEM micrographs in the next chapter).

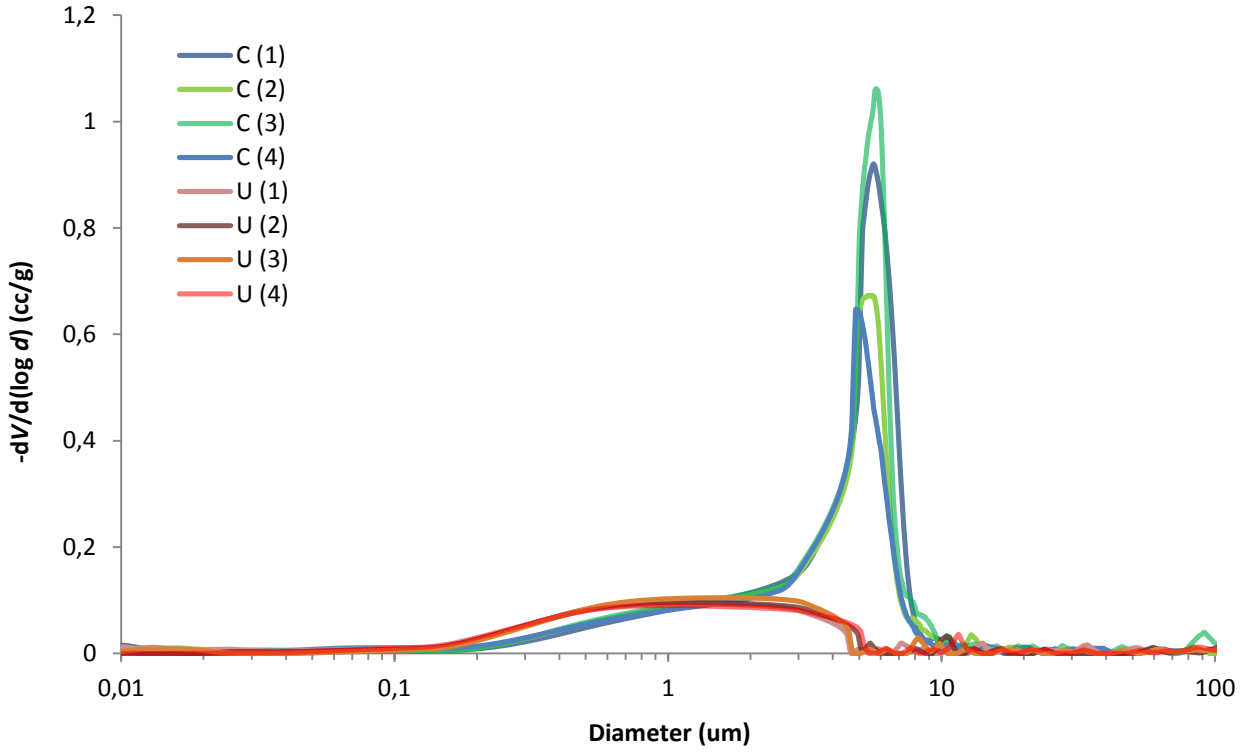

Figure 55: *Comparison of average porosity between classified (C) and unclassified (U) GGBFS-based mixture membranes determined using MIP.*

In the diagrams below (Figure 56) where only the relevant results are included can be seen that mixtures with mid to high content of water vary in pore size distributions in the range between approximately 0.07 to 0.65 µm but are not ordered by their water content. The lowest water content mixture which was number 2 had a through-pores sizes ranging from 0.7 to 6 µm. The second driest mixture which was number 12 however had pore sizes ranging from 0.3 to 0.8 µm and it shows greater pore content then most of the given series.

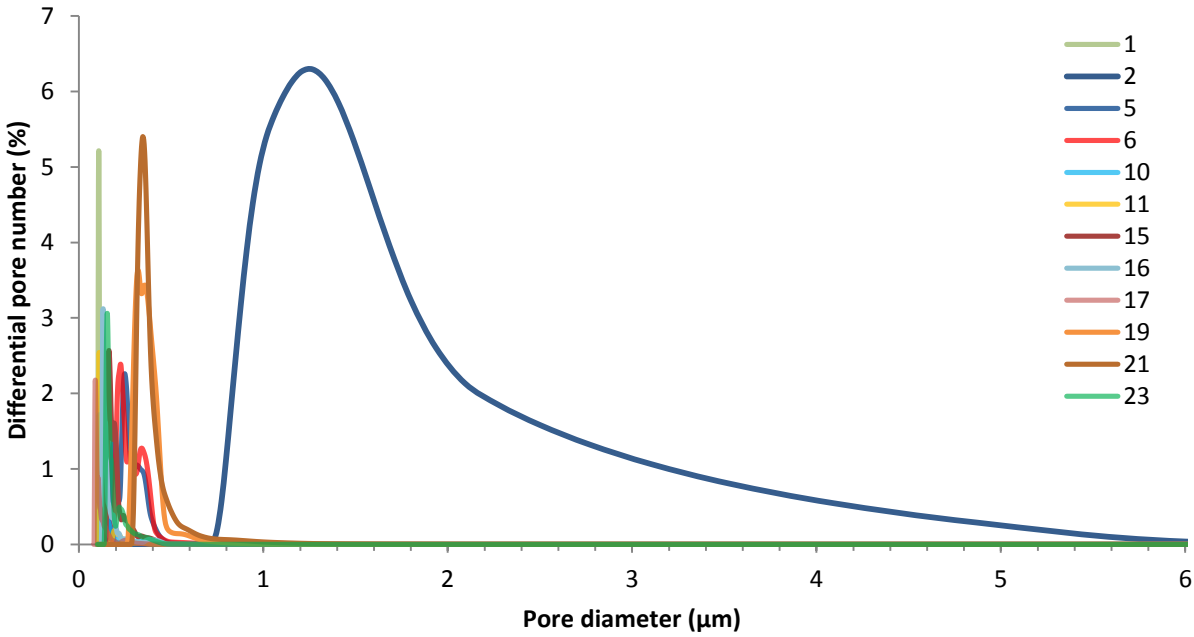

Figure 56: *CFP-based differential porosity curves of chosen MATLAB samples.*

The next diagram (Figure 57) was cropped to show closely the range where most of the pore size distributions of the series are located and how its typical results look like. Nearly all the results (except sample 12) are located in this range but it is important to note that the reproducibility of the CFP measurements for more accurate specifications was not perfect due to manual production of the barriers. A lot of results also overlapped and the diagrams were then illegible. Therefore only the representative results were left to reveal the range of the pore diameters and the overall through-porosity of the samples that can be taken as certain for given feedstock granulometries and preparation conditions.

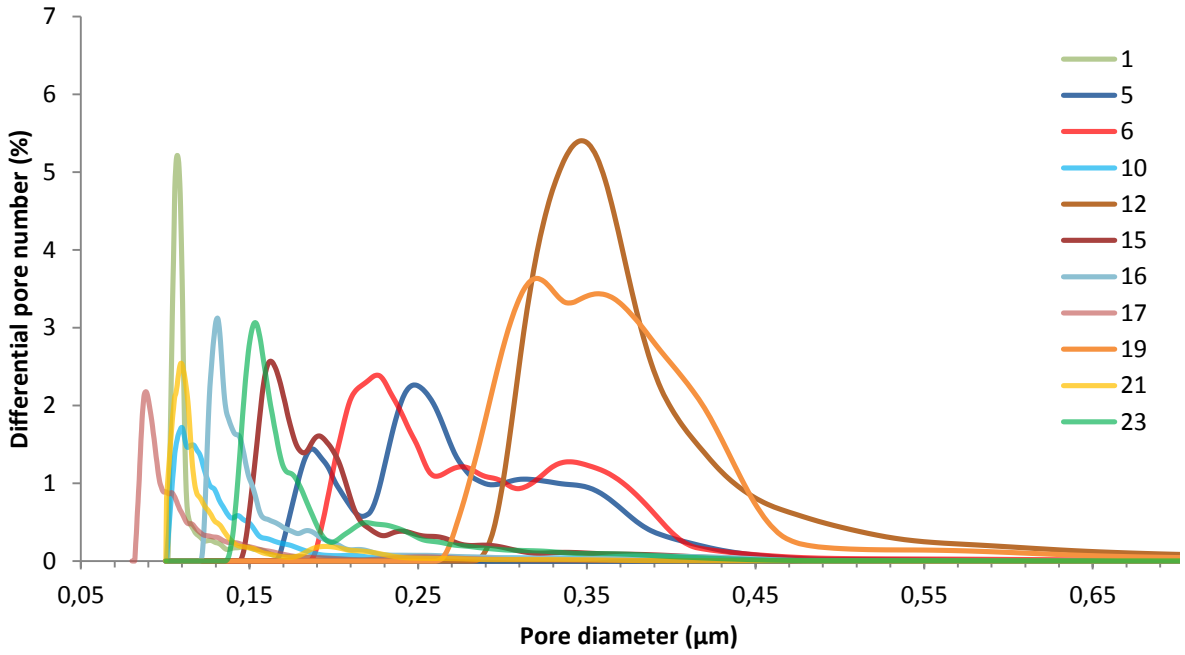

Figure 57: *CFP-based differential porosity curves of chosen MATLAB samples.*

The FA and S series were also subjected to pore-distribution measurements via CFP and also MIP (Mercury Intrusion Porosimetry). The results are shown in Figures 58 to 65. It is important to note that both these techniques gave similar results regarding the observed trends when one significant peak occurs around certain pore diameter for every mixture composition, but the exact values of pore diameter differ significantly when compared the same mixture measurements by both methods. This is not surprising since the working principles of these methods are totally different and different is also evaluation of the results. While the CFP results are given in the percentual number of the pores of certain size with respect to the total amount of detected pores, the MIP results show volume changes of intruded mercury between the two different pore diameters normalized to the sample weight. It should also be noted that while MIP measures all opened pores including dead-end pores in the porous network, CFP is sensitive only to pores through which fluid can flow. CFP therefore better describes potential filtration properties. The MIP results were however converted to differential pore number form (Figures 60, 63 and 65) for better comparison.

Lower alkali-activator content specimens of the F (fly ash) series were very difficult to measure on the porosimetry due to their friability and fragility and therefore their results data were not included. However, the data left and compared in the diagrams below show that between the FA-6 and FA-12 both methods revealed larger pores present in specimens with lower activator dose (Figure 58). It is probably caused by lower N-A-S-H content creating narrower necks between particles as a consequence of lower solids dissolution. Pore size reduction at higher activator dose was also observed by increased intrusions of mercury into the pores smaller than 200 nm (Figure 59). Based on the total amount of intruded mercury and specimen volume, total porosity of FA-6 and FA-12 series was estimated to 38.5 ± 1.5% and 33.8 ± 2.9%, respectively. Despite the fact that the reproducibility was not ideal in some cases the results show very clearly that increased dose of activator lead to a decrease in total porosity.

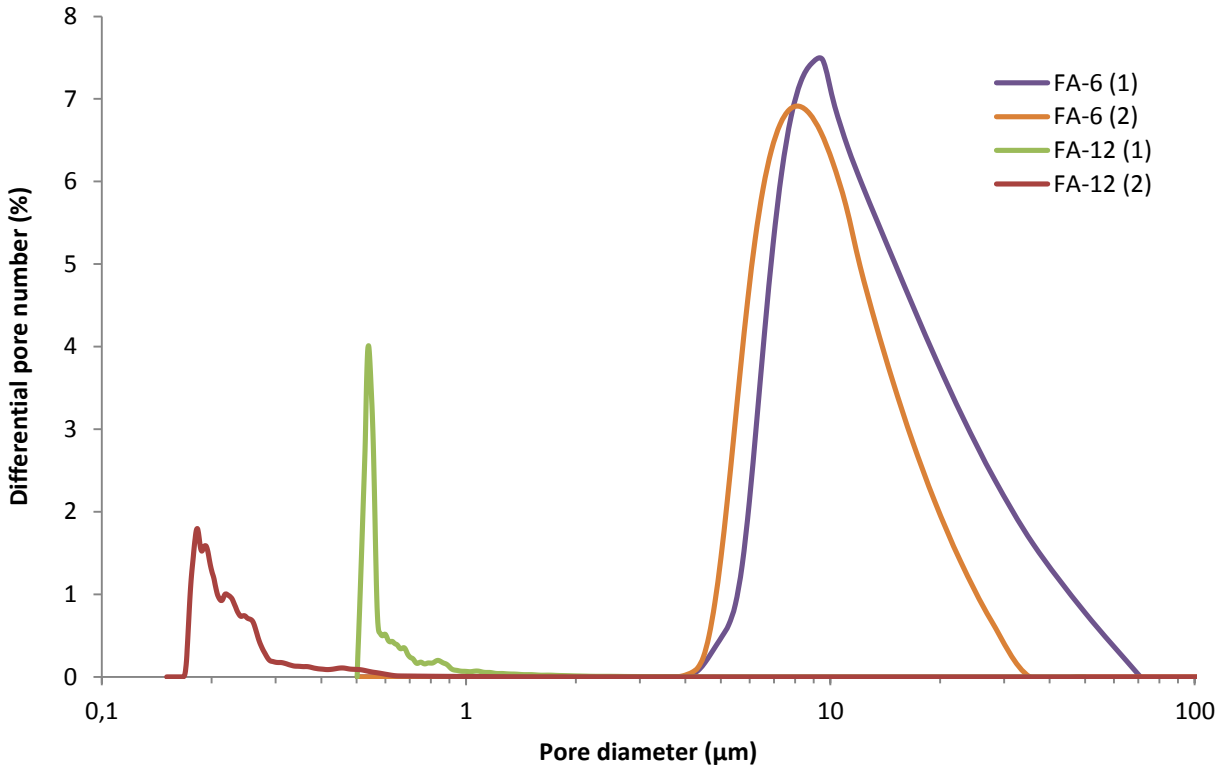

Figure 58: *CFP-based differential porosity curves of fly ash samples.*

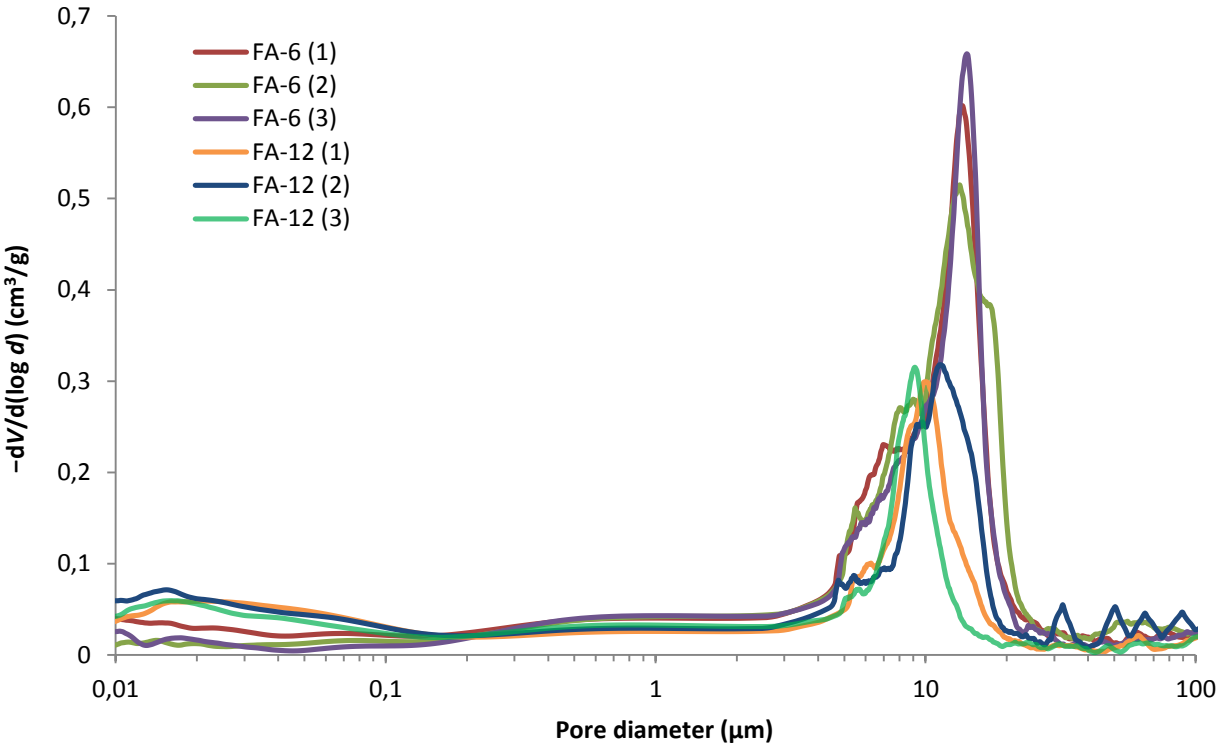

Figure 59: *MIP-based porosity measurements of fly ash samples expressed in volume change of intruded mercury into certain pore diameter normalized to the sample weight.*

To compare the results among each other the MIP data was converted from their natural form of $-dV/d(\log d)$ (differential volume of intruded mercury normalized to one decade of pore-size channel related to the sample weight) to differential pore number dependence like the data from the CFP (see Figure 60). And it is now plain to see that the sample FA-12 (3) has its first peak around 1.3 µm even higher than all the FA-6 samples, which is not visible in the $-dV/d(\log d)$ form on the Figure 59.

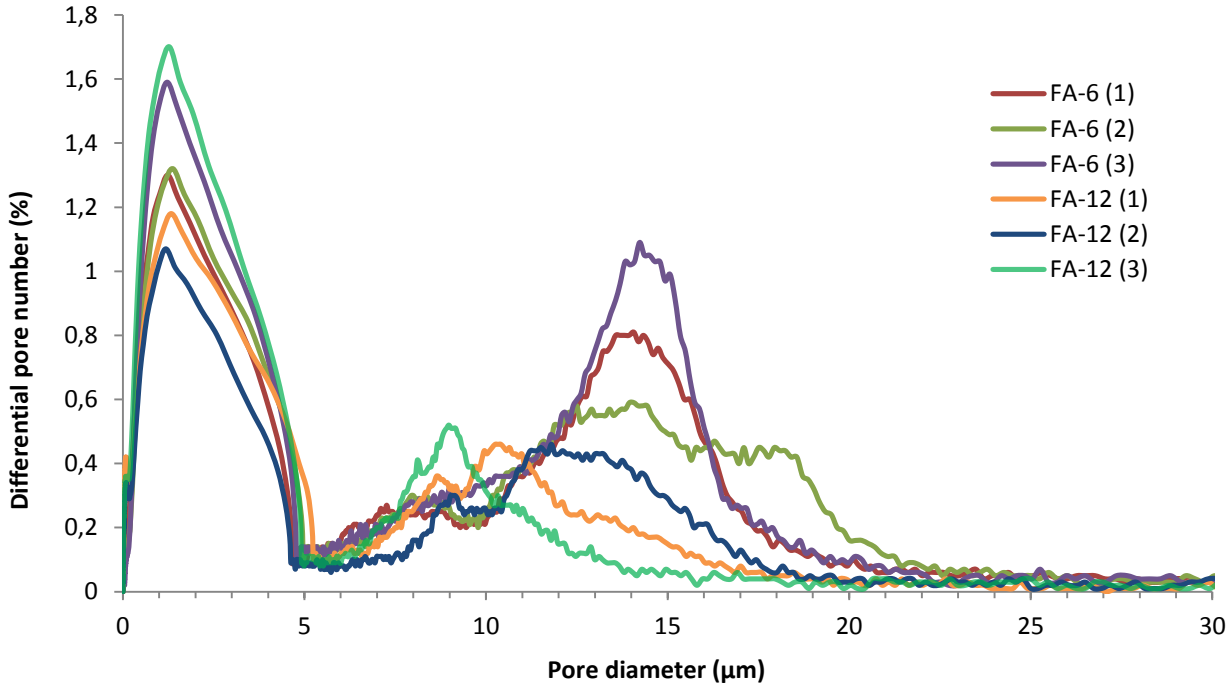

Figure 60: *MIP-based differential porosity measurements of fly ash samples.*

The S (blast furnace slag) series of the samples that due to their higher overall strength (as discussed below) better withstand the porosimetry measurements even with lower dose of activator (except the lowest marked S-1) are shown in the following diagrams.

The CFP data clearly shows that the more concentrated the activator was the finer pores the specimen contained. It is also visible that S-4 and S-5 results were very similar and they seem to delimit maximum of the dependence from both sides. Samples S-6 and S-12 are not present in the following CFP results because they did not show any open-through porosity at all during repeated measurements. Figure 61 illustrate a trend that clarifies that it is possible – samples S-4 and S-5 show a steep decrease in through-porosity at approximately 0.35 µm. The decrease is predictable because more dissolved matter between the particles, thus smaller pores, means of course a greater chance of clogging the channels through the porous body.

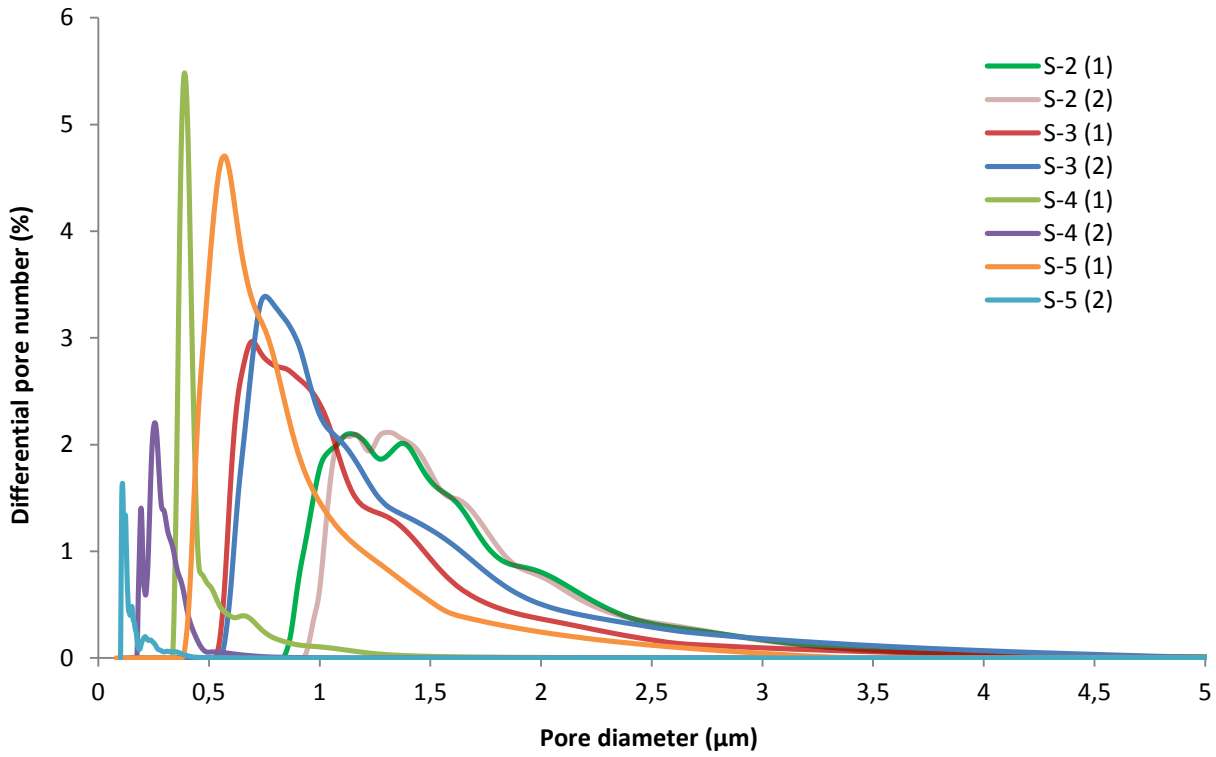

Figure 61: *CFP-based differential porosity curves of GGBFS samples.*

The MIP results of the S series in the diagrams below confirm that both pore diameter and overall porosity decrease with the increasing activator concentration. The original $-dV/d(\log d)$ results from MIP, more precisely their maxima, show the trend more visibly then the differential pore number form in this case. Because this MIP-based porosity data seemed very promising but the differential form (which as all of these results is an average of 4 measurements) did not showed the curves in the expected order even after new series of samples was measured, it was decided to prepare new experimental series under greater pressure that could better regularize the particles. The pressure was set to twice the original one which was 1 ton for the barrier 25mm in diameter (that equals 19.5MPa) so this series was made under 2 tons (~ 39MPa). The results of MIP measurement of these samples can be seen in figures 64 and 65. The S-2 mixture proved to protrude from the row even more clearly than in the 1 ton series (Figures 62 and 63) and again it is more obvious from the $-dV/d(\log d)$ form of results. The total porosity decrease with increasing pressure can be seen on all samples (except the S-2 maxima). The standard deviation does not indicate that the S-2 results to be anyhow inconsistent or irrelevant within the series (Table 16).

Table 16: The average total porosity of the GGBFS samples with their standard deviations.

	S-1		S-2		S-3		S-4		S-5		S-6	
Pressure (Tons)	TP(%)	s.d.	TP(%)	s.d.	TP(%)	s.d.	TP(%)	s.d.	TP(%)	s.d.	TP(%)	s.d.
1	33.65	2.54	31.71	1.14	29.93	1.56	21.81	0.40	23.60	2.12	20.20	2.33
2	32.45	3.16	37.78	1.96	27.98	1.50	18.88	0.05	21.91	0.44	16.24	1.87

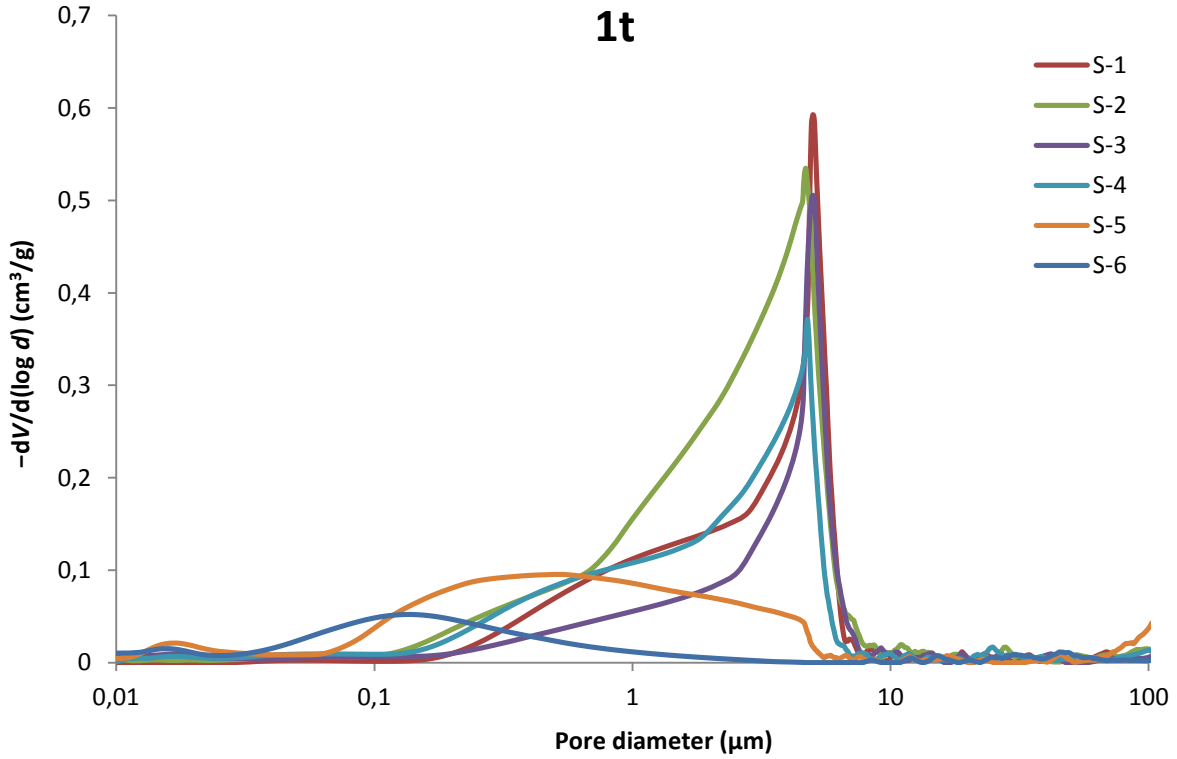

Figure 62: *MIP-based porosity measurements of GGBFS samples expressed in volume change of intruded mercury into certain pore diameter normalized to the sample weight.*

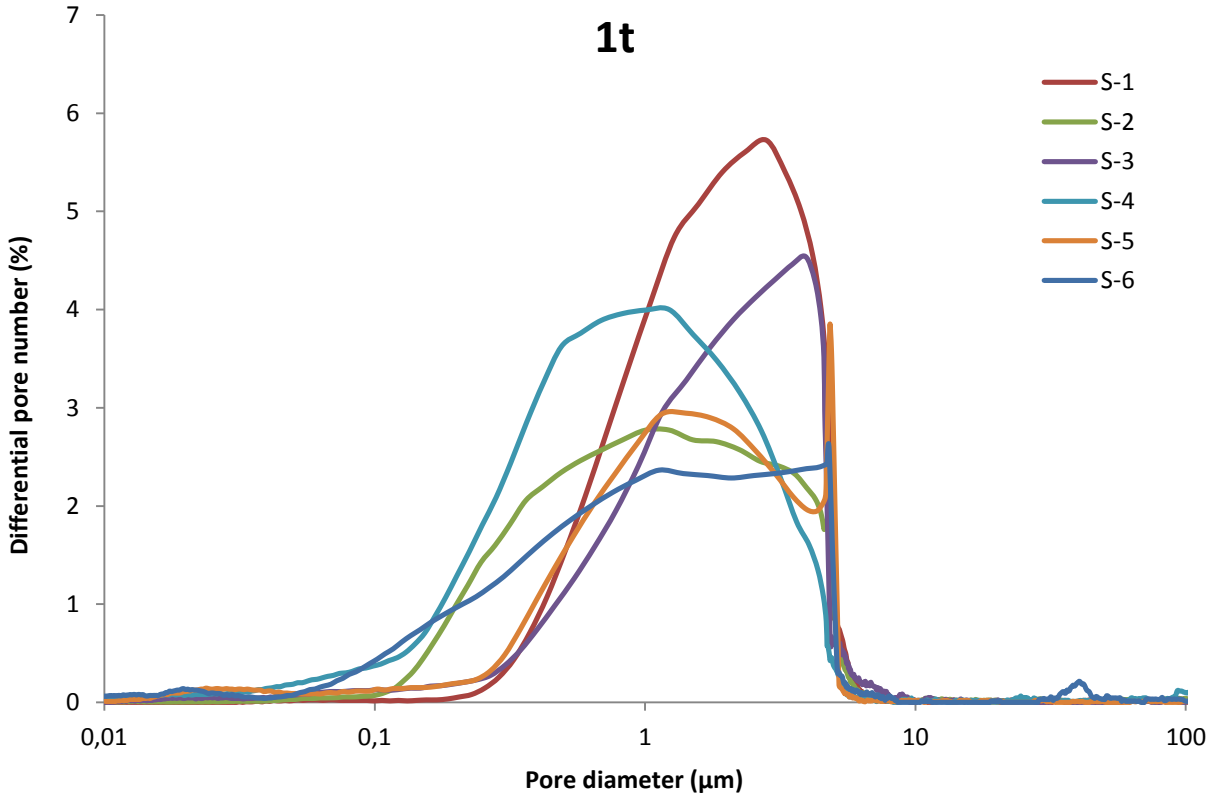

Figure 63: *MIP-based differential porosity measurements of GGBFS samples.*

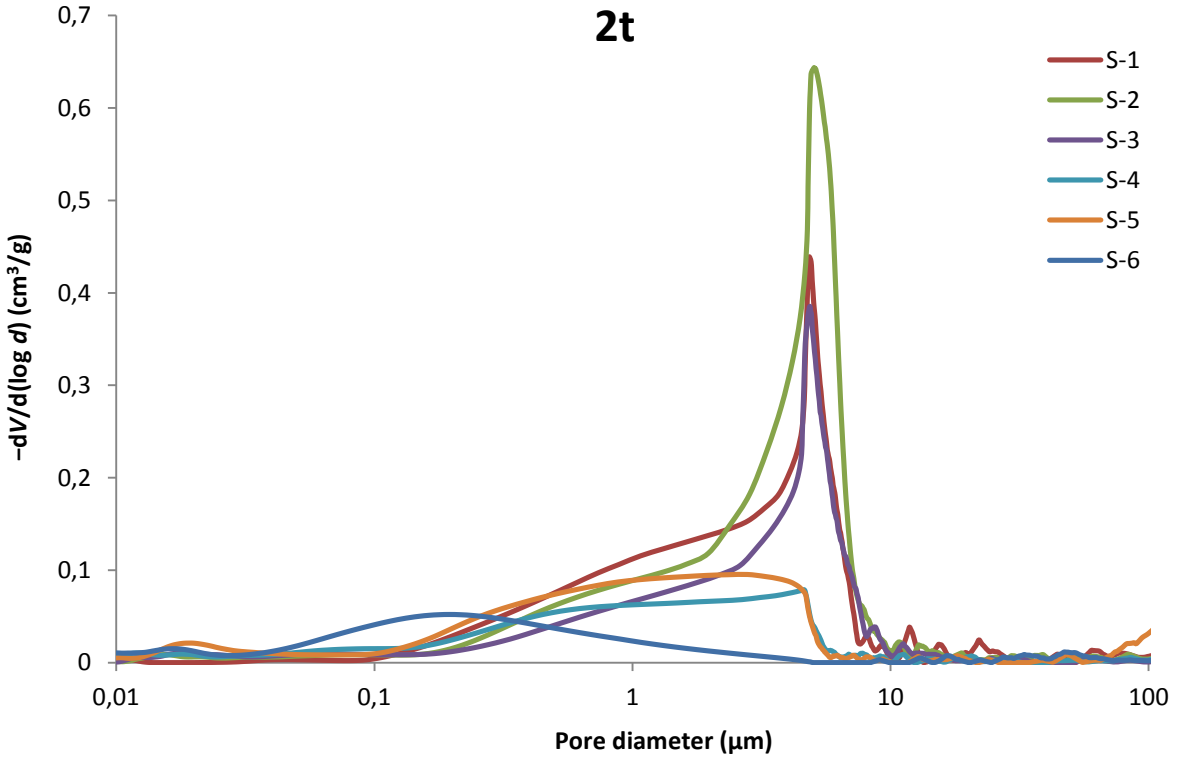

Figure 64: *MIP-based porosity measurements of GGBFS samples expressed in volume change of intruded mercury into certain pore diameter normalized to the sample weight.*

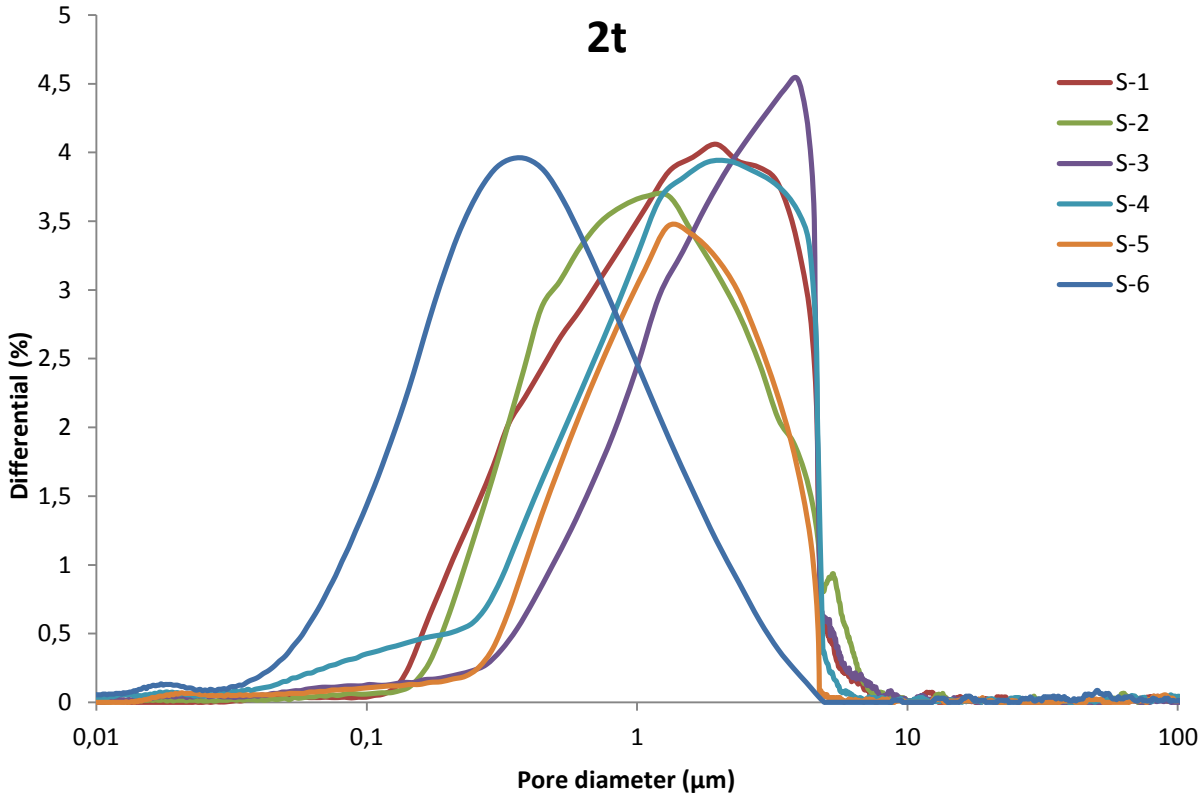

Figure 65: *MIP-based differential porosity measurements of GGBFS samples.*

5.8 MICROSTRUCTURE

For SEM observations a small part of the specimens was taken and its cross-section smoothed with a sand paper and then polished using JEOL IB09010CP ionic polisher. Finally, samples were sputter-coated with gold and investigated by ZEISS EVO LS 10 scanning electron microscope in the mode of secondary electrons (SE) and back scattered electrons (BSE) detection. Accelerating voltage of the microscope was set to 10 kV.

Contacts between fly ash particles are evident from figures obtained by SEM, either in SE mode (Figure 66) or in BSE mode (Figure 67). At lower magnitude, differences in the FA-6 and FA-12 samples are not very clear at the first sight, but with a distance higher binding phase content is definite for higher dose of activator (observable at closer look in the form of rims around the fly ash grains). This fact is even for iron-rich particle, which is probably hematite or magnetite which is the brightest one in Figure 67, identified better below by EDS analysis in Figures 71 and 72. It can be expected that due to its composition such particle can hardly be alkali activated and it is thus likely that formation of binding phase around this particle was a consequence of dissolution of other particles.

It is generally accepted (Marjanović et al. 2015) that hydration product of alkaline activation of fly ash is sodium-aluminium-silicon-hydrate (N-A-S-H). Yet besides the original undisolved material inside the particles and N-A-S-H phase around and between them some crystals can be observed mainly near the borders of fly ash particles which meas some kinf of crystalic phase present in the samples.

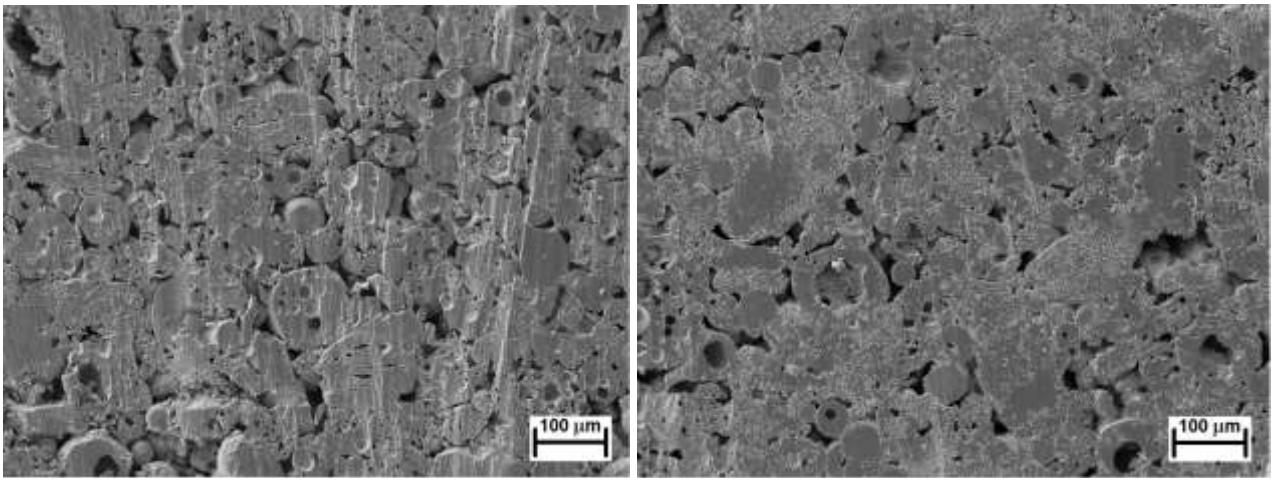

Figure 66: *Microstructure of the prepared specimens (FA 6 on the left and FA-12 on the right) observed by SEM in SE mode, magnitude 200×.*

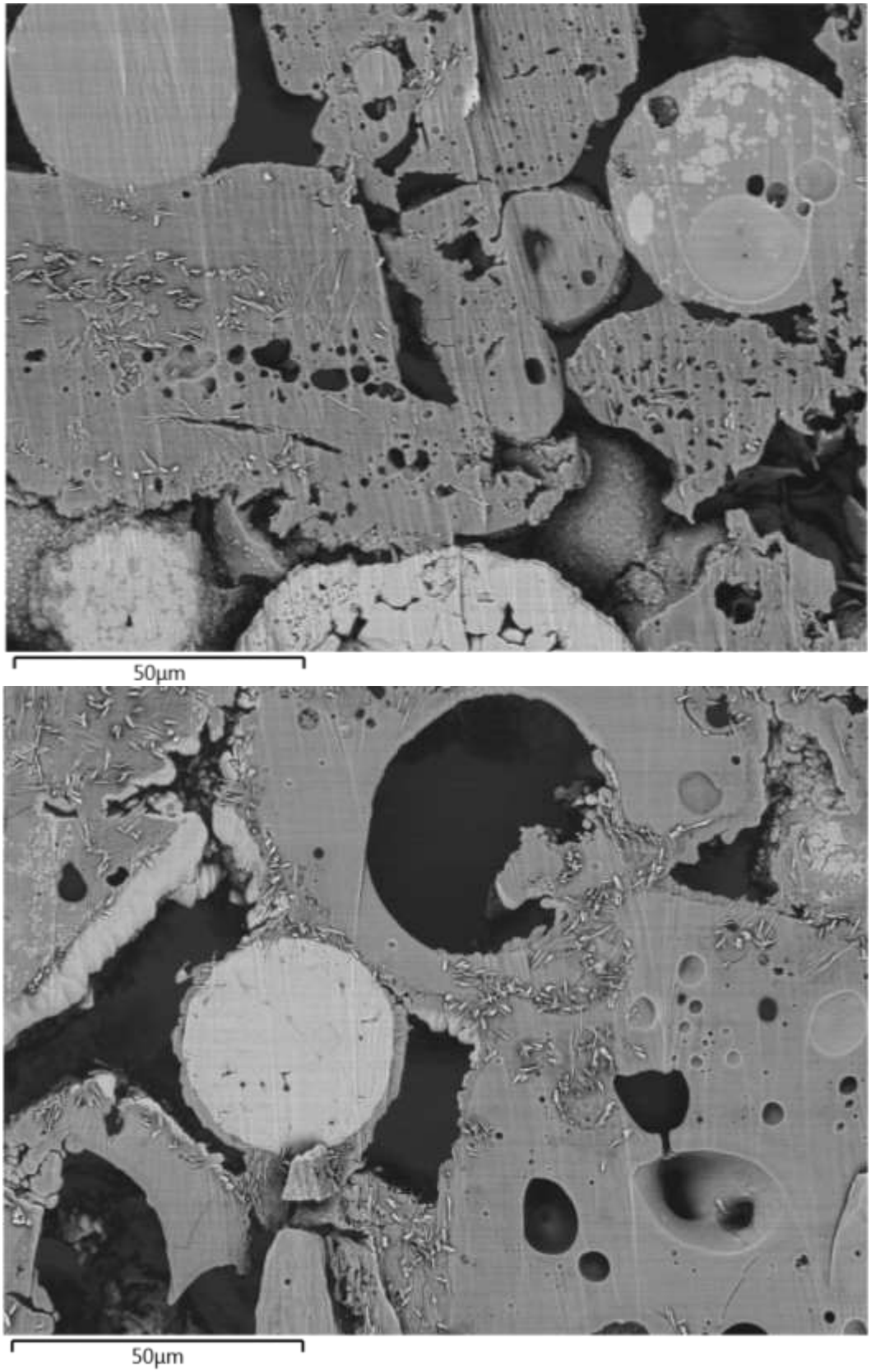

Figure 67: *Comparison of the binder phase between FA particles (FA-6 upwards and FA-12 underneath) as observed by SEM in BSE mode, magnitude 2000×.*

As already mentioned the two regions of the AAFA specimens shown in the pictures above (Figure 67) show as most of the specimens on fly ash basis the occurence of emerging crystals which were observed even in the macroscale. Figure 68 illustrates the exterme case of efflorescence on FA-based AAM testing column. The crystals were also observed under Olympus BX41 optical microscope and some of the micrographs are presented in Figure 68. It is believed the crystals visible in the micrographs in Figure 67 were formed during the several hours between the polishing of the specimens and their microscope-scanning and are also simply a consequence of efflorescence.

Due to this phenomenon the lower more varied sample from Figure 67 was subjected to the energy-dispersive spectrometry (SEM EDS) which revealed that these particles are rich in sodium and it is believed that the crystals are products of gradual carbonation of sodium hydroxide by atmospheric carbon dioxide.

Figure 68: *Extreme case of efflorescence – crystals slowly emerging on one of the AAFA samples (the front edge of the sample is 2cm wide).*

Figure 69: *Detail pictures of macroscopic crystals from the specimen in the previous figure.*

Among other things (like the strength of the material discussed above) the efflorescence phenomena proved during the work lead the author to aim the research of the potential production of porous media from the mixtures based predominantly on the basis of BFS. The pure BFS-based samples had shown considerable shrinkage, but the hybrid samples with a share of FA and bauxite did not.

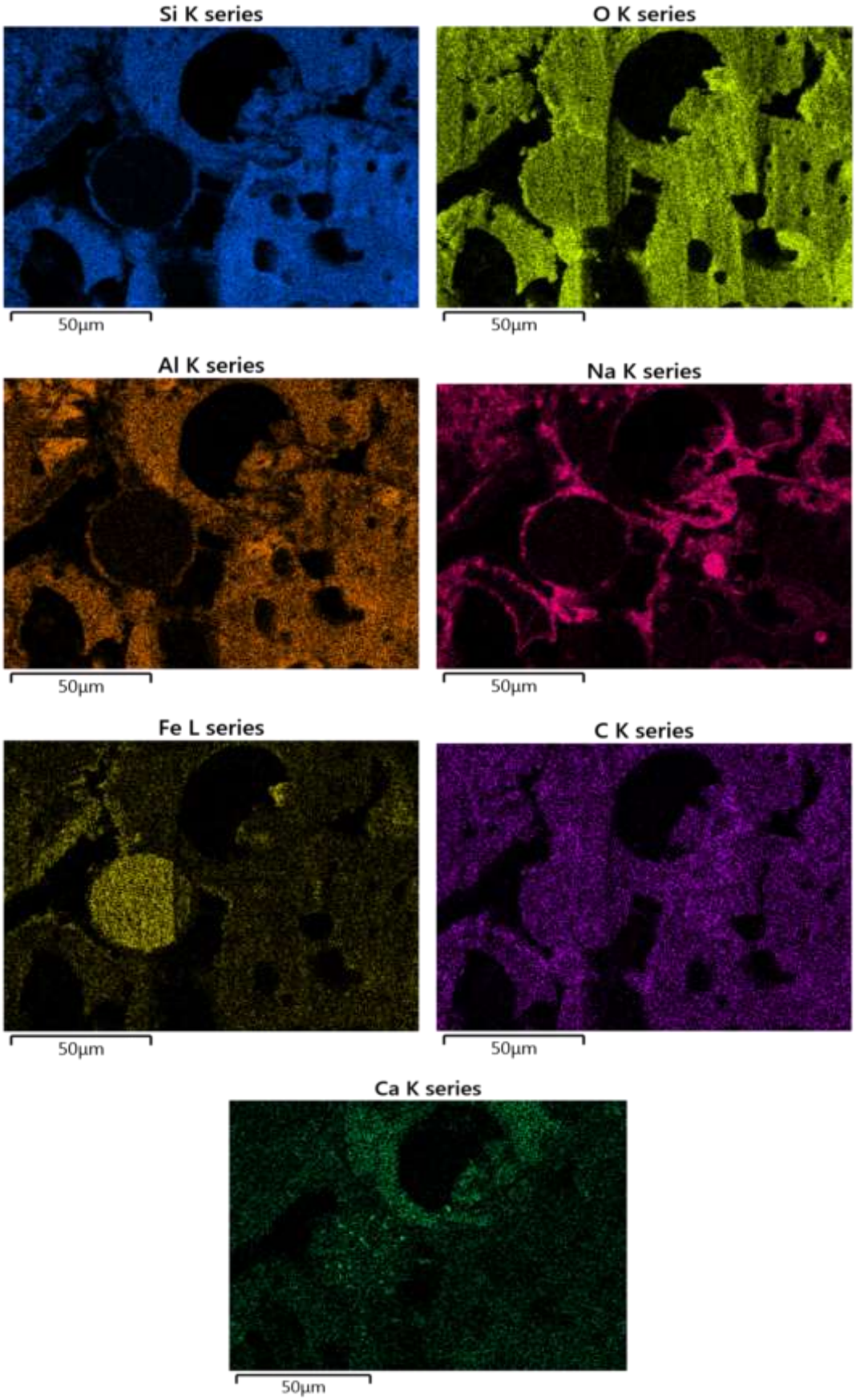

Figure 70: *Individual images of each element investigated on the FA-based specimen by EDS.*

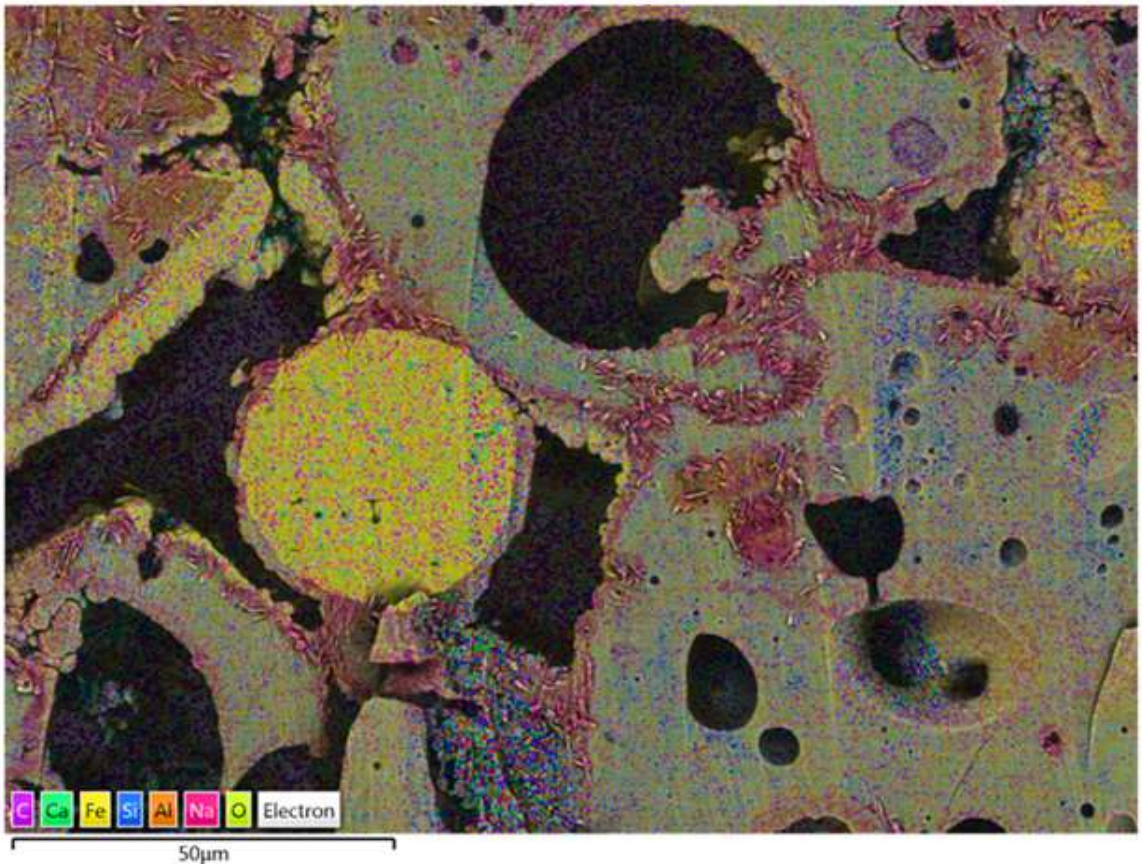

Figure 71: *Layered image made from the individual EDS analysis of FA-based specimen.*

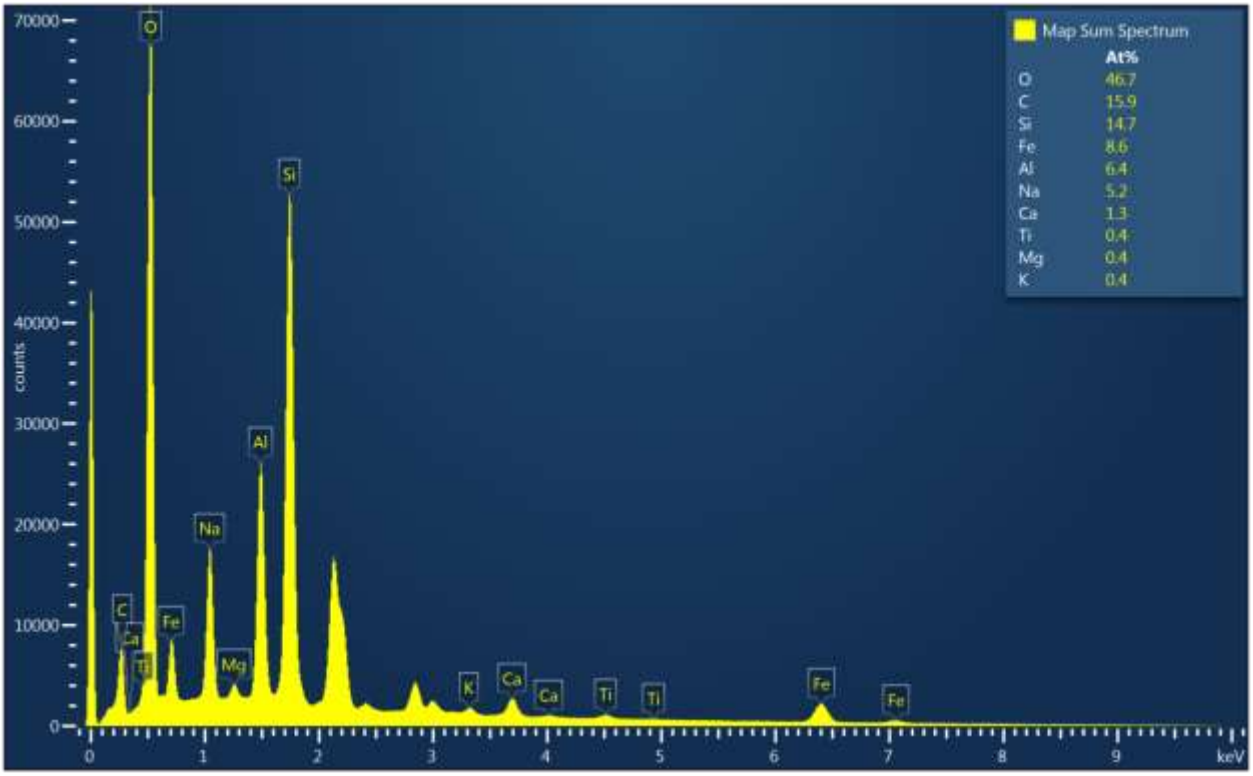

Figure 72: *EDS quantitative analysis of the scanned area of the FA-based specimen.*

The EDS revealed that the regions affected by crystal growth are rich in sodium and oxygen which was not a surprise and it can be therefore concluded that the crystals are pure sodium hydroxide. The only confusing fact for attentive person at this point is that the macroscopic crystals in Figure 69 are of two different forms – round and opaque (what is typical for NaOH), and oblong and transparent. It was assumed that the second type has undergone the carbonation process by reaction with atmospheric CO_2 while consuming the inner moisture during its growth to form sodium carbonate crystals.

To be sure, the crystals were scrubbed of the body to carry out the X-Ray powder Diffraction analysis (XRD) which confirmed that the crystals were sodium carbonate hydrate (see Figure 73).

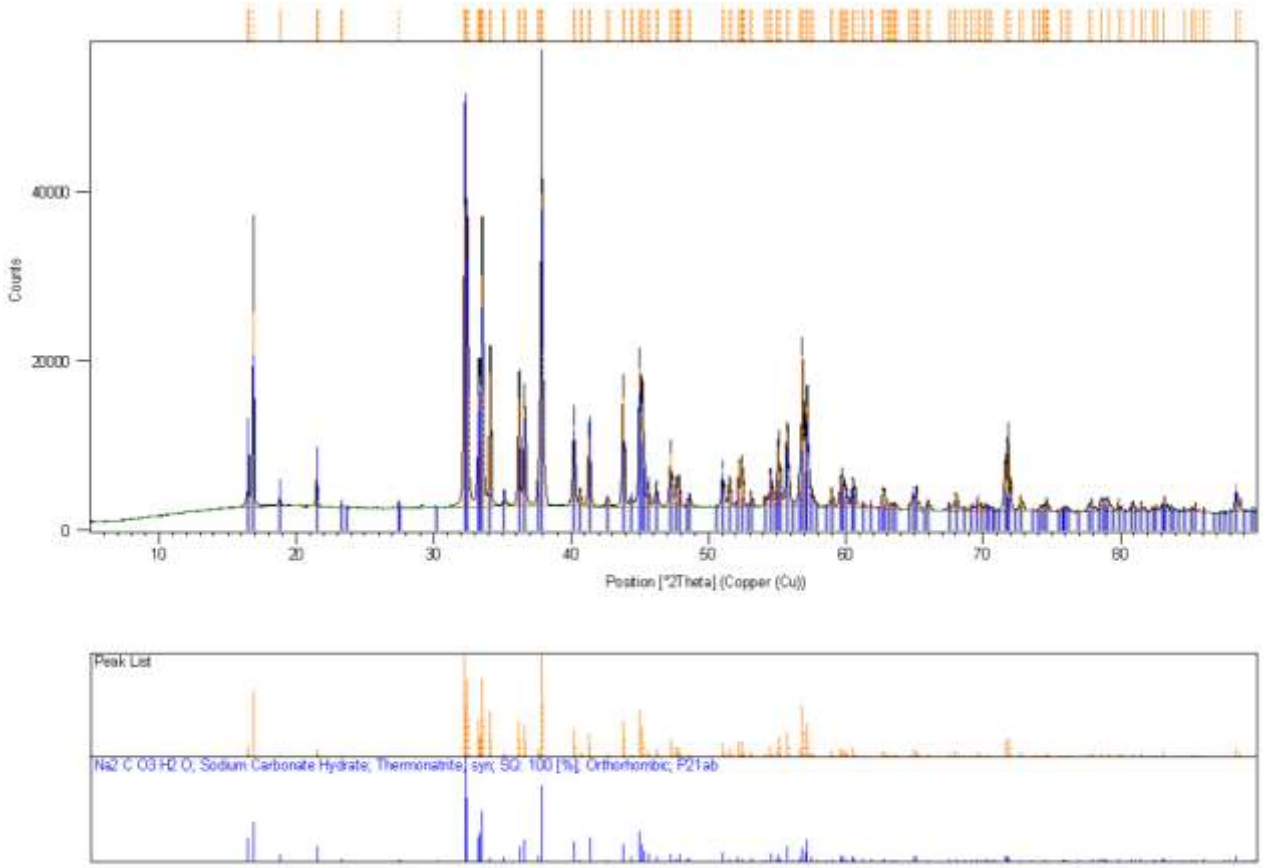

Figure 73: *XRD analysis of crystals emerging on FA-based samples*

The BFS specimens were also investigated using SEM and the microstructure overview of the prepared membranes is given in Figure 74. There is also a comparison of barriers of the same composition prepared from unclassified slag to prove that the classification of the powders is necessary to obtain better porosity results. It can be seen that both types of membranes preserve porosity although it clearly illustrates that membranes based on unclassified GGBFS contain a lot of places where potentially larger pores are stuck by finer particles and thus number of desired pores decrease considerably. Moreover, microstructure of the membrane prepared from unclassified GGBFS is less homogenous compared to classified ones.

On the other hand increase in porosity is connected with decrease in strength and despite the fact that strength of unclassified-slag-based membranes was not investigated those prepared from classified GGBFS were more prone to cracking during the sample preparation and easier to abrade.

The main binding phase forming during alkaline activation of GGBFS is calcium-aluminium-silicate-hydrate (C-A-S-H) (Myers et al.,2013; Puertas et al. 2011). Thank to this phase, GGBFS grains are connected together and form filtration membrane (Figures 74 and 75). Its amount is sufficiently high to facilitate compactness of the body but it was low to satisfactorily determine its composition by EDS (see Figures 76, 77 and 78). The micrographs however confirm that the GGBFS-based materials do not tend to efflorescence because the crystals do not occur in them.

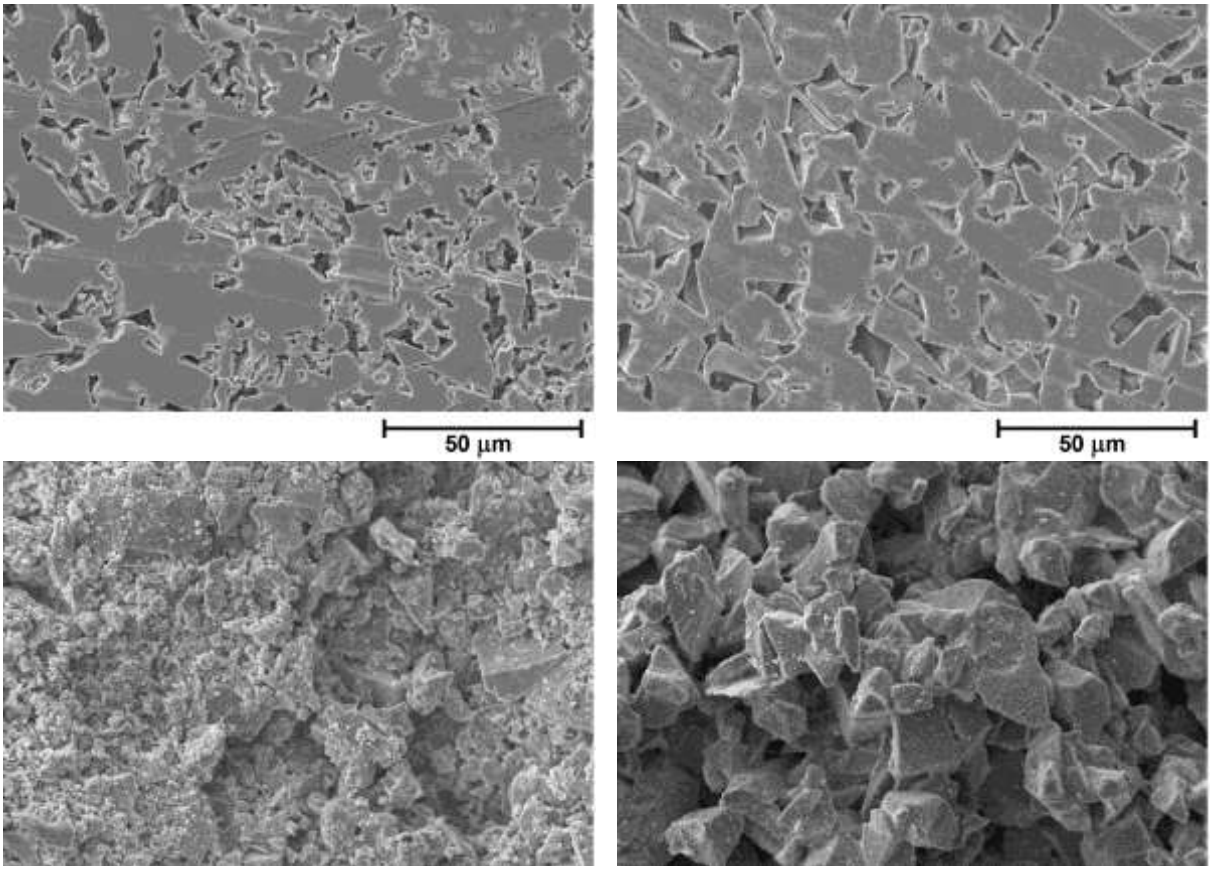

Figure 74: *Microstructure of polished (up) and unpolished (down) parts of the membrane from unclassified (left) and classified (right) GGBFS; magnitude 2 000x.*

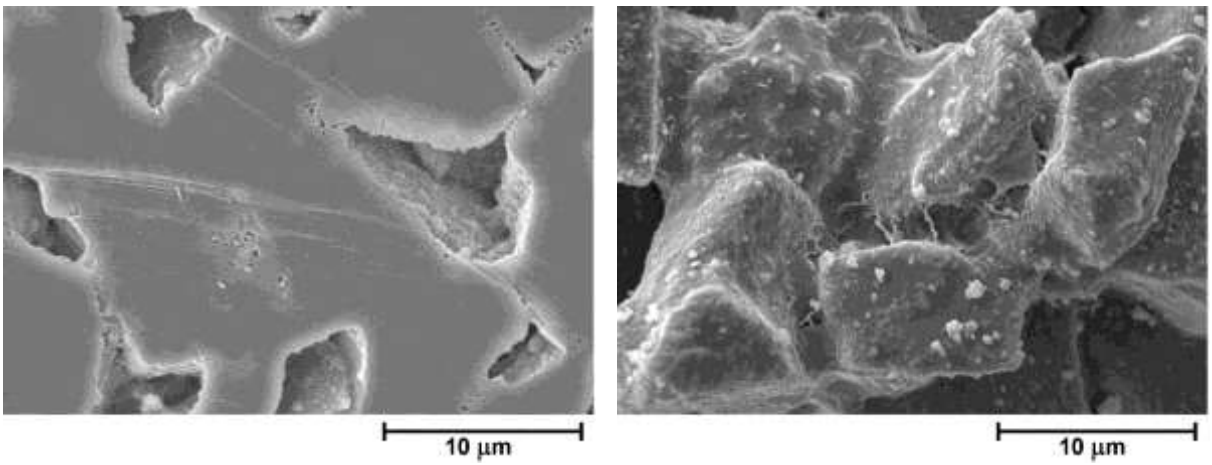

Figure 75: *Detail of polished (left) and unpolished (right) part of the membrane from classified GGBFS; magnitude 10 000x.*

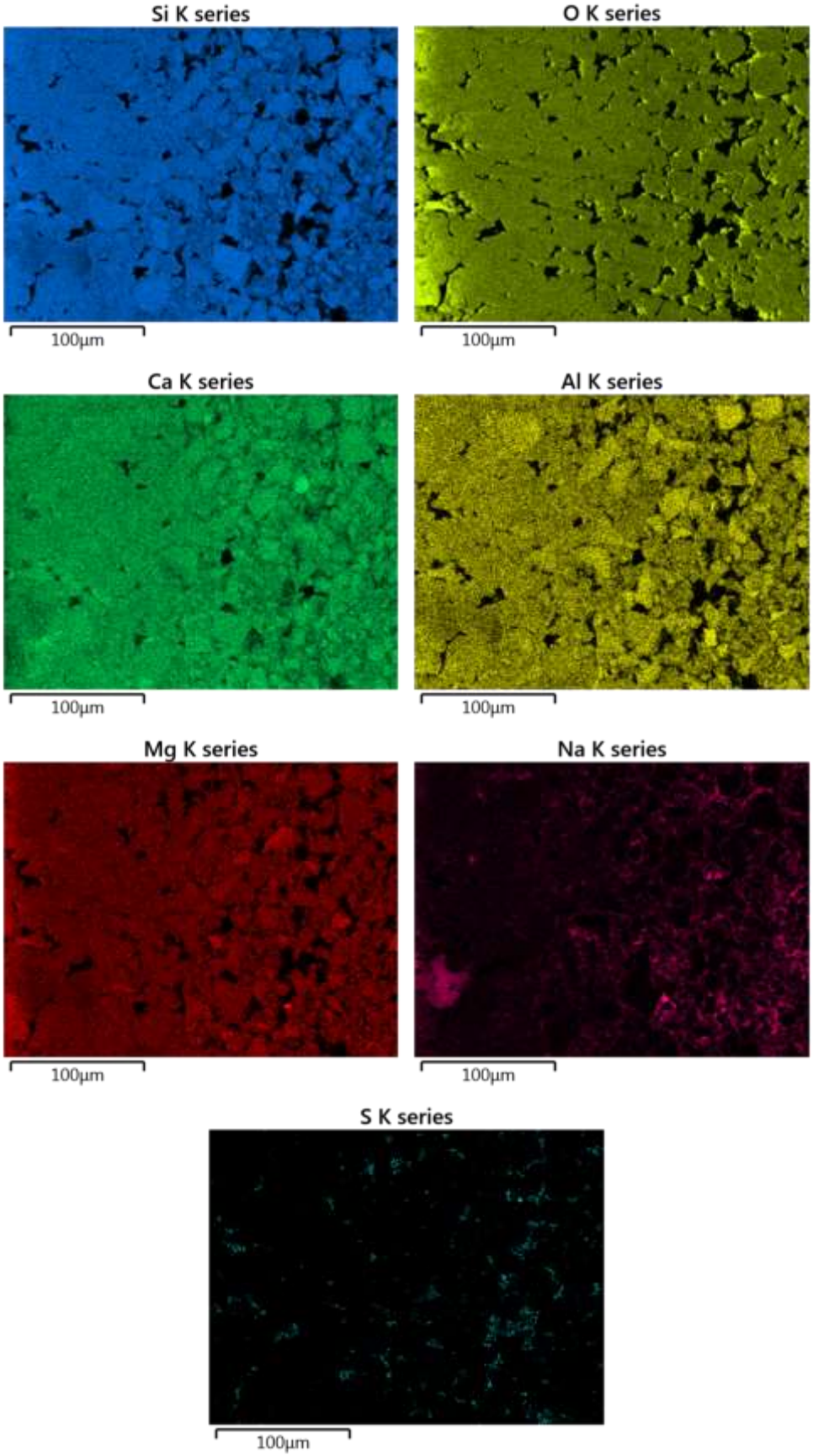

Figure 76: *Individual images of each element investigated on the GGBFS specimen by EDS.*

Figure 77: *Layered image from the individual EDS analysis of GGBFS-based specimen.*

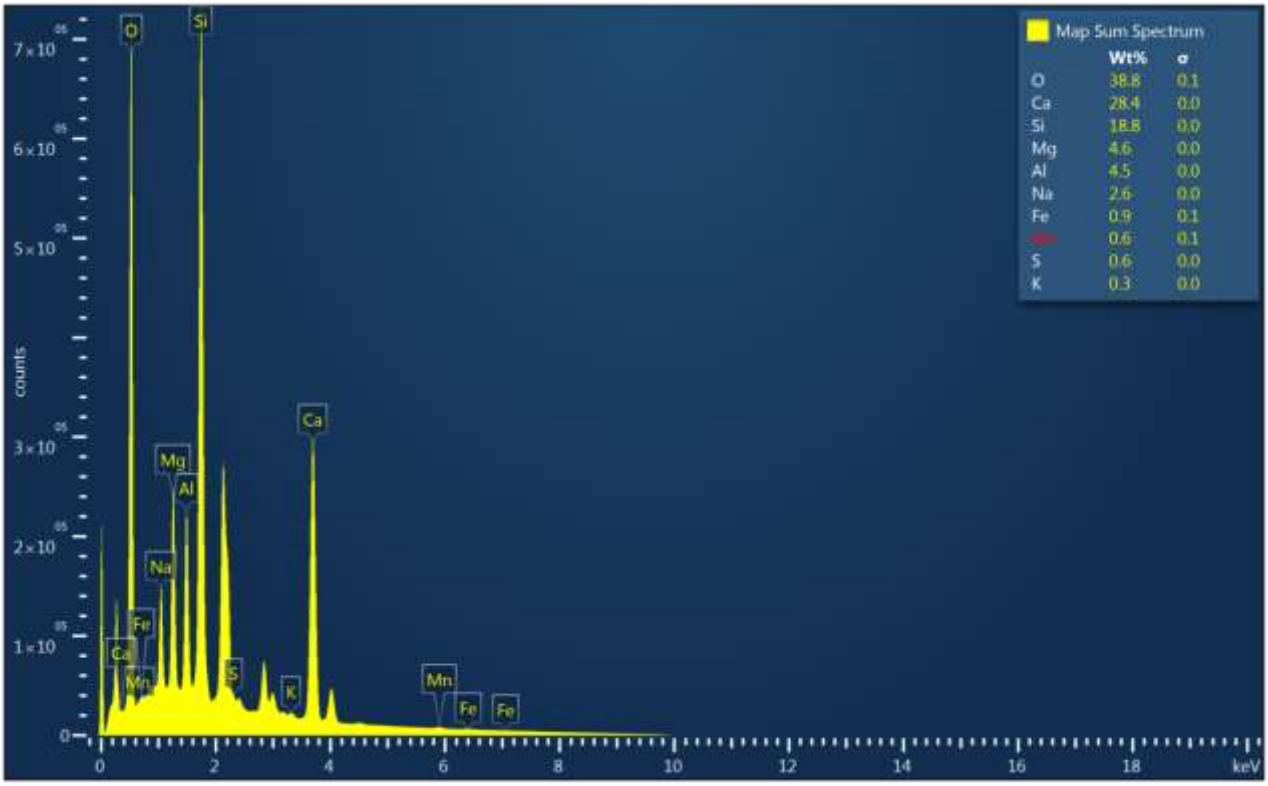

Figure 78: *EDS quantitative analysis of the scanned area of the GGBFS-based specimen.*

5.9 FINAL POROUS MATERIAL COMPOSITION

On the basis of the previous results and subsequent findings it was clear that the ideal mixture should have the SiO_2/Al_2O_3 ratio around 3, it should be based on GGBFS for the most part to be as strong as possible but contain minor part of FA and bauxite to reduce the GGBFS shrinkage and preserve the oxides ratio and it also has to be as dry as possible to maintain good porosity. After these conclusions the dataset of possible mixture compositions was searched through and one particular composition was chosen for the findings verification (the composition is listed in Table 17). The bodies from this material were prepared and the results of the mechanical and porosity tests as well as micrographs from SEM are listed below.

It is important to note at this point that with this level of dryness it is very difficult to mix the components well and obtain a homogenous structure. For good results the combination of manual mixing and planetary mixing machine treatment had to be applied. The machine mixing routine was amended to 5 times 15 seconds alternating with manual disruption of the material which tended to lodge to a firm aggregate in the mixing container under the planetary centrifugal motion.

Table 17: Composition and parameters of the final porous material X.

#	P1 (SiO_2/Al_2O_3)	P2 (Na_2O/Al_2O_3)	P3 (H_2O/Na_2O)	Glass	NaOH	Ash	Baux.	Slag	w/s
X	2.98	0.92	5.02	1.06	19.76	10.78	8.26	60.14	0.159

The material of this composition achieved in uniaxial tensile strength tests the results of 6.31 ± 0.20 MPa for the testing columns and 6.65 ± 0.49 MPa for the bodies grinded from the pressed barriers while maintaining very good level of fine porosity – see Figure 79 and for realistic idea of the material structure see Figure 80 and 81 showing ion beam polished samples.

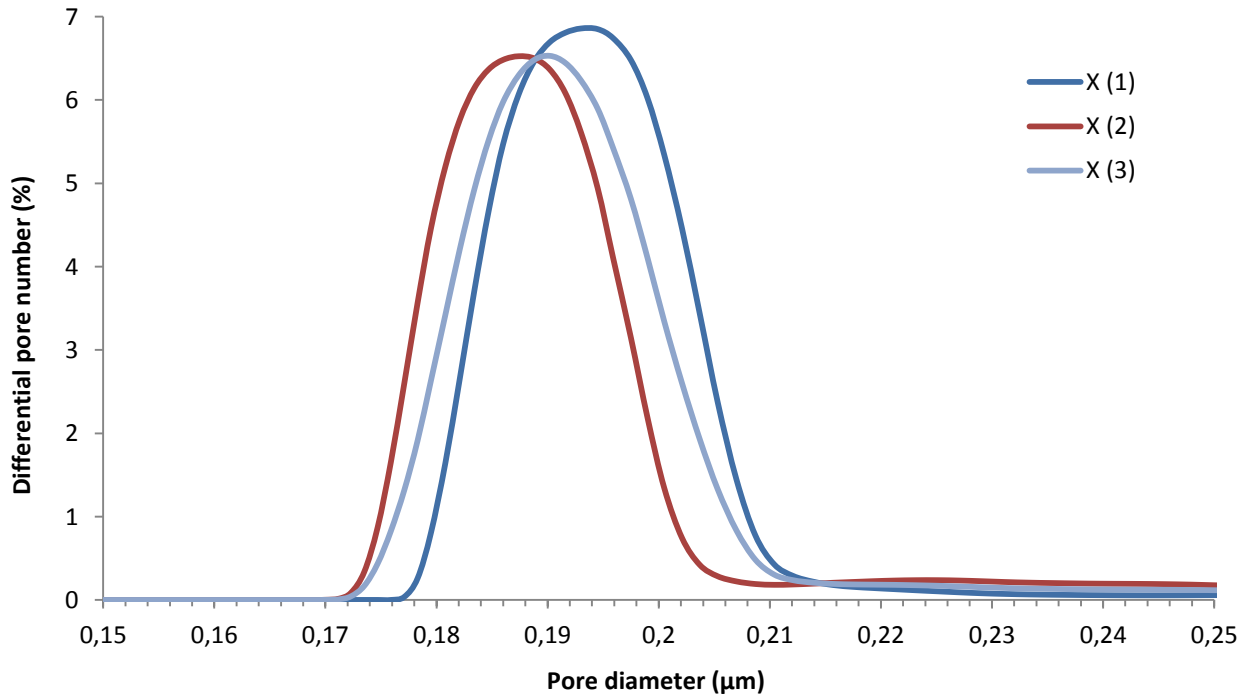

Figure 79: *CFP-based differential porosity curves of the X composition samples.*

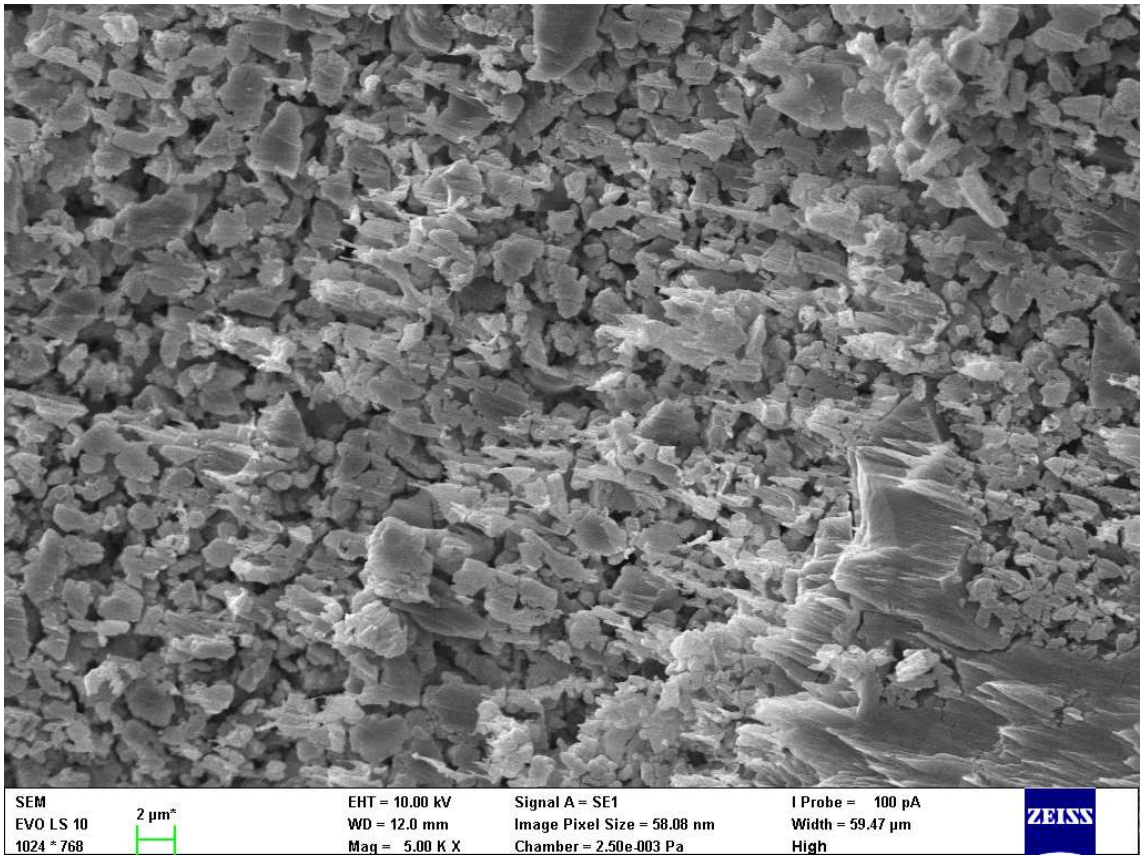

Figure 80: *SEM image of the X composition structure; magnitude 5000x.*

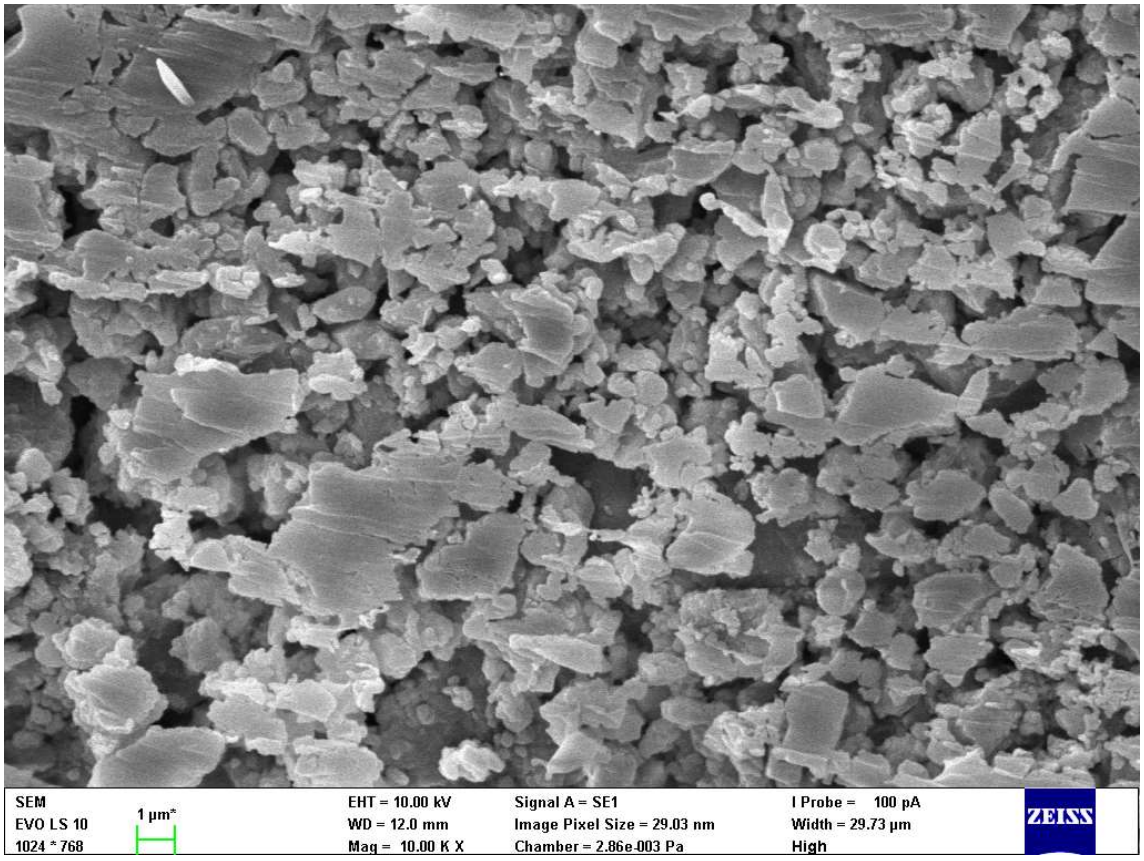

Figure 81: *SEM image of the X composition structure; magnitude 10000x.*

5.10 PERMEABILITY TESTING

After the strength and porosity of the final composition bodies were tested and the potential of the composition verified the permeability had to be proved using the filtration post. The first results had shown that the filtration barrier withstands even the maximal pressure of the filtration post (nearly 6 bar) but the uniform barrier of such pore-fineness to thickness ratio puts too much resistance to the flow and the permeability was only about 15 L/m^2.h.bar which correlate with the results in literature (Qin et al. 2015) but a lot less than the results of Fang et al. (2013) which was using asymmetrical filtration barriers so it was decided to prepare the barriers asymmetrically – coarser support with thin layer of the fine filtering material.

For the preparation of the coarser supporting layer an S-5 mixture analogue was chosen due to its best strength characteristics within the whole mixtures spectrum. The unground blast furnace slag had to be used and thus it had to be also classified. To cut the sharper fraction by classification of the powder ALPINE E200 LS air jet sieve with 125μm and 250μm sieves were used. The resulting granulometry of the coarser powder which can be seen in Figure 82 shows overlaps against the used sieves mesh diameters. This is caused due to unground blast furnace slag particles morphology which is oblong needle-like (see Figure 83) so the particles entering the sieve perpendicularly can pass through.

At first two different approaches were tested for the preparation – 'wet on wet' (pressing and curing two layers together while both freshly mixed) and 'wet on dry' (pressing the finer layer on fully hardened support). The issue with the readily hardened supports is that they tend to collapse under the pressing the finer mixture on top of them. The 'wet on wet' method had also a disadvantage which hides in an uneven thickness of the layers after pressing them, both soft, together. The results of these two approaches turned out not suitable and therefore the simple third technique was used in form of depositing the upper finer layer by laboratory spatula on the surface of the fully cured support, then cure it and sand off the surface to reduce its thickness and level the surface. The only issue of this method is that it is time consuming while measuring of the layer has to be done during the sanding to obtain comparable thicknesses on multiple pieces.

Regardless of the way of preparation the results of the asymmetrical barriers were different from each other because predictably the repeatability of the asymmetrical barriers made by hand is not perfect. The cured membranes made by the third above mentioned technique were then tested on the filtration post for permeability with water and the average results were 138 L/h.m^2.bar. Air permeability measured using Quantachrome 3Gzh porometer showed the permeability results of 1320 L/h.m^2.bar.

The resulting structures were observed under SEM and they are depicted below. Figure 84 shows ion beam polished cut of the asymmetrical filtration body from the side. Figure 85 shows the coarse supporting structure and Figures 86 and 87 are showing ion polished surfaces of the fine filtering layer under greater magnitudes.

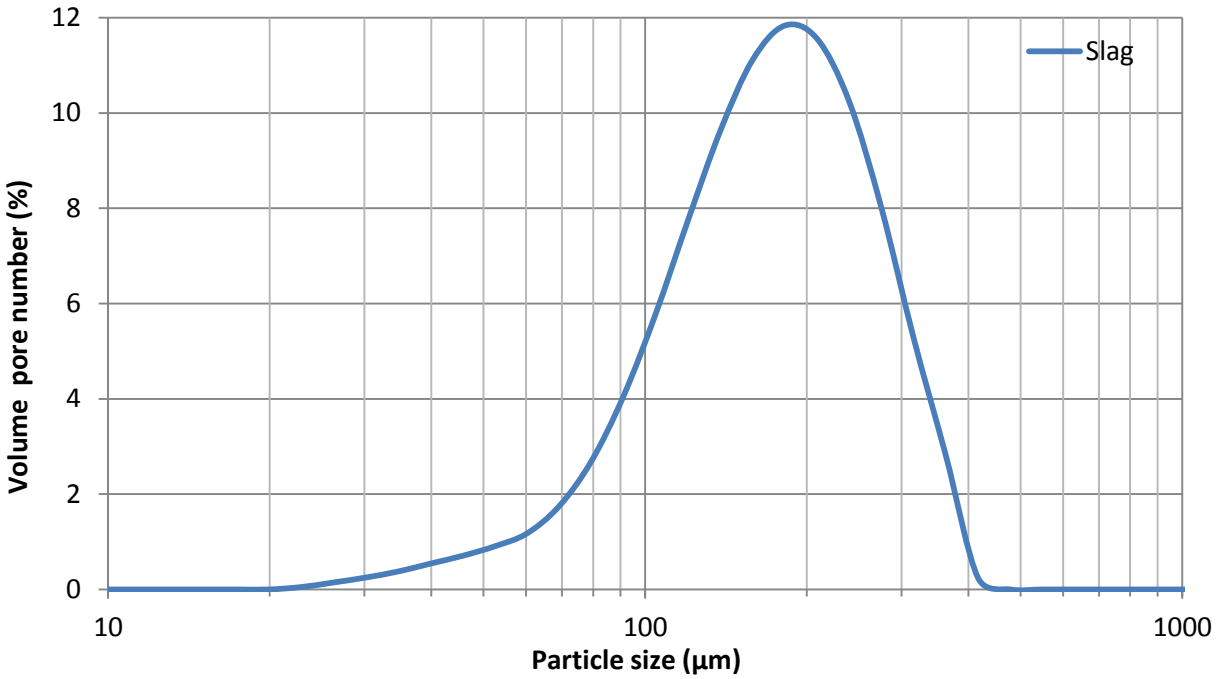

Figure 82: *Coarse GBFS after classification.*

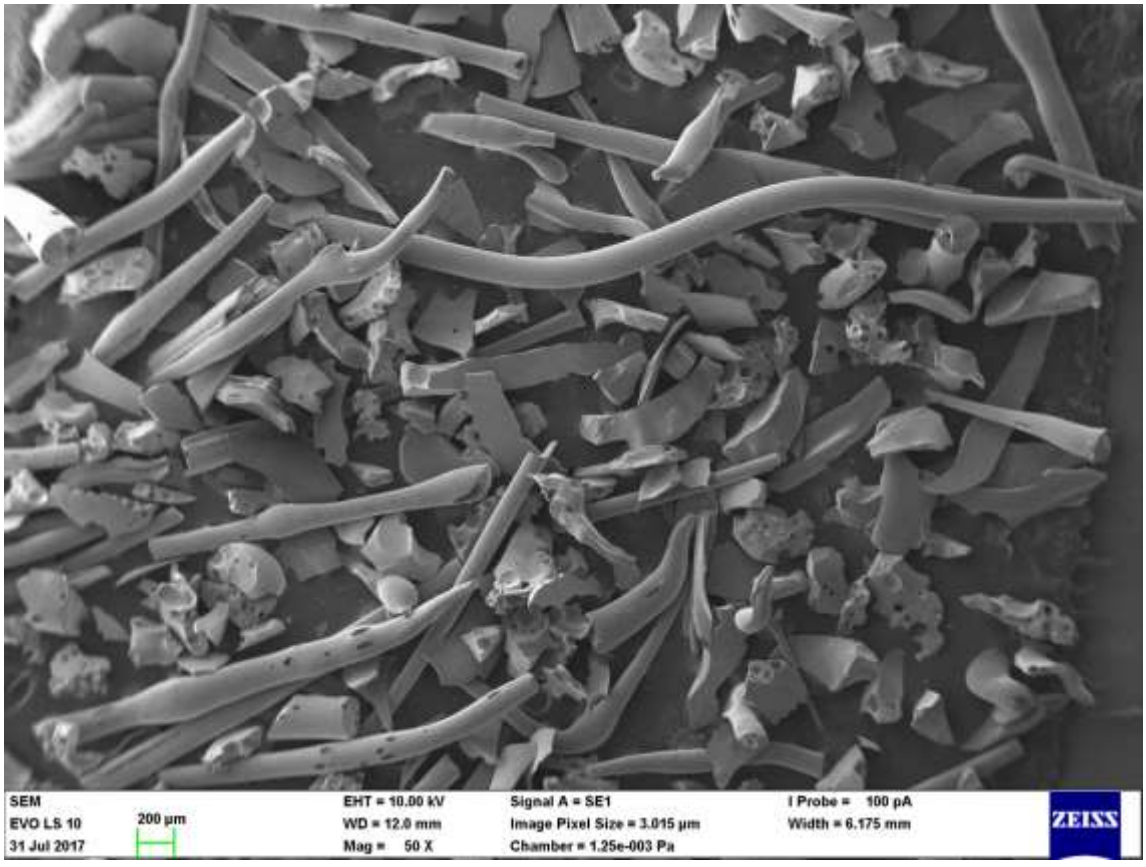

Figure 83: *SEM image of GBFS morphology; magnitude 50x.*

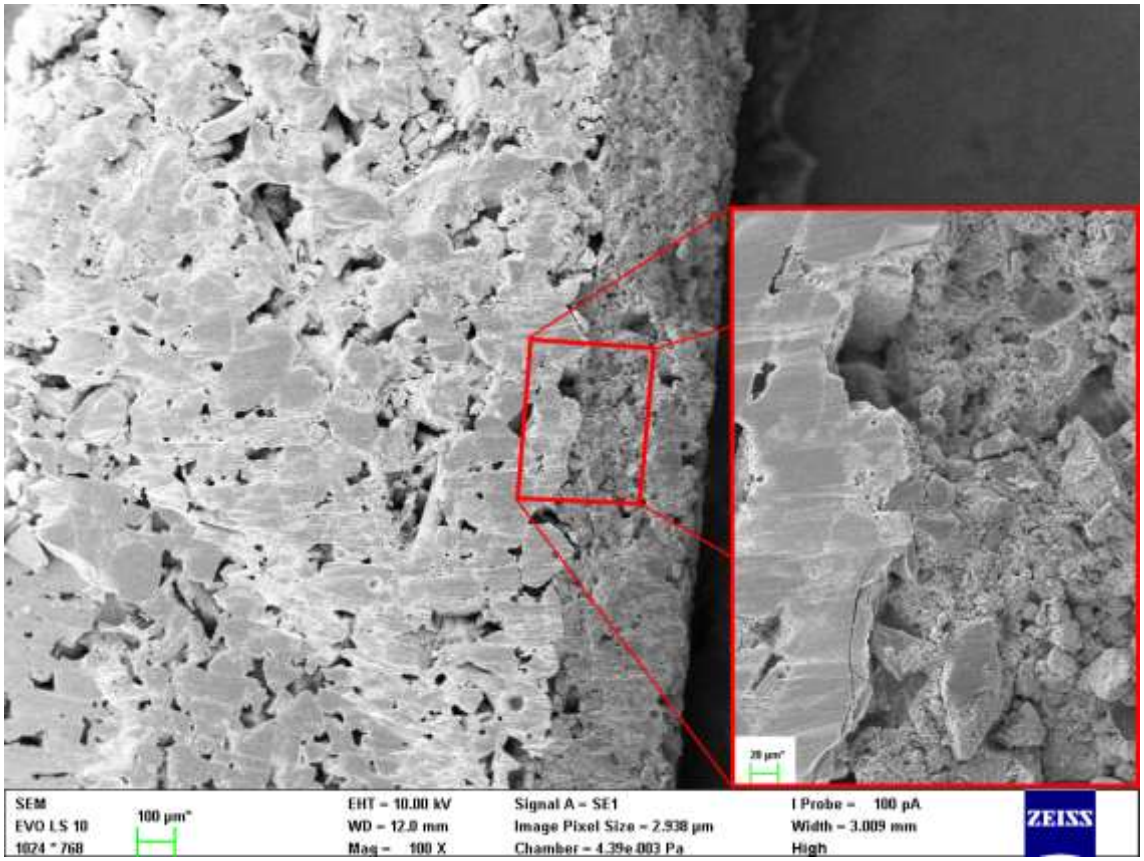

Figure 84: *Asymmetrical porous body SEM image; magnitude 100x + 500x cutout.*

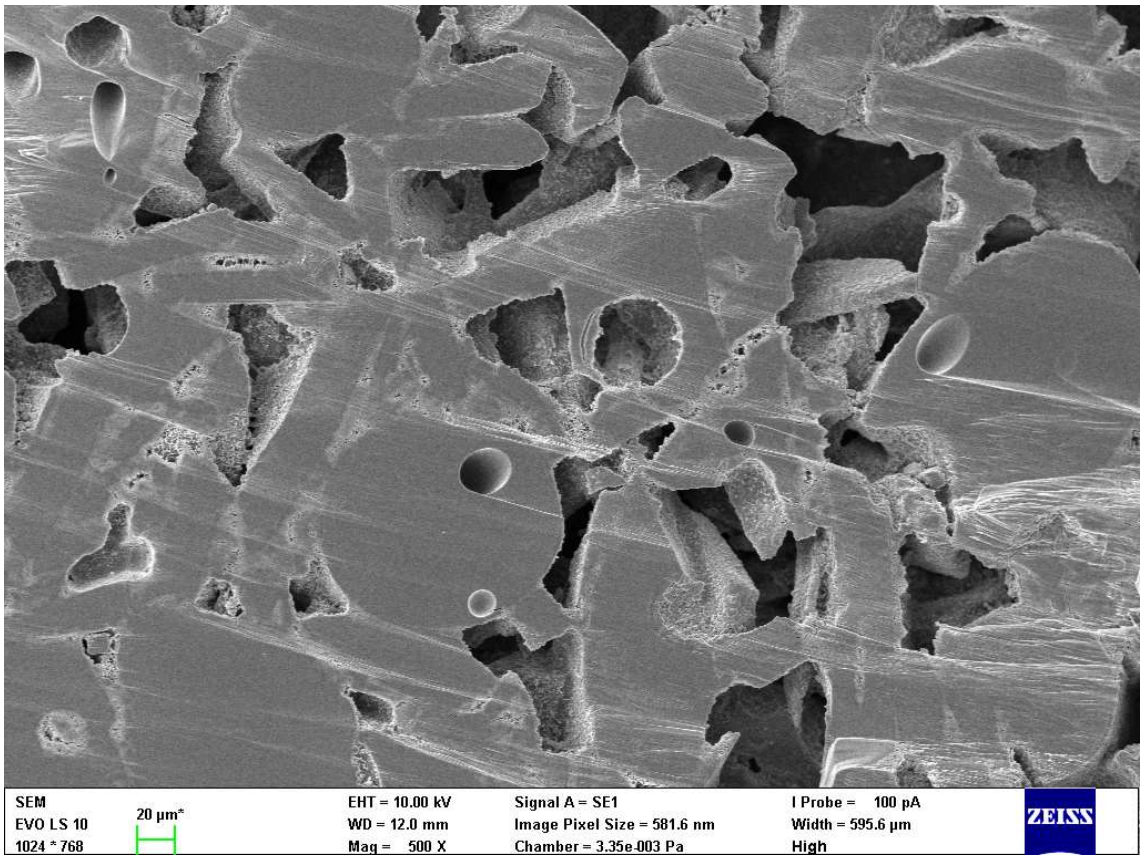

Figure 85: *Coarse supporting body structure; magnitude 500x.*

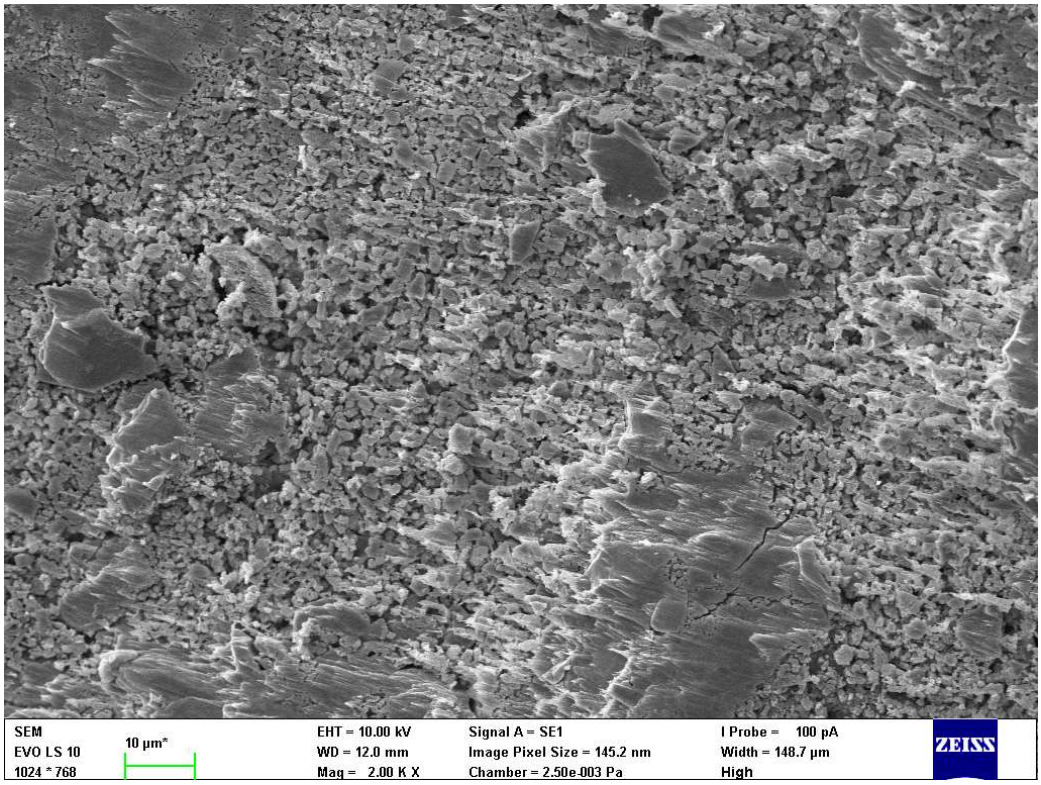

Figure 86: *Fine filtering layer; magnitude 2000x.*

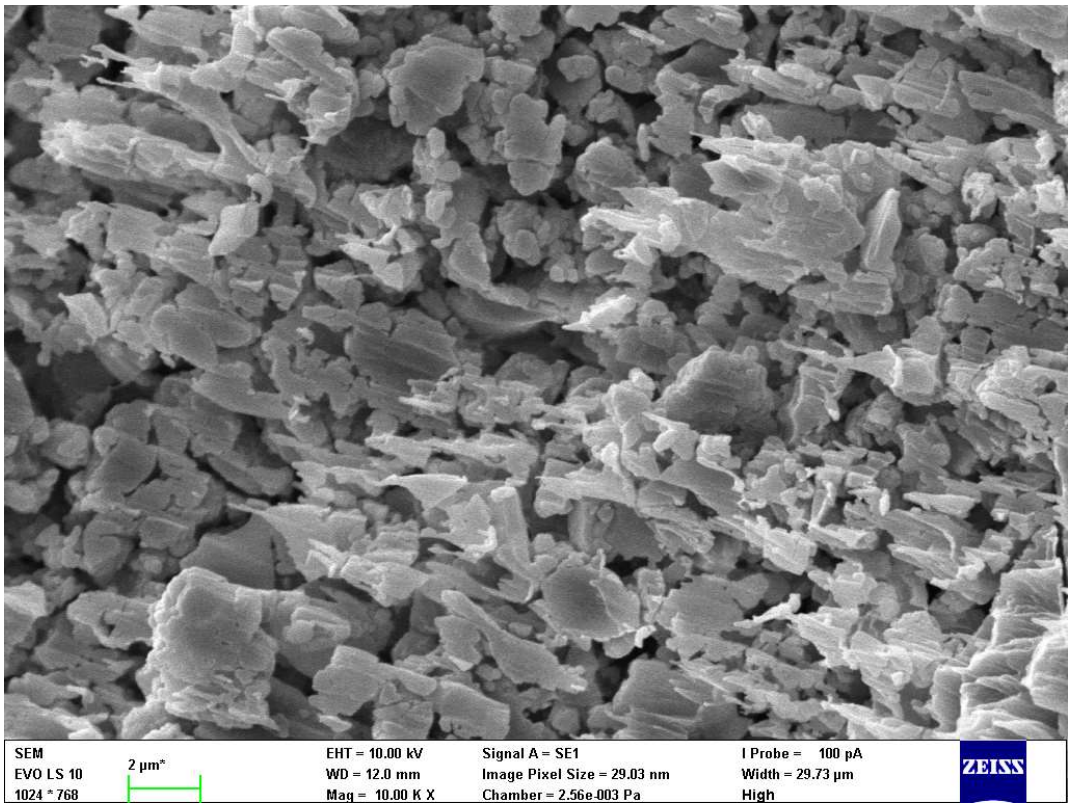

Figure 87: *Fine filtering layer; magnitude 10000x.*

Note: *The previous micrographs from SEM show ion beam polished surfaces on the cut of assymetrical barrier (Figure 84), supporting coarse layer of the asymmetrical barrier (Figure 85) and the fine filtering layer alone (Figure 86 and 87). The peaked sharply pointed structures that can be seen especially in the micrographs of the fine-structure material (Figures 80, 86 and 87) were caused by the ion beam polishing of the very fine porous structure. The principle of the polishing/BIB milling process is shown in Figure 88. An ion beam removes approximately 100 µm of sample material in most cases leaving a planar surface that allows high-resolution imaging (Philipp et Amann-Hildenbrand; 2017).*

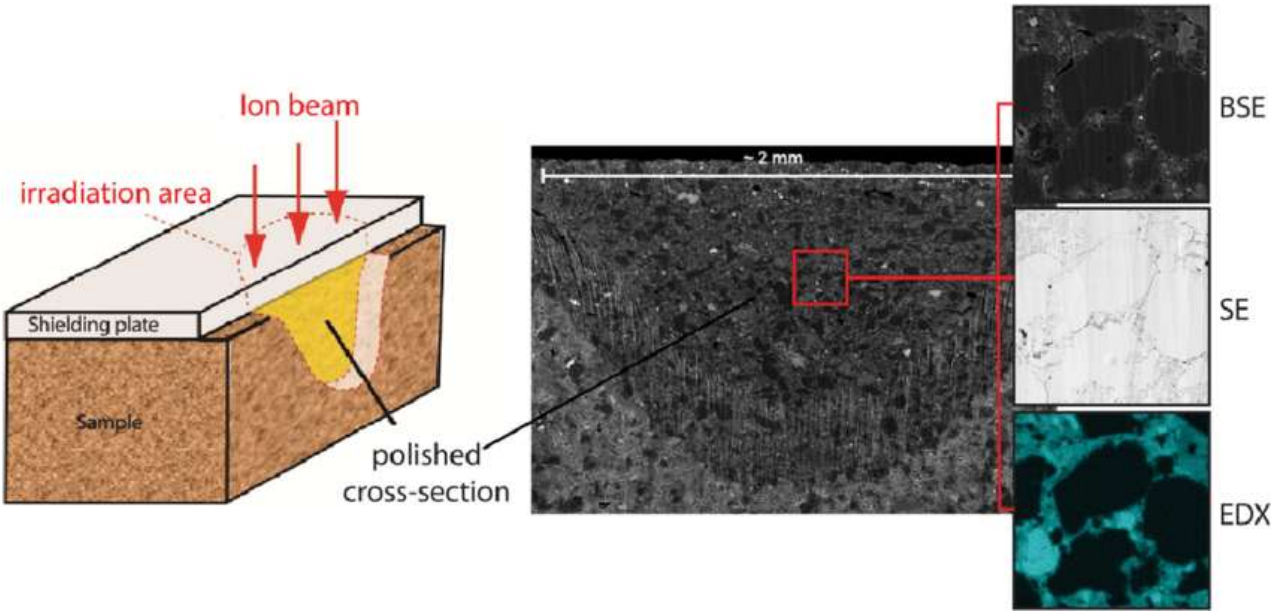

Figure 88: *BIB milling principle (Philipp et Amann-Hildenbrand; 2017).*

The results showed that the material is suitable for use in filtration media production. The only thing that remains to be resolved in the future is the optimization of the production procedures to improve the uniformity of the produced filtration barriers. Mainly the mechanism of application of the fine layer on top of the coarse layer is an issue. In ceramics this type of membrane could be manufactured via dipping the surface of the coarser support into the sludge or slurry of the fine material dispersed in water one or multiple times to build up an even and very thin layer. In this case though the mixture is necessarily in form of loose and lightly moist bulk material and further dilution would directly affect the mechanism of reaction and resulting mechanical properties. Therefore the deposition has to be done only mechanical way.

By other means the overall practicability of the material seems very promising and with other sharp fractions segregated it can be applied similar to other inorganic filters, to tailor the filtration media of different pore diameters and overall geometries with emphasis on the particular application.

6 DISCUSSION

The results of the study confirm that alkali activated secondary raw materials emphasizing blast furnace slag can be utilized to produce porous media with good strength parameters. The strength of the best porous materials prepared in the experimental part of the work are comparable to those of fly-ash based filtration membranes sintered at 800 °C du to literature (Singh et Bularasa, 2013).

Based on the strength results listed in this work, GGBFS seems to be more suitable for membrane material preparation than FA. However BFS issue when compared to FA is that its particles are angular, and when they are in contact with each other along their edges or walls, continuous porosity is reduced compared to round FA particles. On the other hand, through this principle GGBFS has a greater potential to build firmer links between the particles.

Understanding the main processes and patterns in the given alkali-activated materials' behavior led to the choice of one composition which could optimally combine strength and porosity. The composition chosen in this step was the driest possible one from the MATLAB-based dataset which combined the majority of the GGBFS to maintain the best strength, yet still maintained some of the fly ash and bauxite to preserve the best oxide ratios, better porosity and to reduce the inconsiderable shrinkage and tendency to crack while drying which the purely slag-based materials suffered from (Bílek et al., 2016). Addressing the shrinkage, the measurements showed that while purely FA-based bodies had, on average, a diameter of 25.55 mm after curing, purely slag-based samples' diameter was 25.36 mm, and the bodies made from the final mixture were 25.46 mm, which indicates a reduction in filter shrinkage by approximately half.

The data from the four-point uniaxial tensile tests of the columns made of various composition mixtures follow the regularities known for geopolymers. For the purpose of the work parameters P1 (SiO_2/Al_2O_3 ratio), P2 (Na_2O/Al_2O_3 ratio), P3 (H_2O/Na_2O ratio) and w/s (water to solids ratio) were established and the properties were observed from these parameters point of view.

The strength dependence on the SiO_2/Al_2O_3 ratio was proved to follow the precedent that, in the given range of approx. 2.7–3.2, the homogeneity of the material structure and thus its overall strength increases (and porosity decreases) with an increase in the ratio value corresponding to the results published by Duxson et al (2005).

The strong influence of the Na_2O/Al_2O_3 ratio on strength was verified in the strength results of the FA and S series of mixtures, which all have the same SiO_2/Al_2O_3 ratio within their groups. The Na_2O/Al_2O_3 ratio was very convincingly proved to show the best strength results when around unity as assumed based on the literature (Rowles et O'Connor, 2003; Duxson et al, 2005). In this case, the strength results do not match the conclusion that the concentration of the alkali activator for optimum strength of alkali activated BFS is 14 M (Singh et al, 2016). The literature-presented concentration is closest to composition S-4 (approx. 13.4M) but S-5 (approx. 16.2 M) had an 18% higher flexural strength than S-4.

The H_2O/M_2O ratio, that Kriven, Barbosa, Hos etc. had used for geopolymer characterization was found to be insufficient to characterize the material consistency and workability which was intended to be the main role of the parameter. Additionally, no visible dependence on the strength of the materials was observed due to the results, but it was not the main aim of this work so the compositions were not well-suited for the task. For ongoing work, the simple water to solids ratio (w/s) was adopted instead. This parameter was found to be the most appropriate for the workability characterization and in terms of final material strength influence was shown to be

important. The data show that within the examined w/s range, the strength of the final material decreases with an increase in the w/s ratio of the mixture.

The porosimetry measurements were performed via the MIP and CFP methods. The MIP method measures all opened pores, including dead-ends in the pore network, thus it better describes the overall nature of the material's porous structure. The CFP method is sensitive only to through-pores and better describes the permeability and potential filtering ability of the media. The results of the two methods therefore not only differ but show the porosity from two different perspectives. Both, however, mostly share the same final conclusions in terms of mixture-composition parameters to final material porosity dependencies for the FA and S series. Only in most cases one method shows it more visibly then the other. Both the FA and S series matched the assumption that by increasing the alkali activator concentration the strength increases significantly – in terms of porosity this means that pores are getting smaller, apparently due to the increasing ability of the activator to dissolve the surface layers of the particles and create thicker and thus stronger necks between them in the condensation stage. A downside of this process is that the material becomes more homogenous (with a greater amount of gepolymer gel, which binds the mass together) and the overall porosity thus decreases with the decrease in average pore diameter and also closure of many pores. The process of concentrating the alkali activator can be perceived as an increase in the sintering temperature of ceramics, which, also due to more material melting, creates wider and stronger necks between the particles but also decreases the porosity of the final product.

All of these facts make perfect sense when imagining the process on the scale of individual particles and wetting of their surface by the activator, which in a specific range of amounts only fills the spaces around the contact sites of the particles due to capillary drag and until a certain w/s limit the necks are only getting wider. It is, however, important to note that the range where this phenomenon occurs is specific to certain particles' granulometry, and even their morphology and the fluid ingredient resulting gel thickness. The overall importance of the finding is that this range should be always found in cases where the porosity of the final material is of interest and the amount of alkali activator should be optimized for the given case to create strong bonds but subvert the porosity as little as possible.

The SEM microphotographs show the necking phenomenon very clearly when comparing the pictures of classified raw material and the final AAM structure. The main factor which changes between them is the occurrence of necks bonding them together. Of course, with GGBFS the effect of smoothing the edges of the particles by etching caused by the alkali activator can also be observed in the unpolished surface micrographs.

One of the limitations of this study's results clarity is in one of its main focuses, the MATLAB computational mixture compositions. Although these were chosen to cover the intended range of values of all the parameters, they were mostly divergent in other variables. Then in certain cases their results do not follow the dependencies in the diagrams as clearly as they would if there were more series of samples compiled with only one variable changing through each of them. Without extensive understanding of the effects influencing the material properties, the diagrams of the MATLAB-designed series may seem disordered in some cases. Therefore, the otherwise unclear patterns were covered by designing the pure FA and S series, which plainly change only

the variables P2 (Na_2O/Al_2O_3 ratio) and P3 (H_2O/Na_2O ratio) to show the regularities in the observed properties they affect.

A second limitation is that the materials used (GGBFS and FA) may vary widely in composition depending on the factory they came from and also the production conditions. Every batch of blast furnace slag can differ which applies even more to every batch of fly ash that largely depends on the quality and composition of the coal used and the conditions it was burned in. This is, however, one of the reasons why it is very useful to utilize such instruments as the MATLAB calculation scheme when designing the AAM mixtures that takes the composition of the specific material into account and adapts the dose of every component accordingly.

The last thing to note was the manual compaction of the tensile testing columns when compared to the filtering barriers made by press molding under defined pressure, which translates to slightly different uniformity (and thus porosity and strength parameters) of the resulting bodies. The only other way to achieve the desired specimen cross section would be to apply the same pressure molding method (as with barriers) in a vertical oriented mold. This process was, however, found to be inapplicable due to high energy dissipation to the walls of the mold, causing very uneven longwise compaction of the samples. It was almost impossible to demold the columns without damaging them even though different types of mold separators and techniques were applied to improve the demolding process. The tensile testing columns were therefore made in ordinary dismountable molds by manual compaction. With such dry mixtures, however, the utilization of a vibrational stool would not properly compact the material, therefore the manual compaction was applied. Although the ultimate strength of the manually compacted columns may not exactly meet the strenght of press-molded bodies, the tensile testing results are a good indicator of the materials' mutual mechanical properties because the manual compaction procedure was normalized to increase the uniformity of the products as much as possible.

Addressing the final composition X, it must be said that approximately 7% of pores in the narrow distribution of approx. 0.19 μm in diameter from the CFP analysis may not seem very convincing. However, it is important to note that those are only the pores which go all the way through 2 mm-thick bodies, which gives an aspect ratio of 1:5,000 width to length of the through-pores (furthermore neglecting the tortuosity). This is of great importance and should be taken into consideration. This also applies to pores of the ambient widths (see Figure 79).

A fact that also plays a role is that the mixtures were spread manually across the molds and some regions were, unfortunately, more compacted than others. To verify this idea, some bodies from the same material were pressed under twice the pressure and they clearly showed significantly lower porosity. As a part of the conclusion it should therefore be noted that the production process should be further optimized, or, in the best case, automated to exploit better spreading, lower pressure, better uniformity and lower thicknesses. This would lead to a significant increase in the number of through-pores. This, however, is one of the suggestions for further research.

7 CONCLUSION

The aim of this work was to prepare and optimize inorganic porous media based on alkali-activated secondary raw materials to find out whether such material could be suitable for filtration praxis. The main reason for this research was that conventional inorganic materials use primary resources, a lot of energy and are thus more expensive and harmful to the environment.

The obvious goal of every filtration technique is to separate maximal quantum of one phase with minimal resistance to the other phase flow, because apart from the collection effectivity, one of the most important properties for every porous material used for filtration applications is its permeability. In general, a higher permeability can be obtained by either increasing the pore volume fraction, the pore size (which reduces the capture performance), or in best case increasing the pore-connectivity. It has to be also taken into account that the overall higher porosity always tend to impair the mechanical properties of the product. The optimization between porosity and mechanical strength is therefore always a key feature of filtration media design because it is impossible to obtain maximum values in both these factors. In this case the obtained through-porosity of the final material was good considering the fact that the filtration bodies' thicknesses were 4 orders of magnitude higher than the width of individual pores. The strength of the material of over 6 MPa is also perfectly acceptable.

The combination of a majority of GGBFS due to its better strength while bonded via alkali activation and minor fraction of FA due to the round shape of its particles, which properly complement the microstructure, seem very promising. Furthermore, it was observed that the FA admixture has the ability to reduce the unfavorable GGBFS shrinkage which was further proved by literature found later (Ye et Radlińska, 2016) and it possibly even improves the chemical resistance of the final material (Pařízek et al, 2016).

The idea for the topic of this work and its main aim came from the fact that contemporary inorganic porous materials share the same principle – connecting particles of inorganic material together to form a porous structure of certain properties, only each of them different way. But why to use primary resources which are more and more precious, expensive and need an extra step which consumes a lot of energy (e.g. sintering ceramics or clinker production)? Fly ash and blast furnace slag, even already used in a few applications, are still high-volume industrial wastes but because they possess favorable properties in the form of their pozzolanic activity, should be utilized much more to avoid the practice of landfilling them without further attention and consuming more primary resources instead.

Partial objectives of the work were sufficiently met with available resources. The first – to demonstrate a low-cost method for making porous filter media accompanied the whole work and the only issue is that for future utilization, some level of automation of spreading out and pressing the material is needed to obtain even better values and repeatability of the results.

Second partial aim was to tailor the pore microstructure by varying the content and size of ingredients. This objective was met by fractionation of the ingredients and varying their content into various mixtures due to very robust experimental design based on calculation rather than tentative determination of the compositions.

The third and fourth partial aims were to affect the pore microstructure with attention to permeability and with attention to mechanical strength. These two objectives have clearly contradictory goals but share the main idea of porous structure research – to find an optimum in

which the porosity and strength of the final material meet in the best ratio within the preset conditions. The optimal zone of the investigated AAM strength and porosity was found to be shifted towards the BFS, although the FA admixture (along with bauxite) still plays an important role in the system.

The last partial aim was to illustrate a novel filtration material which is both fast and effective, which the final composition of the alkali-activated mixtures is perfectly capable of accomplishing with sufficiently developed technology for the barriers preparation. The microstructure of the material looks very promising and the level of strength the material exhibits with that level of porosity is very good. The issue and subject for further research is to prepare the membrane (from this kind of very dry mixture) sufficiently thin in order to verify the filtration properties of such barriers in practical applications.

8 REFERENCES

AZARSHAB, Mohammadreza, Farzaneh MOHAMMADI, Hojjatollah MAGHSOODLOORAD a Toraj MOHAMMADI. Ceramic membrane synthesis based on alkali activated blast furnace slag for separation of water from ethanol. Ceramics International [online]. 2016, 42(14), 15568-15574 [cit. 2018-06-06]. DOI: 10.1016/j.ceramint.2016.07.005. ISSN 02728842. Dostupné z: http://linkinghub.elsevier.com/retrieve/pii/S0272884216310598

BAKHAREV, T. Geopolymeric materials prepared using Class F fly ash and elevated temperature curing. Cement and Concrete Research [online]. 2005, 35(6), 1224-1232 [cit. 2018-04-30]. DOI: 10.1016/j.cemconres.2004.06.031. ISSN 00088846. Dostupné z: http://linkinghub.elsevier.com/retrieve/pii/S0008884604002844

BARBOSA, Valeria F.F, Kenneth J.D MACKENZIE a Clelio THAUMATURGO. Synthesis and characterisation of materials based on inorganic polymers of alumina and silica: sodium polysialate polymers. International Journal of Inorganic Materials [online]. 2000, 2(4), 309-317 [cit. 2018-05-29]. DOI: 10.1016/S1466-6049(00)00041-6. ISSN 14666049. Dostupné z: http://linkinghub.elsevier.com/retrieve/pii/S1466604900000416

BELL, Jonathan L., Patrick E. DRIEMEYER a Waltraud M. KRIVEN. 2009. Formation of Ceramics from Metakaolin-Based Geopolymers: Part I-Cs-Based Geopolymer. *Journal of the American Ceramic Society*. 92(1): 1-8. DOI: 10.1111/j.1551-2916.2008.02790.x.

BÍLEK, Vlastimil, Lukáš KALINA, Radoslav NOVOTNÝ, Jakub TKACZ a Ladislav PAŘÍZEK. Some Issues of Shrinkage-Reducing Admixtures Application in Alkali-Activated Slag Systems. Materials [online]. 2016, 9(6), 462- [cit. 2018-04-30]. DOI: 10.3390/ma9060462. ISSN 1996-1944. Dostupné z: http://www.mdpi.com/1996-1944/9/6/462

BILIM, Cahit, Okan KARAHAN, Cengiz Duran ATIŞ a Serhan İLKENTAPAR. Effects of chemical admixtures and curing conditions on some properties of alkali-activated cementless slag mixtures. KSCE Journal of Civil Engineering [online]. 2015, 19(3), 733-741 [cit. 2018-04-30]. DOI: 10.1007/s12205-015-0629-0. ISSN 1226-7988. Dostupné z: http://link.springer.com/10.1007/s12205-015-0629-0

BILIM, Cahit, Okan KARAHAN, Cengiz Duran ATIŞ a Serhan İLKENTAPAR. Influence of admixtures on the properties of alkali-activated slag mortars subjected to different curing conditions. Materials & Design [online]. 2013, 44, 540-547 [cit. 2018-04-30]. DOI: 10.1016/j.matdes.2012.08.049. ISSN 02613069. Dostupné z: http://linkinghub.elsevier.com/retrieve/pii/S0261306912005882

BULEJKO, Pavel, Tomáš SVĚRÁK, Pavel KEJÍK, Ondřej KRIŠTOF a Kateřina SIKOROVÁ. The potential use of geopolymer-based materials in filtration applications. In: 21st International Congress of Chemical and Process Engineering, CHISA 2014 and 17th

Conference on Process Integration, Modelling and Optimisation for Energy Saving and Pollution Reduction, PRES 2014. Praha: Czech Society of Chemical Engineering, 2014, s. 600.

BULEJKO, Pavel a Tomáš SVĚRÁK. Mechanical and filtering properties of non-sintered porous solids for filtration applications. In: 20th International Conference on Engineering Mechanics 2014. Svratka: Czech Society of Chemical Engineering, 2014, s. 112-115.

BULEJKO, Pavel a Vlastimil BÍLEK Jr. Influence of chemical additives and curing conditions on the mechanical properties and carbonation resistance of alkali-activated slag composites. Materiali in tehnologije [online]. 2017, 51(1), 49-53 [cit. 2018-04-30]. DOI: 10.17222/mit.2015.185. ISSN 15802949. Dostupné z: http://mit.imt.si/Revija/izvodi/mit171/bulejko.pdf

CAO, Jingjie, Xinfa DONG, Lingling LI, Yingchao DONG a Stuart HAMPSHIRE. Recycling of waste fly ash for production of porous mullite ceramic membrane supports with increased porosity. Journal of the European Ceramic Society [online]. 2014, 34(13), 3181-3194 [cit. 2018-06-02]. DOI: 10.1016/j.jeurceramsoc.2014.04.011. ISSN 09552219. Dostupné z: http://linkinghub.elsevier.com/retrieve/pii/S095522191400199X

Carl Zeiss AG. ZEISS EVO: Scanning Electron Microscope [online]. 07745 Jena, Germany: Carl Zeiss Microscopy, 2017 [cit. 2017-11-17]. Dostupné z: https://www.zeiss.com/microscopy/int/products/scanning-electron-microscopes/evo.html

COLLEPARDI, Mario. The New Concrete. 2nd ed. Grafiche Tintoretto, 2010, 346 s. ISBN 8890377720. 9788890377723.

ČERŇANSKÝ, A., PECIAR, M. Separačné procesy I: Hydromechanické procesy. 1st ed. Bratislava: Vydavateľstvo STU, 2008. 277 p. ISBN 978-80-227-2800-3.

DAVIDOVITS, Joseph. 2008. *Geopolymer: chemistry*. 2nd ed. Saint-Quentin: Institute Géopolymère, 587 s. ISBN 29-514-8201-9.

DUAN, Ping, Chunjie YAN, Wei ZHOU a Daming REN. Development of fly ash and iron ore tailing based porous geopolymer for removal of Cu(II) from wastewater. Ceramics International [online]. 2016, 42(12), 13507-13518 [cit. 2018-06-06]. DOI: 10.1016/j.ceramint.2016.05.143. ISSN 02728842. Dostupné z: http://linkinghub.elsevier.com/retrieve/pii/S0272884216307490

DULLIEN, F. 1979. *Porous media: fluid transport and pore structure*. New York: Academic Press, xx, 396 p. ISBN 29-514-8201-9.

DUXSON, Peter, John L. PROVIS, Grant C. LUKEY, Seth W. MALLICOAT, Waltraud M. KRIVEN a Jannie S.J. VAN DEVENTER. Understanding the relationship between

geopolymer composition, microstructure and mechanical properties. Colloids and Surfaces A: Physicochemical and Engineering Aspects [online]. 2005, 269(1-3), 47-58 [cit. 2018-05-28]. DOI: 10.1016/j.colsurfa.2005.06.060. ISSN 09277757. Dostupné z: http://linkinghub.elsevier.com/retrieve/pii/S0927775705004966

ENGELHARDT, Günter, Endel LIPPMAA a Märt MÄGI. Ordering of silicon and aluminium ions in the framework of NaX zeolites. A solid-state high-resolution 29 Si n.m.r. study. J. Chem. Soc., Chem. Commun [online]. 1981, (14), 712-713 [cit. 2018-05-29]. DOI: 10.1039/C39810000712. ISSN 0022-4936. Dostupné z: http://xlink.rsc.org/?DOI=C39810000712

EOM, Jung-Hye, Young-Wook KIM, Santosh RAJU, David Stanley SMITH, Sylvie ROSSIGNOL a S. ROSSIGNOL. 2013. Processing and properties of macroporous silicon carbide ceramics: A review. *Journal of Asian Ceramic Societies*. 1(3): 220-242. DOI: 10.1016/j.jascer.2013.07.003. ISSN 21870764. Dostupné z: http://linkinghub.elsevier.com/retrieve/pii/S2187076413000523

ESPINAL, Laura, F. GOLESTANI-FARD, A.R. MIRHABIBI, G.M. NASAB, K.J.D. MACKENZIE a M.H SHAHRAKI. 2002. Porosity and Its Measurement. *Characterization of Materials*. Hoboken, NJ, USA: John Wiley, 41(6): 7872-7880. DOI: 10.1002/0471266965.com129. ISBN 0471266965. ISSN 02728842. Dostupné z: http://doi.wiley.com/10.1002/0471266965.com129

EVERETT, D. H. 1972-01-1. Manual of Symbols and Terminology for Physicochemical Quantities and Units, Appendix II: Definitions, Terminology and Symbols in Colloid and Surface Chemistry. *Pure and Applied Chemistry*. 31(4): -. DOI: 10.1351/pac197231040577. ISSN 1365-3075. Dostupné z: http://www.degruyter.com/view/j/pac.1972.31.issue-4/pac197231040577/pac197231040577.xml

FANG, Jing, Guotong QIN, Wei WEI, Xinqing ZHAO a Lei JIANG. Elaboration of new ceramic membrane from spherical fly ash for microfiltration of rigid particle suspension and oil-in-water emulsion. Desalination [online]. 2013, 311, 113-126 [cit. 2018-04-30]. DOI: 10.1016/j.desal.2012.11.008. ISSN 00119164. Dostupné z: http://linkinghub.elsevier.com/retrieve/pii/S0011916412006030

FENG, Dingwu, John L. PROVIS, Jannie S. J. DEVENTER, A. Van RIESSEN, W. RICKARD a J. SANJAYAN. 2011. Thermal Activation of Albite for the Synthesis of One-Part Mix Geopolymers. *Journal of the American Ceramic Society*. 95(2): 315-342. DOI: 10.1533/9781845696382.2.315.

FOX, John M. Fly Ash Classification: Old and New Ideas. In: 2017 World of Coal Ash [online]. Lexington, KY, 2017, s. 1-19 [cit. 2018-04-30].. Dostupné z: http://www.flyash.info/2017/026-Fox-woca2017p.pdf

GIASUDDIN, Haider M., Jay G. SANJAYAN, P.G. RANJITH, C. PEYRATOUT, A. SMITH, S. ARRII-CLACENS, J.M. CLACENS a S. ROSSIGNOL. 2013. Strength of geopolymer cured in saline water in ambient conditions: A review. *Fuel*. 107(7): 34-39. DOI: 10.1016/j.fuel.2013.01.035. ISSN 00162361. Dostupné z: http://linkinghub.elsevier.com/retrieve/pii/S0016236113000446

HE, Peigang, Dechang JIA, Meirong WANG a Yu ZHOU. 2011. Thermal evolution and crystallization kinetics of potassium-based geopolymer. *Ceramics International*. 37(1): 59-63. DOI: 10.1016/j.ceramint.2010.08.008.

HENON, Joseph, Arnaud ALZINA, Joseph ABSI, David Stanley SMITH, Sylvie ROSSIGNOL a S. ROSSIGNOL. 2012. Porosity control of cold consolidated geomaterial foam: Temperature effect. *Ceramics International*. 38(1): 77-84. DOI: 10.1016/j.ceramint.2011.06.040. ISSN 02728842. Dostupné z: http://linkinghub.elsevier.com/retrieve/pii/S0272884211005827

HARDJITO, Djwantoro, Steenie E. WALLAH, Dody M. J. SUMAJOUW a Rangan B. V. Factors Influencing the Compressive Strength of Fly ash-Based Geopolymer Concrete. In: Civil Engineering Dimension. Vol. 6, No. 2. 2004, s. 88-93. DOI: 10.9744/ced.6.2.pp.%2088-93. ISSN 1410-9530.

HARDJITO, Djwantoro, Chua Chung CHEAK a Carrie Ho LEE ING. Strength and Setting Times of Low Calcium Fly Ash-based Geopolymer Mortar. Modern Applied Science [online]. 2009, 2(4), - [cit. 2018-04-30]. DOI: 10.5539/mas.v2n4p3. ISSN 1913-1852. Dostupné z: http://www.ccsenet.org/journal/index.php/mas/article/view/2403

Hosokawa Alpine Turboplex Classifier ATP: Centrifugal Force Classifier. Hosokawa Micron Corporation [online]. [cit. 2016-03-10]. Dostupné z: http://www.hosokawamicron.co.jp/en/machines/136

Hosokawa Alpine Isolator + Jet Mill AS. 2011. SCHMID-SCHWARZER, B. YouTube [online]. [cit. 2015-06-18]. Dostupné z: https://www.youtube.com/watch?v=ib7LFQM-NCA

Hosokawa Alpine Air Jet Sieve e200 LS: Principle of Operation. 2012. SCHMID-SCHWARZER, B. YouTube [online]. [cit. 2015-06-18]. Dostupné z: https://www.youtube.com/watch?v=5QCFt21WhqA

HUANG, Yi a Minfang HAN. 2011. The influence of α-Al2O3 addition on microstructure, mechanical and formaldehyde adsorption properties of fly ash-based geopolymer products. *Journal of Hazardous Materials*. 193: 90-94. DOI: 10.1016/j.jhazmat.2011.07.029.

HLAVÁČEK, Petr. Engineering properties of alkali activated composites. Praha, 2014. Doctoral Thesis. Czech Technical University in Prague. Supervisor Vít Šmilauer.

CHAOUCHE, Mohend, Xiao Xiao GAO, Martin CYR, Marine COTTE a Laurent FROUIN. On the origin of the blue/green color of blast-furnace slag-based materials: Sulfur K-edge XANES investigation. Journal of the American Ceramic Society [online]. 2017, 100(4), 1707-1716 [cit. 2018-03-21]. DOI: 10.1111/jace.14670. ISSN 00027820. Dostupné z: http://doi.wiley.com/10.1111/jace.14670

CHEREMISINOFF, Nicholas P, J ROUQUEROL, K SING, P LLEWELLYN a G MAURIN. *Liquid filtration: principles, methodology and applications*. 2nd ed. /. Boston: Butterworth-Heinemann, 1998, xi, 319 p. ISBN 07-506-7047-9.

ICHIKAWA, Tsuneki a Masazumi MIURA. 2007. Modified model of alkali-silica reaction. *Cement and Concrete Research*. 37(9): 1291-1297. DOI: 10.1016/j.cemconres.2007.06.008. ISSN 00088846. Dostupné z: http://linkinghub.elsevier.com/retrieve/pii/S0008884607001329

ISHIZAKI, Kōzō, Sridhar KOMARNENI a M NANKO. 1998. *Porous materials: process technology and applications*. Boston: Kluwer Academic Publishers, viii, 240 p. Materials technology series (Kluwer Academic Publishers). ISBN 04-127-1110-9.

JEDIDI, Ilyes, Sabeur KHEMAKHEM, Sami SAÏDI, et al. Preparation of a new ceramic microfiltration membrane from mineral coal fly ash: Application to the treatment of the textile dying effluents. Powder Technology [online]. 2011, 208(2), 427-432 [cit. 2018-03-14]. DOI: 10.1016/j.powtec.2010.08.039. ISSN 00325910. Dostupné z: http://linkinghub.elsevier.com/retrieve/pii/S0032591010004316

JO, Y.M., R. HUCHISON a J.A. RAPER. Preparation of Ceramic Membrane Filters, From Waste Fly Ash, Suitable for Hot Gas Cleaning. Waste Management & Research [online]. 1996, 14(3), 281-295 [cit. 2018-04-30]. DOI: 10.1177/0734242X9601400304. ISSN 0734-242X. Dostupné z: http://journals.sagepub.com/doi/10.1177/0734242X9601400304

KAUR, Mandeep, Jaspal SINGH a Manpreet KAUR. Synthesis of fly ash based geopolymer mortar considering different concentrations and combinations of alkaline activator solution. Ceramics International[online]. 2018, 44(2), 1534-1537 [cit. 2018-03-14]. DOI: 10.1016/j.ceramint.2017.10.071. ISSN 02728842. Dostupné z: http://linkinghub.elsevier.com/retrieve/pii/S0272884217322630

KEJÍK, P. *Rozpustnost elektrárenských popílků ve vysoce alkalickém prostředí*. Brno: Vysoké učení technické v Brně, Fakulta chemická, 2010. 41 s. Vedoucí bakalářské práce Ing. František Šoukal, Ph.D.

KIM, Eric Heysung. Understanding effects of silicon/aluminumide ratio and calcium hydroxide on chemical composition, nanostructure and compressive strength for metakaolin geopolymers. Urbana, Illinois, 2012. Master Thesis. University of Illinois. Adviser: Leslie Struble.

KIM, Min Sik, Yubin JUN, Changha LEE a Jae Eun OH. Use of CaO as an activator for producing a price-competitive non-cement structural binder using ground granulated blast furnace slag. Cement and Concrete Research [online]. 2013, 54, 208-214 [cit. 2018-03-14]. DOI: 10.1016/j.cemconres.2013.09.011. ISSN 00088846. Dostupné z: http://linkinghub.elsevier.com/retrieve/pii/S000888461300197X

KING, C. 1980. *Separation processes*. 2d ed. New York: McGraw-Hill, xxvi, 850 p. ISBN 00-703-4612-7.

KOLEŻYŃSKI, Andrzej, Magdalena KRÓL a Mikołaj ŻYCHOWICZ. The structure of geopolymers – Theoretical studies. Journal of Molecular Structure [online]. 2018, 1163, 465-471 [cit. 2018-06-25]. DOI: 10.1016/j.molstruc.2018.03.033. ISSN 00222860. Dostupné z: http://linkinghub.elsevier.com/retrieve/pii/S0022286018303223

KONG, Daniel L.Y. a Jay G. SANJAYAN. Damage behavior of geopolymer composites exposed to elevated temperatures. Cement and Concrete Composites [online]. 2008, 30(10), 986-991 [cit. 2018-05-21]. DOI: 10.1016/j.cemconcomp.2008.08.001. ISSN 09589465. Dostupné z: http://linkinghub.elsevier.com/retrieve/pii/S0958946508001005

LANDI, Elena, Valentina MEDRI, Elettra PAPA, Jiri DEDECEK, Petr KLEIN, Patricia BENITO a Angelo VACCARI. 2013. Alkali-bonded ceramics with hierarchical tailored porosity. *Applied Clay Science*. Hoboken, NJ, USA: John Wiley, 73(6): 56-64. DOI: 10.1016/j.clay.2012.09.027. ISBN 0471266965. ISSN 01691317. Dostupné z: http://linkinghub.elsevier.com/retrieve/pii/S0169131712002578

LEE, N.K., Hammad R. KHALID a H.K. LEE. Adsorption characteristics of cesium onto mesoporous geopolymers containing nano-crystalline zeolites. Microporous and Mesoporous Materials [online]. 2017, 242, 238-244 [cit. 2018-04-30]. DOI: 10.1016/j.micromeso.2017.01.030. ISSN 13871811. Dostupné z: http://linkinghub.elsevier.com/retrieve/pii/S1387181117300306

LEE, Yu-Ri, June Thet SOE, Siqian ZHANG, Ji-Whan AHN, Min Bum PARK a Wha-Seung AHN. Synthesis of nanoporous materials via recycling coal fly ash and other solid wastes: A mini review. Chemical Engineering Journal [online]. 2017B, 317, 821-843 [cit. 2018-05-21]. DOI: 10.1016/j.cej.2017.02.124. ISSN 13858947. Dostupné z: http://linkinghub.elsevier.com/retrieve/pii/S1385894717302899

LIU, Jing, Yan HE, Yuan YUAN, Jing Lin HUANG a Xue Min CUI. The Preparation and Characterization of Geopolymer Based Inorganic Membranes. Key Engineering Materials

[online]. 2014, 602-603, 80-83 [cit. 2018-04-30]. DOI: 10.4028/www.scientific.net/KEM.602-603.80. ISSN 1662-9795. Dostupné z: http://www.scientific.net/KEM.602-603.80

LOTHENBACH, B. a A. GRUSKOVNJAK. Hydration of alkali-activated slag: thermodynamic modelling. Advances in Cement Research[online]. 2007, 19(2), 81-92 [cit. 2018-03-21]. DOI: 10.1680/adcr.2007.19.2.81. ISSN 0951-7197. Dostupné z: http://www.icevirtuallibrary.com/doi/10.1680/adcr.2007.19.2.81

LUYTEN, Jan, Steven MULLENS a Ivo THIJS. 2010. Designing with Pores - Synthesis and Applications. *KONA Powder and Particle Journal*. 28: 131-142. DOI: 10.14356/kona.2010012. ISSN 0288-4534. Dostupné z: http://jlc.jst.go.jp/DN/JST.JSTAGE/kona/2010012?lang=en

MARJANOVIĆ, N., M. KOMLJENOVIĆ, Z. BAŠČAREVIĆ, V. NIKOLIĆ a R. PETROVIĆ. Physical–mechanical and microstructural properties of alkali-activated fly ash–blast furnace slag blends. Ceramics International [online]. 2015, 41(1), 1421-1435 [cit. 2018-04-30]. DOI: 10.1016/j.ceramint.2014.09.075. ISSN 02728842. Dostupné z: http://linkinghub.elsevier.com/retrieve/pii/S0272884214014606

MASSAZZA, Franco. Pozzolanic cements. Cement and Concrete Composites [online]. 1993, 15(4), 185-214 [cit. 2018-06-06]. DOI: 10.1016/0958-9465(93)90023-3. ISSN 09589465. Dostupné z: http://linkinghub.elsevier.com/retrieve/pii/0958946593900233

MEDPELLI, Dinesh, Jung-Min SEO, Dong-Kyun SEO a F. GLASSER. Geopolymer with Hierarchically Meso-/Macroporous Structures from Reactive Emulsion Templating. Journal of the American Ceramic Society [online]. 2014, 97(1), 70-73 [cit. 2018-06-02]. DOI: 10.1111/jace.12724. ISSN 00027820. Dostupné z: http://doi.wiley.com/10.1111/jace.12724

MEDRI, Valentina a Andrea RUFFINI. 2012. Alkali-bonded SiC based foams. *Journal of the European Ceramic Society*. 32(9): 1907-1913. DOI: 10.1016/j.jeurceramsoc.2011.10.030. ISSN 09552219. Dostupné z: http://linkinghub.elsevier.com/retrieve/pii/S0955221911005401

MEDRI, Valentina, Elena LANDI, Santosh RAJU, David Stanley SMITH, Sylvie ROSSIGNOL a S. ROSSIGNOL. 2014. Recycling of porcelain stoneware scraps in alkali bonded ceramic composites: A review. *Ceramics International*. 40(1): 307-315. DOI: 10.1016/j.ceramint.2013.06.003. ISSN 02728842. Dostupné z: http://linkinghub.elsevier.com/retrieve/pii/S0272884213006573

MEMON, Fareed Ahmed, Muhd Fadhil NURUDDIN, Samuel DEMIE a Nasir SHAFIQ. Effect of Curing Conditions on Strength of Fly ash-based Self-Compacting Geopolymer Concrete. Construction and Architectural Engineering. 2011, 5(8), 1-4. DOI: doi.org/10.5281/zenodo.1070949.

MOHAMMADI, Farzaneh a Toraj MOHAMMADI. Optimal conditions of porous ceramic membrane synthesis based on alkali activated blast furnace slag using Taguchi method. Ceramics International [online]. 2017, 43(16), 14369-14379 [cit. 2018-06-06]. DOI: 10.1016/j.ceramint.2017.07.197. ISSN 02728842. Dostupné z: http://linkinghub.elsevier.com/retrieve/pii/S0272884217316450

MYERS, Rupert J., Susan A. BERNAL, Rackel SAN NICOLAS a John L. PROVIS. Generalized Structural Description of Calcium–Sodium Aluminosilicate Hydrate Gels: The Cross-Linked Substituted Tobermorite Model. Langmuir [online]. 2013, 29(17), 5294-5306 [cit. 2018-04-30]. DOI: 10.1021/la4000473. ISSN 0743-7463. Dostupné z: http://pubs.acs.org/doi/10.1021/la4000473

NASVI, M.C.M., P.G. RANJITH, J. SANJAYAN, J.-M. CLACENS, S. ARII-CLACENS, I. SOBRADOS, C. PEYRATOUT, A. SMITH, J. SANZ, et al. 2013. The permeability of geopolymer at down-hole stress conditions: Application for carbon dioxide sequestration wells. *Applied Energy*. 102(21): 1391-1398. DOI: 10.1016/j.apenergy.2012.09.004. ISSN 03062619. Dostupné z: http://linkinghub.elsevier.com/retrieve/pii/S0306261912006447

NASVI, M.C.M., P.G. RANJITH, J. SANJAYAN a H. BUI. 2014. Effect of temperature on permeability of geopolymer: A primary well sealant for carbon capture and storage wells. *Fuel*. 117: 354-363. DOI: 10.1016/j.fuel.2013.09.007. ISSN 00162361. Dostupné z: http://linkinghub.elsevier.com/retrieve/pii/S0016236113008363

NEDELJKOVIĆ, Marija, Branko ŠAVIJA, Yibing ZUO, Mladena LUKOVIĆ a Guang YE. Effect of natural carbonation on the pore structure and elastic modulus of the alkali-activated fly ash and slag pastes. Construction and Building Materials [online]. 2018, 161, 687-704 [cit. 2018-06-11]. DOI: 10.1016/j.conbuildmat.2017.12.005. ISSN 09500618. Dostupné z: http://linkinghub.elsevier.com/retrieve/pii/S0950061817324005

NEMATOLLAHI, Behzad a Jay SANJAYAN. Effect of different superplasticizers and activator combinations on workability and strength of fly ash based geopolymer. Materials & Design [online]. 2014, 57, 667-672 [cit. 2018-05-21]. DOI: 10.1016/j.matdes.2014.01.064. ISSN 02613069. Dostupné z: http://linkinghub.elsevier.com/retrieve/pii/S0261306914000934

NIKLIOĆ, I., S. MARKOVIĆ, I. JANKOVIĆ – ČASTVAN, V.V. RADMILOVIĆ, Lj. KARANOVIĆ, Biljana BABIĆ a V.R. RADMILOVIĆ. Modification of mechanical and thermal properties of fly ash-based geopolymer by the incorporation of steel slag. Materials Letters [online]. 2016, 176, 301-305 [cit. 2018-06-06]. DOI: 10.1016/j.matlet.2016.04.121. ISSN 0167577X. Dostupné z: http://linkinghub.elsevier.com/retrieve/pii/S0167577X16306267

PAGNI, John. Amroy aims to become nano-leader. *Plastics news Europe* [online]. 5 March 2010. [cit. 2015-06-09]. Dostupné z: http://www.europeanplasticsnews.com/subscriber/headlines2.html?cat=1

PACHECO-TORGAL, Fernando, João CASTRO-GOMES a Said JALALI. 2008. Alkali-activated binders: A review: Part 1. Historical background, terminology, reaction mechanisms and hydration products. *Construction and Building Materials*. 22(7): 1305-1314. DOI: 10.1016/j.conbuildmat.2007.10.015. ISSN 09500618. Dostupné z: http://linkinghub.elsevier.com/retrieve/pii/S0950061807002462

PAŘÍZEK, Ladislav, Vlastimil BÍLEK a Matěj BŘEZINA. Chloride Resistance of Alkali Activated Slag Pastes with Fly Ash Replacement. Materials Science Forum [online]. 2016, 851, 98-103 [cit. 2018-03-13]. DOI: 10.4028/www.scientific.net/MSF.851.98. ISSN 1662-9752. Dostupné z: http://www.scientific.net/MSF.851.98

PÉRA, Jean, Jean AMBROISE a Michel CHABANNET. Properties of blast-furnace slags containing high amounts of manganese. Cement and Concrete Research [online]. 1999, 29(2), 171-177 [cit. 2019-01-16]. DOI: 10.1016/S0008-8846(98)00096-9. ISSN 00088846. Dostupné z: http://linkinghub.elsevier.com/retrieve/pii/S0008884698000969

PHAIR, J.W., J.S.J. VAN DEVENTER a J.D. SMITH. Effect of Al source and alkali activation on Pb and Cu immobilisation in fly-ash based "geopolymers". Applied Geochemistry [online]. 2004, 19(3), 423-434 [cit. 2018-06-06]. DOI: 10.1016/S0883-2927(03)00151-3. ISSN 08832927. Dostupné z: http://linkinghub.elsevier.com/retrieve/pii/S0883292703001513

PHILIPP, T., A. AMANN-HILDENBRAND, B. LAURICH, G. DESBOIS, R. LITTKE a J. L. URAI. The effect of microstructural heterogeneity on pore size distribution and permeability in Opalinus Clay (Mont Terri, Switzerland): insights from an integrated study of laboratory fluid flow and pore morphology from BIB-SEM images. Geological Society, London, Special Publications [online]. 2017, 454(1), 85-106 [cit. 2018-07-17]. DOI: 10.1144/SP454.3. ISSN 0305-8719. Dostupné z: http://sp.lyellcollection.org/lookup/doi/10.1144/SP454.3

PIMRAKSA, K., P. CHINDAPRASIRT, A. RUNGCHET, K. SAGOE-CRENTSIL, T. SATO, C. LEONELLI, E. KAMSEU a V. M. SGLAVO. 2011. Lightweight geopolymer made of highly porous siliceous materials with various Na2O/Al2O3 and SiO2/Al2O3 ratios. *Materials Science and Engineering: A*. 528(21): 155-164. DOI: 10.1002/9780470456200.ch15.

POSTMA, H. W. Ch. 2001. Carbon Nanotube Single-Electron Transistors at Room Temperature. *Science*. 293(5527): 76-79. DOI: 10.1126/science.1061797. ISSN 00368075. Dostupné z: http://www.sciencemag.org/cgi/doi/10.1126/science.1061797

PRUD'HOMME, E., P. MICHAUD, E. JOUSSEIN, C. PEYRATOUT, A. SMITH, S. ARRII-CLACENS, J.M. CLACENS a S. ROSSIGNOL. 2010. Silica fume as porogent agent in geo-materials at low temperature: A review. *Journal of the European Ceramic Society*. 30(7): 307-

315. DOI: 10.1016/j.jeurceramsoc.2010.01.014. ISSN 09552219. Dostupné z: http://linkinghub.elsevier.com/retrieve/pii/S0272884213006573

PRUD'HOMME, E., P. MICHAUD, E. JOUSSEIN, C. PEYRATOUT, A. SMITH a S. ROSSIGNOL. 2011A. In situ inorganic foams prepared from various clays at low temperature. *Applied Clay Science*. 51(1-2): 15-22. DOI: 10.1016/j.clay.2010.10.016. ISSN 01691317. Dostupné z: http://linkinghub.elsevier.com/retrieve/pii/S0169131710003443

PRUD'HOMME, E., P. MICHAUD, E. JOUSSEIN, J.-M. CLACENS, S. ARII-CLACENS, I. SOBRADOS, C. PEYRATOUT, A. SMITH, J. SANZ, et al. 2011B. Structural characterization of geomaterial foams — Thermal behavior: A review. *Journal of Non-Crystalline Solids*. 357(21): 3637-3647. DOI: 10.1016/j.jnoncrysol.2011.06.033. ISSN 00223093. Dostupné z: http://linkinghub.elsevier.com/retrieve/pii/S0022309311004418

PUERTAS, F., M. PALACIOS, H. MANZANO, J.S. DOLADO, A. RICO a J. RODRÍGUEZ. A model for the C-A-S-H gel formed in alkali-activated slag cements. Journal of the European Ceramic Society [online]. 2011, 31(12), 2043-2056 [cit. 2018-04-30]. DOI: 10.1016/j.jeurceramsoc.2011.04.036. ISSN 09552219. Dostupné z: http://linkinghub.elsevier.com/retrieve/pii/S0955221911002159

PUERTAS, F., C. VARGA a M.M. ALONSO. Rheology of alkali-activated slag pastes. Effect of the nature and concentration of the activating solution. Cement and Concrete Composites [online]. 2014, 53, 279-288 [cit. 2018-03-14]. DOI: 10.1016/j.cemconcomp.2014.07.012. ISSN 09589465. Dostupné z: http://linkinghub.elsevier.com/retrieve/pii/S0958946514001309

PURDON, A. O. The action of alkalis on blast-furnace slag. J. Soc. Chem. Ind.- Trans. Commun. 1940, 59, 191-202.

PYTLÍK, Petr. Technologie betonu. 2. vyd. Brno: VUTIUM, 2000. Učebnice (VUTIUM). ISBN 80-214-1647-5.

QIN, Guotong, Xueqian LÜ, Wei WEI, Jiajia LI, Ruyue CUI a Shixuan HU. Microfiltration of kiwifruit juice and fouling mechanism using fly-ash-based ceramic membranes. Food and Bioproducts Processing [online]. 2015, 96, 278-284 [cit. 2018-04-30]. DOI: 10.1016/j.fbp.2015.09.006. ISSN 09603085. Dostupné z: http://linkinghub.elsevier.com/retrieve/pii/S0960308515001157

RASOULI, H.R., F. GOLESTANI-FARD, A.R. MIRHABIBI, G.M. NASAB, K.J.D. MACKENZIE a M.H SHAHRAKI. 2015. Fabrication and properties of microporous metakaolin-based geopolymer bodies with polylactic acid (PLA) fibers as pore generators. *Ceramics International*. 41(6): 7872-7880. DOI: 10.1016/j.ceramint.2015.02.125. ISSN 02728842. Dostupné z: http://linkinghub.elsevier.com/retrieve/pii/S0272884215003442

ROUQUEROL, J., D. AVNIR, C. W. FAIRBRIDGE, D. H. EVERETT, J. M. HAYNES, N. PERNICONE, J. D. F. RAMSAY, K. S. W. SING a K. K. UNGER. 1994-01-1. Recommendations for the characterization of porous solids (Technical Report). *Pure and Applied Chemistry*. 66(8). DOI: 10.1351/pac199466081739. ISSN 1365-3075. Dostupné z: http://www.degruyter.com/view/j/pac.1994.66.issue-8/pac199466081739/pac199466081739.xml

ROUQUEROL, Françoise, J ROUQUEROL, K SING, P LLEWELLYN a G MAURIN. *Adsorption by powders and porous solids: principles, methodology and applications*. Second edition. Boston, MA: Elsevier, 2008, xix, 626 pages. ISBN 00-809-7035-4.

EDITED BY NICOLAS ROUSSEL. Understanding the rheology of concrete. Cambridge: Woodhead Publishing, 2012. ISBN 9780857095282.

ROVNANÍK, Pavel. Effect of curing temperature on the development of hard structure of metakaolin-based geopolymer. Construction and Building Materials [online]. 2010, 24(7), 1176-1183 [cit. 2018-04-30]. DOI: 10.1016/j.conbuildmat.2009.12.023. ISSN 09500618. Dostupné z: http://linkinghub.elsevier.com/retrieve/pii/S0950061809004346

ROWLES, Matthew R. a Brian H. O'CONNOR. Chemical and Structural Microanalysis of Aluminosilicate Geopolymers Synthesized by Sodium Silicate Activation of Metakaolinite. Journal of the American Ceramic Society [online]. 2009, 92(10), 2354-2361 [cit. 2018-05-28]. DOI: 10.1111/j.1551-2916.2009.03191.x. ISSN 00027820. Dostupné z: http://doi.wiley.com/10.1111/j.1551-2916.2009.03191.x

RUNTTI, Hanna, Tero LUUKKONEN, Mikko NISKANEN, et al. Sulphate removal over barium-modified blast-furnace-slag geopolymer. Journal of Hazardous Materials [online]. 2016, 317, 373-384 [cit. 2018-04-30]. DOI: 10.1016/j.jhazmat.2016.06.001. ISSN 03043894. Dostupné z: http://linkinghub.elsevier.com/retrieve/pii/S0304389416305568

SAKULICH, A. R. a D. P. BENTZ. Mitigation of autogenous shrinkage in alkali activated slag mortars by internal curing. Materials and Structures [online]. 2013, 46(8), 1355-1367 [cit. 2018-04-30]. DOI: 10.1617/s11527-012-9978-z. ISSN 1359-5997. Dostupné z: http://link.springer.com/10.1617/s11527-012-9978-z

SARIKAYA, Ayhan a Fatih DOGAN. 2013. Effect of various pore formers on the microstructural development of tape-cast porous ceramics. Ceramics International. 39(1): 403-413. DOI: 10.1016/j.ceramint.2012.06.041. ISSN 02728842. Dostupné z: http://linkinghub.elsevier.com/retrieve/pii/S0272884212005706

SARKER, Prabir Kumar, Sean KELLY a Zhitong YAO. 2014. Effect of fire exposure on cracking, spalling and residual strength of fly ash geopolymer concrete. *Materials*. 63: 584-

592. DOI: 10.1016/j.matdes.2014.06.059. ISSN 02613069. Dostupné z: http://linkinghub.elsevier.com/retrieve/pii/S0261306914005147

SHI, Caijun, P KRIVENKO a D ROY. 2006. *Alkali-activated cements and concretes*. London: Taylor, ix, 376 s. ISBN 04-157-0004-3.

SCHNEIDER, M., M. ROMER, M. TSCHUDIN a H. BOLIO. Sustainable cement production—present and future. Cement and Concrete Research [online]. 2011, 41(7), 642-650 [cit. 2018-05-21]. DOI: 10.1016/j.cemconres.2011.03.019. ISSN 00088846. Dostupné z: http://linkinghub.elsevier.com/retrieve/pii/S0008884611000950

SINGH, Gurpreet a Vijaya Kumar BULASARA. Preparation of low-cost microfiltration membranes from fly ash. Desalination and Water Treatment [online]. 2013, , 1-9 [cit. 2018-04-30]. DOI: 10.1080/19443994.2013.855677. ISSN 1944-3994. Dostupné z: http://www.tandfonline.com/doi/abs/10.1080/19443994.2013.855677

SINGH, B., M.R. RAHMAN, R. PASWAN a S.K. BHATTACHARYYA. Effect of activator concentration on the strength, ITZ and drying shrinkage of fly ash/slag geopolymer concrete. Construction and Building Materials [online]. 2016, 118, 171-179 [cit. 2018-03-14]. DOI: 10.1016/j.conbuildmat.2016.05.008. ISSN 09500618. Dostupné z: http://linkinghub.elsevier.com/retrieve/pii/S0950061816307267

SING, K. S. W. 1985-01-1. Reporting physisorption data for gas/solid systems with special reference to the determination of surface area and porosity (Recommendations 1984): Definitions, Terminology and Symbols in Colloid and Surface Chemistry. *Pure and Applied Chemistry*. 57(4): -. DOI: 10.1351/pac198557040603. ISSN 1365-3075. Dostupné z: http://www.degruyter.com/view/j/pac.1985.57.issue-4/pac198557040603/pac198557040603.xml

SUTHERLAND, Ken. *Filters and filtration handbook*. Boston, MA: Elsevier, 2008, p. cm. ISBN 978-185-6174-640.

SVOBODA, P, J DOLEŽAL, F ŠKVÁRA, L KOPECKÝ a M LUCUK. Současný stav výzkumu v oblasti geopolymerů. Praha: Česká rozvojová agentura, 2005.

SWICOFIL: Undestanding Geotextiles [online]. [cit. 2015-06-09]. Dostupné z: http://www.swicofil.com/othermarket_geotextiles.html

ŠESTÁK, Jaroslav, Miroslav HOLEČEK a Jiří MÁLEK, ed. Some thermodynamic, structural and behavioral aspects of materials accentuating non-crystalline states. Nymburk: OPS, 2009. ISBN 978-80-87269-06-0.

ŠKVÁRA, František. Alkalicky aktivované materiály: geopolymery [online]. In: . Praha: Ústav skla a keramiky VŠCHT, 2007, s. 1-49 [cit. 2016-10-10]. Dostupné z: http://old.vscht.cz/sil/pojiva/geo_2007.pdf

ŠNITA, Dalimil. 2005. Chemické inženýrství I. 1. vyd. Praha: VŠCHT, 318 s. ISBN 80-708-0589-7.

ŠOUKAL, F, T OPRAVIL, P PTÁČEK, B FOLLER a J BRANDŠTETR. Geopolymers-amorphous ceramics via solution. In: Some Thermodynamic, Structural and Behavioral Aspects of Materials Accentuating Non-Crystalline States. Plzeň: OPS Nymburk, 2009, s. 556-584. ISBN 978-80- 87269-06-0.

TEMUUJIN, J., R.P. WILLIAMS a A. VAN RIESSEN. Effect of mechanical activation of fly ash on the properties of geopolymer cured at ambient temperature. Journal of Materials Processing Technology [online]. 2009, 209(12-13), 5276-5280 [cit. 2018-05-21]. DOI: 10.1016/j.jmatprotec.2009.03.016. ISSN 09240136. Dostupné z: http://linkinghub.elsevier.com/retrieve/pii/S0924013609001058

TEWARI, P.K., R.K. SINGH, V.S. BATRA a M. BALAKRISHNAN. Membrane bioreactor (MBR) for wastewater treatment: Filtration performance evaluation of low cost polymeric and ceramic membranes. Separation and Purification Technology [online]. 2010, 71(2), 200-204 [cit. 2018-06-02]. DOI: 10.1016/j.seppur.2009.11.022. ISSN 13835866. Dostupné z: http://linkinghub.elsevier.com/retrieve/pii/S1383586609004791

THO-IN, Tawatchai, Vanchai SATA, Prinya CHINDAPRASIRT a Chai JATURAPITAKKUL. Pervious high-calcium fly ash geopolymer concrete. Construction and Building Materials [online]. 2012, 30, 366-371 [cit. 2018-05-21]. DOI: 10.1016/j.conbuildmat.2011.12.028. ISSN 09500618. Dostupné z: http://linkinghub.elsevier.com/retrieve/pii/S0950061811007057

VAN JAARSVELD, J.G.S., J.S.J. VAN DEVENTER a L. LORENZEN. The potential use of geopolymeric materials to immobilise toxic metals: Part I. Theory and applications. Minerals Engineering [online]. 1997, 10(7), 659-669 [cit. 2018-06-06]. DOI: 10.1016/S0892-6875(97)00046-0. ISSN 08926875. Dostupné z: http://linkinghub.elsevier.com/retrieve/pii/S0892687597000460

VAN JAARSVELD, J.G.S, J.S.J VAN DEVENTER a G.C LUKEY. The effect of composition and temperature on the properties of fly ash- and kaolinite-based geopolymers. Chemical Engineering Journal [online]. 2002, 89(1-3), 63-73 [cit. 2018-04-30]. DOI: 10.1016/S1385-8947(02)00025-6. ISSN 13858947. Dostupné z: http://linkinghub.elsevier.com/retrieve/pii/S1385894702000256

WAESELMANN, Naëmi. Structural transformations in complex perovskite-type relaxor and relaxor-based ferroelectrics at high pressures and temperatures. Hamburg, 2012. Dissertation. University of Hamburg. Vedoucí práce Dr. habil. Boriana Mihaylova.

WANG, S, M SOUDI, L LI a Z ZHU. Coal ash conversion into effective adsorbents for removal of heavy metals and dyes from wastewater. Journal of Hazardous Materials [online]. 2006, 133(1-3), 243-251 [cit. 2018-06-11]. DOI: 10.1016/j.jhazmat.2005.10.034. ISSN 03043894. Dostupné z: http://linkinghub.elsevier.com/retrieve/pii/S0304389405006321

XIE, Jiting a Obada KAYALI. Effect of initial water content and curing moisture conditions on the development of fly ash-based geopolymers in heat and ambient temperature. Construction and Building Materials [online]. 2014, 67, 20-28 [cit. 2018-04-30]. DOI: 10.1016/j.conbuildmat.2013.10.047. ISSN 09500618. Dostupné z: http://linkinghub.elsevier.com/retrieve/pii/S0950061813009689

YE, Hailong a Aleksandra RADLIŃSKA. Fly ash-slag interaction during alkaline activation: Influence of activators on phase assemblage and microstructure formation. Construction and Building Materials[online]. 2016, 122, 594-606 [cit. 2018-03-14]. DOI: 10.1016/j.conbuildmat.2016.06.099. ISSN 09500618. Dostupné z: http://linkinghub.elsevier.com/retrieve/pii/S0950061816310273

YE, Hailong a Aleksandra RADLIŃSKA. Shrinkage mitigation strategies in alkali-activated slag. Cement and Concrete Research [online]. 2017, 101, 131-143 [cit. 2018-06-11]. DOI: 10.1016/j.cemconres.2017.08.025. ISSN 00088846. Dostupné z: http://linkinghub.elsevier.com/retrieve/pii/S000888461630093X

YUSUF, Moruf Olalekan, Megat Azmi MEGAT JOHARI, Zainal Arifin AHMAD a Mohammed MASLEHUDDIN. Effects of H_2O/Na_2O molar ratio on the strength of alkaline activated ground blast furnace slag-ultrafine palm oil fuel ash based concrete. Materials & Design (1980-2015) [online]. 2014, 56, 158-164 [cit. 2018-03-14]. DOI: 10.1016/j.matdes.2013.09.078. ISSN 02613069. Dostupné z: http://linkinghub.elsevier.com/retrieve/pii/S0261306913009722

ZDRAVKOV, Borislav, Jiří ČERMÁK, Martin ŠEFARA a Josef JANKŮ. Pore classification in the characterization of porous materials: A perspective. Open Chemistry [online]. 2007, 5(2), - [cit. 2018-03-26]. DOI: 10.2478/s11532-007-0017-9. ISSN 2391-5420. Dostupné z: http://www.degruyter.com/view/j/chem.2007.5.issue-2/s11532-007-0017-9/s11532-007-0017-9.xml

ZHANG, Jin, Yan HE, Yi-pin WANG, Jin MAO a Xue-min CUI. Synthesis of a self-supporting faujasite zeolite membrane using geopolymer gel for separation of alcohol/water mixture. Materials Letters [online]. 2014, 116, 167-170 [cit. 2018-04-30]. DOI: 10.1016/j.matlet.2013.11.008. ISSN 0167577X. Dostupné z: http://linkinghub.elsevier.com/retrieve/pii/S0167577X13015255

ZHANG, Mo, Tahar EL-KORCHI, Guoping ZHANG, Jianyu LIANG a Mingjiang TAO. Synthesis factors affecting mechanical properties, microstructure, and chemical composition of red mud–fly ash based geopolymers. Fuel [online]. 2014, 134, 315-325 [cit. 2018-05-21]. DOI: 10.1016/j.fuel.2014.05.058. ISSN 00162361. Dostupné z: http://linkinghub.elsevier.com/retrieve/pii/S0016236114005201

ZHANG, Yaojun a Licai LIU. Fly ash-based geopolymer as a novel photocatalyst for degradation of dye from wastewater. Particuology [online]. 2013, 11(3), 353-358 [cit. 2018-05-21]. DOI: 10.1016/j.partic.2012.10.007. ISSN 16742001. Dostupné z: http://linkinghub.elsevier.com/retrieve/pii/S1674200113000680

ZHANG, Zuhua, Liangfeng LI, Dongning HE, Xue MA, Chunjie YAN a Hao WANG. Novel self-supporting zeolitic block with tunable porosity and crystallinity for water treatment. Materials Letters [online]. 2016, 178, 151-154 [cit. 2018-06-02]. DOI: 10.1016/j.matlet.2016.04.214. ISSN 0167577X. Dostupné z: http://linkinghub.elsevier.com/retrieve/pii/S0167577X16307194

ZHANG, Zuhua, Hao WANG, Yingcan ZHU, Andrew REID, John L. PROVIS a Frank BULLEN. Using fly ash to partially substitute metakaolin in geopolymer synthesis. Applied Clay Science [online]. 2014B, 88-89, 194-201 [cit. 2018-05-21]. DOI: 10.1016/j.clay.2013.12.025. ISSN 01691317. Dostupné z: http://linkinghub.elsevier.com/retrieve/pii/S0169131713004420

9 LIST OF FIGURES

Figure 1: Hypothetical porous grain cross section showing various types of pores: closed (C), blind (B), through (T), interconnected (I), together with some roughness (R) (Rouquerol, 1990). 13
Figure 2: Positions of hydraulic and pozzolan compounds in CaO-SIO_2-Al_2O_3(Fe_2O_3) ternary diagram of minerals. 1 – Portland cements, 2 – blast furnace slags, 3 – silica fumes, 4 – CaO-rich fly ash, 5 – SiO_2-rich (siliceous) fly ash, 6 – pozzolan fly ash. (Pytlík, 2000) 20
Figure 3: Typical composition of pozzolanic materials (Šesták et al., 2009). 20
Figure 4: Schematic diagram of pozzolan types due to Massazza (1993) 22
Figure 5: Q^4(mAl) structures (Barbosa et al, 2000). 26
Figure 6: Visualization of alkali activation mechanism. Note: the gel formation begins from supersaturated solution. 28
Figure 7: A closer schematic look at randomly distributed and cross-linked tetrahedron polymeric structure of geopolymer (Šoukal et al., 2009). 28
Figure 8: Terminology of poly(sialate) geopolymers (Davidovits, 2008). 29
Figure 9: Poly(sialate), poly(sialate-siloxo) and poly(sialate-disiloxo)structure illustrations (colorized)(Davidovits, 2008). 30
Figure 10: Left – The overview of the spiral jet mill assembly (including vibratory dispenser, air pressure controller and collecting container); Right – Illustration of movement inside the milling chamber (Hosokawa, 2011). 35
Figure 11: Air jet sieve assembly overview and sieving chamber air movement illustration above (Hosokawa, 2012). 36
Figure 12: ALPINE 50 ATP Turboplex and a scheme of the classifying chamber function. (Hosokawa Alpine Turboplex Classifier ATP) 37
Figure 13: Olympus BX41. 38
Figure 14: Zeiss EVO scanning electron microscope with control and display componens; measurement cell insight (A); rotable specimen holder (B). (Carl Zeiss AG, 2017) 39
Figure 15: Malvern Mastersizer 2000 with wet-measurement cell plugged in the middle and dry-measurement cell in the holder (left). 40
Figure 16: Planetary centrifugal vacuum mixer Thinky ARV-310 and a scheme of the mixing cell movement during operation 41
Figure 17: The control/CPU module (left) and the sample holder of the 3Gzh porometer. 42
Figure 18: LaborTech LabTest 6.0051 uniaxial testing machine. 43
Figure 19: Schematic representation of Braggs law (Waeselmann, 2012). 44
Figure 20: XRD goniometer of Siemens D5005 set accordingly to the scheme of the function. 44
Figure 21: Experimental filtration post. 45
Figure 22: Prunéřov II fly ash after removal of the fraction above 500µm. 47
Figure 23: Prunéřov II fly ash after second fractionation to remove the finer fractions. 48
Figure 24: Non-fractionated GGBFS. 49
Figure 25: GGBFS after fractionation 50
Figure 26: Particular materials granulometries before classification. 51
Figure 27: Particular materials granulometries after classification. 52
Figure 28: The MATLAB-based compositions illustrated in 3D coordinate system. 60
Figure 29: Convex hull of the set in Fig.20 view on the coordinate system. 60
Figure 30: The MATLAB-based compositions illustrated in 3D coordinate system. 61
Figure 31: Convex hull of the set in Fig.22 view on the coordinate system. 61

Figure 32: The MATLAB-based compositions illustrated in 3D coordinate system. 62
Figure 33: Convex hull of the set in Fig.24 view on the coordinate system. 62
Figure 34: Hydraulic manual press with pressure gauge. 65
Figure 35: The exhibition of the molding layout during the 25mm barriers preparation. 66
Figure 36: Examples of 25mm and 50mm barriers, ordinary (left) and experimentaly reinforced with short-chopped silanized E-glassfiber roving (right). 67
Figure 37: Molds and punches manufactured for 25mm and 50mm barriers production and an experimental mold with built-in support for filtration testing post. 68
Figure 38: Horizontal mold manufactured for uniaxial strength testing columns production (column size lxhxw = 100x10x10mm). 69
Figure 39: Experimental vertical mold and punch manufactured for uniaxial strength testing columns production by pressing column size lxhxw = 100x10x10mm. 69
Figure 40: Example of unsuccessfully made testing columns with pressure dissipation between layers pressed at each other visible due to color-changing phenomena. 70
Figure 41: A spread of mixture extremely manifesting the color-changing phenomena after leaving it for 5 weeks in laboratory conditions. 71
Figure 42: A barrier and a leftover material showing the color-changing phenomena after leaving it for 3 weeks in laboratory conditions. 71
Figure 43: Two identical mixture filtration barriers after 1 week in laboratory conditions, bottom surface (left) to top surface (right) comparison. 72
Figure 44: Uniaxial tensile strength testing layout scheme with two bodies loading (ČSN EN 12390-5). 73
Figure 45: Uniaxial tensile strength measuring clamping bracket designed and manufactured to follow the ČSN EN 12390-5 rules. 74
Figure 46: Strength-testing of the prepared geopolymer columns prepared 100 mm in length to assure 3 measurements from each body (broken in halves and those tested separately). 74
Figure 47: Parameter P1 to uniaxial tensile strength dependence diagram. 76
Figure 48: Parameter P2 to uniaxial tensile strength dependence diagram. 76
Figure 49: Parameter P3 to uniaxial tensile strength dependence diagram. 77
Figure 50: Water to solid ratio to uniaxial tensile strength dependence diagram. 77
Figure 51: Fly ash content to uniaxial tensile strength dependence diagram. 78
Figure 52: Blast furnace slag content to uniaxial tensile strength dependence diagram. 78
Figure 53: Alkali activator (sodium hydroxide) concentration to uniaxial tensile strength dependence diagram of the fly ash and GGBFS based mixtures series. 79
Figure 54: Concentrations of Na_2O in the alkali-activated fly ash paste specimens. The prism 40x40x160mm was leached in regularly replaced deionized water.(Hlaváček, 2014) 80
Figure 55: Comparison of average porosity between classified (C) and unclassified (U) GGBFS-based mixture membranes determined using MIP. 81
Figure 56: CFP-based differential porosity curves of chosen MATLAB samples 82
Figure 57: CFP-based differential porosity curves of chosen MATLAB samples 83
Figure 58: CFP-based differential porosity curves of fly ash samples 84
Figure 59: MIP-based porosity measurements of fly ash samples expressed in volume change of intruded mercury into certain pore diameter normalized to the sample weight 84
Figure 60: MIP-based differential porosity measurements of fly ash samples 85

Figure 61: CFP-based differential porosity curves of GGBFS samples 86
Figure 62: MIP-based porosity measurements of GGBFS samples expressed in volume change of intruded mercury into certain pore diameter normalized to the sample weight 87
Figure 63: MIP-based differential porosity measurements of GGBFS samples 87
Figure 64: MIP-based porosity measurements of GGBFS samples expressed in volume change of intruded mercury into certain pore diameter normalized to the sample weight 88
Figure 65: MIP-based differential porosity measurements of GGBFS samples 88
Figure 66: Microstructure of the prepared specimens (FA 6 on the left and FA-12 on the right) observed by SEM in SE mode, magnitude 200× 89
Figure 67: Comparison of the binder phase between FA particles (FA-6 upwards and FA-12 underneath) as observed by SEM in BSE mode, magnitude 2000×. 90
Figure 68: Extreme case of efflorescence – crystals slowly emerging on one of the AAFA samples (the front edge of the sample is 2cm wide) 91
Figure 69: Detail pictures of macroscopic crystals from the specimen in the previous figure. 92
Figure 70: Individual images of each element investigated on the FA-based specimen by EDS. 93
Figure 71: Layered image made from the individual EDS analysis of FA-based specimen. 94
Figure 72: EDS quantitative analysis of the scanned area of the FA-based specimen. 94
Figure 73: XRD analysis of crystals emerging on FA-based samples 95
Figure 74: Microstructure of polished (up) and unpolished (down) parts of the membrane from unclassified (left) and classified (right) GGBFS; magnitude 2 000×. 96
Figure 75: Detail of polished (left) and unpolished (right) part of the membrane from classified GGBFS; magnitude 10 000×. 96
Figure 76: Individual images of each element investigated on the GGBFS specimen by EDS. 97
Figure 77: Layered image from the individual EDS analysis of GGBFS-based specimen. 98
Figure 78: EDS quantitative analysis of the scanned area of the GGBFS-based specimen. 98
Figure 79: CFP-based differential porosity curves of the X composition samples. 99
Figure 80: SEM image of of the X composition structure; magnitude 5000x. 100
Figure 81: Coarse GBFS after classification. 102
Figure 82: SEM image of GBFS morphology; magnitude 50x. 102
Figure 83: Asymmetrical porous body SEM image; magnitude 100x. 103
Figure 84: Coarse supporting body structure; magnitude 500x. 103

10 LIST OF TABLES

Table 1: The separation processes spectrum (Sutherland, 2008). 10
Table 2: Porous solids - definitions of selected important terms (Rouquerol et al., 2008). 12
Table 3: The overview of filter media types by material (Sutherland, 2008). 15
Table 4: The overview of filter media types by format (Sutherland, 2008). 16
Table 5: Typical composition of FA, GGBFS and Portland cement comparison (GCPAT, 2016). 22
Table 6: Prunéřov II fly ash oxide composition. 46
Table 7: Kotouč Štramberk slag oxide composition. 49
Table 8: Bauxite oxide composition. 50
Table 9: Sodium hydroxide 50%wt. (left) and water glass (right) activators oxide compositions. 52
Table 10: Material costs. 53
Table 11: MATLAB-based compositions chosen for experiments. 63
Table 12: Pure two-component fly ash (FA) and slag (S) mixtures compositions. 64
Table 13: FA and S compositions for investigation of the activator concentration influences. 64
Table 14: Uniaxial tensile strength measurements results in context with mixtures compositions and parameters, each result averaged from 4 measurements. 75
Table 15: Uniaxial tensile strength results of the fly ash and GGBFS based mixtures in context with compositions and parameters, each result averaged from 4 measurements. 79
Table 16: The average total porosity of the GGBFS samples with their standard deviations. 86
Table 17: Composition and parameters of the final porous material X. 99

11 LIST OF ABREVIATIONS AND SYMBOLS

AAFA	alkali-activated fly ash
AAM	alkali-activated material
AAS	alkali-activated slag
AFm	phase of Portland cements (hydrated calcium aluminates $4CaO \cdot Al_2O_3 \cdot 13–19\ H_2O$)
API	American petroleum industry
BFS	blast furnace slag
BIB	broad ion beam
BSE	back scattered electron
CASH	calcium aluminosilicate hydrate
CFP	capillary flow porosimetry
CSH	calcium silicate hydrate
ČSN EN	Czech technical standard introducing a European standard into Czech standard system
DFT	density functional theory
EDS	energy dispersive spectroscopy
FA	fly ash
GBFS	granulated blast furnace slag
GGBFS	ground granulated blast furnace slag
MIP	mercury intrusion porosimetry
NASH	sodium aluminosilicate hydrate
P1	SiO_2:Al_2O_3 ratio
P2	Na_2O:Al_2O_3 ratio
P3	H_2O: Na_2O ratio
SE	scattered electron
SEM	scanning electron microscopy
SOP	standard operating procedure
TEM	transmission electron microscopy
XRD	X-ray diffraction

d	distance of two adjacent crystallographic planes
d_1	dimensions of the cross section of the testing column
d_2	dimensions of the cross section of the testing column
F	maximal loading strain
f_{ct}	the uniaxial tensile strength
l	distance between supporting rollers
V_{Pores}	pores volume fraction
V_{Total}	total volume of teh specimen
w/s	water:solid ratio
ε	porosity
ϑ	diffraction angle
λ	wavelength

12 AUTHOR'S CURRICULUM VITAE

Personal information	
Name	**Ing. et Bc. Pavel Kejík**
E-mail	pavelkejik@vut.cz
Phone	+420 54114 4912
Date of Birth	16.12.1987
Education	
Dates	2012 - 2018
Degree	Doctoral
Discipline	Applied Sciences in Engineering
Organization	Brno University of Technology, Faculty of Mechanical Engineering
Dates	2010 - 2012
Degree	Master's
Discipline	Chemistry, Technology and Properties of Materials
Organization	Brno University of Technology, Faculty of Chemistry
Dates	2008 - 2013
Degree	Bachelor's
Discipline	Microbiology
Organization	Masaryk University, Faculty of Science
Dates	2007 - 2010
Degree	Bachelor's
Discipline	Chemistry, Technology and Properties of Materials
Organization	Brno University of Technology, Faculty of Chemistry
Selected Experience	
Dates	2010
Discipline	Materials Engineering, Winter Semestral Traineeship
Organization	Istituto Superior Técnico, Lisbon, Portugal
Dates	2013 – 2014
Discipline	Solid/Liquid Separation Internship
Organization	Lappeenranta University of Technology, Finland

13 AUTHOR'S RESEARCH ACTIVITIES

13.1 PUBLICATIONS AND CONFERENCE ATTENDANCES

2018

KEJÍK, P.; BÍLEK Jr., V.; BULEJKO, P.; HAJZLER, J.; BŘEZINA, M.; GALVÁNKOVÁ, L.; KALINA, L. Porous Systems Based on Alkali-Activated Fly Ash. In Binders, Materials and Technologies in Modern Construction IV. Solid State Phenomena. Switzerland: Trans Tech Publications, 2018. s. 179-184. ISBN: 978-3-0357-1348-0. ISSN: 1662-9779.

BÍLEK Jr., V.; BULEJKO, P.; KEJÍK, P.; HAJZLER, J.; MÁSILKO, J.; BEDNÁREK, J.; TKACZ, J.; KALINA, L. Potential use of blast furnace slag for filtration membranes preparation: A pilot study. In International Conference Building Materials, Products and Technologies. IOP Conference Series: Materials Science and Engineering. Bristol: IOP Publishing, 2018. s. 1-6. ISSN: 1757-899X.

BULEJKO, P.; DOHNAL, M.; POSPÍŠIL, J.; KRIŠTOF, O.; SVĚRÁK, T.; KEJÍK, P. Air filtration using hollow-fibre membranes for nanoparticle removal. In FILTECH 2018, March 13-15, Cologne – Germany. 2018. s. 1-12. ISBN: 978-3-941655-15-7.

2017

KRIŠTOF, O.; SVĚRÁK, T.; BULEJKO, P.; KEJÍK, P.; KALIVODA, J. Experimental and CFD investigation of gas and liquid phase in scrubber for absorption processes. In 44th International Conference of the Slovak Society of Chemical Engineering. 2017. s. 448-453. ISBN: 978-80-89597-58- 1.

SVĚRÁK, T.; BULEJKO, P.; OSTREZI, J.; KRIŠTOF, O.; KALIVODA, J.; KEJÍK, P.; MAYEROVÁ, K.; ADAMČÍK, M. Separation of gaseous air pollutants using membrane contactors. IOP Conference Series: Earth and Environmental Science, 2017, roč. 92, č. 1, s. 1-5. ISSN: 1755-1315.

BÓGYIOVÁ, C.; BULEJKO, P.; FEKETE, R.; KEJÍK, P.; KALIVODA, J.; KRIŠTOF, O.; TKACZ, J.; VLASÁK, J.; WASSERBAUER, J.; SVĚRÁK, T. BULK PROPERTIES OF PYROLYSIS COKE. Brno: Brno University of Technology, Faculty of Chemistry, 2017. s. 1-44.

BULEJKO, P.; DOHNAL, M.; POSPÍŠIL, J.; KRIŠTOF, O.; KEJÍK, P.; SVĚRÁK, T. Efficiency of hollow- fiber membranes for air filtration of submicron particles. In 44th International Conference of the Slovak Society of Chemical Engineering. 2017. s. 495-499. ISBN: 978-80-89597-58- 1.

SVĚRÁK, T.; BULEJKO, P.; KRIŠTOF, O.; KEJÍK, P.; KALIVODA, J.; HORSKÝ, J. Covering ability of aluminum pigments prepared by milling processes. POWDER TECHNOLOGY, 2017, roč. 305, č. 1, s. 396-404. ISSN: 0032-5910.

2016

SVĚRÁK, T.; BULEJKO, P.; MAYEROVÁ, K.; KEJÍK, P.; KRIŠTOF, O.; RAUDENSKÝ, M. Hiding Power of Aluminum Metal Pigments Development in the Ball Mill Grinding Process. Solid State Phenomena, 2016, roč. 244, č. 1, s. 19-25. ISSN: 1662-9779.

BULEJKO, P.; SVĚRÁK, T.; DOHNAL, M.; POSPÍŠIL, J.; KRIŠTOF, O.; KEJÍK, P.; KALIVODA, J. Filtrační účinnost membrán na bázi dutých vláken při odstraňování částic ze vzduchu. In Sborník XVII. výroční konference České aerosolové společnosti, 25. – 26. října 2016, Mikulov. Praha: Česká aerosolová společnost, 2016. s. 65-68. ISBN: 978-80-86186-85- 6.

KEJÍK, P.; BULEJKO, P.; SVĚRÁK, T.; KRIŠTOF, O.; MAYEROVÁ, K. Self-supported Geopolymer- based Barriers for Filtration Applications. 24th INTERNATIONAL CONFERENCE ON MATERIALSAND TECHNOLOGY. Ljubljana, Slovenia: Inštitut za kovinske materiale in tehnologije, 2016. ISBN: 978-961-94088-0- 3.

BULEJKO, P.; SVĚRÁK, T.; DOHNAL, M.; KEJÍK, P.; KRIŠTOF, O.; MAYEROVÁ, K. Air filtration using polymeric hollow- fibre membranes. 22nd International Congress of Chemical and Process Engineering CHISA 2016 and the 19th Conference on Process Integration, Modelling and Optimisation for Energy Saving and Pollution Reduction PRES 2016. Praha: Czech Society of Chemical Engineering, 2016.

2015

SVĚRÁK, T.; BAKER, C. G. J.; SIKOROVÁ, K.; KEJÍK, P.; BULEJKO, P.; KRIŠTOF, O. Progress of the IR measurement in the area of the fine, particulate material water content. International Journal of Environmental Engineering, 2015, roč. 2, č. 1, s. 146-149. ISSN: 2374-1724.

KINNARINEN, T.; TUUNILA, R.; HUHTANEN, M.; HÄKKINEN, A.; KEJÍK, P.; SVĚRÁK, T. Wet grinding of CaCO3 with a stirred media mill: Influence of obtained particle size distributions on pressure filtration propertie. POWDER TECHNOLOGY, 2015, roč. 273, č. 1, s. 54-61. ISSN: 0032- 5910.

KINNARINEN T.; TUUNILA R.; HUHTANEN M.; HÄKKINEN A.; KEJÍK, P.; SVĚRÁK, T. Prediction of pressure filtration characteristics of CaCO3 suspensions, ground in a vertical stirred media mill. MINERALS ENGINEERING, 2015, roč. 83, č. 1, s. 201-204. ISSN: 0892-6875.

KEJÍK, P.; SVĚRÁK, T.; BORGUĽOVÁ, E.; BULEJKO, P.; KRIŠTOF, O.; MAYEROVÁ, K.; HURYCHOVA, H.; ŠKLUBALOVA, Z.; PECIAR, P. SURFACTANTS GRINDING ACTIVATION OF CLINKER. Scientifc proceedings, 2015, č. 23, s. 53-56. ISSN: 1338-1954.

SVĚRÁK, T.; BULEJKO, P.; KEJÍK, P.; MAYEROVÁ, K.; KRIŠTOF, O.; RAUDENSKÝ, M. Bulk properties of surface treated limestone powders. In Conference Proceedings, 1st International Conference on Applied Mineralogy & Advanced Materials – AMAM2015. Conference Proceedings, 1st International Conference on Applied Mineralogy & Advanced Materials – AMAM2015. Digilabs S.a.s., 2015. s. 71-76. ISSN: 2283- 5954.

KEJÍK, P.; SVĚRÁK, T.; KRIŠTOF, O.; BULEJKO, P.; MAYEROVÁ, K. Attritor iron content measurement via objective colour determination. 23rd INTERNATIONAL CONFERENCE ON MATERIALSAND TECHNOLOGY PROGRAM AND BOOK OF ABSTRACTS. Ljubljana, Lepi pot 11, Ljubljana, Slovenija: Inštitut za kovinske materiale in tehnologije, 2015. s. 125-125. ISBN: 978-961-92518-8- 1.

2014

KEJÍK, P.; SVĚRÁK, T.; SIKOROVÁ, K.; KRIŠTOF, O.; BULEJKO, P. COIR- BASED FILLERS GRINDING AND BULK PROPERTIES. 22nd INTERNATIONAL CONFERENCE ON MATERIALS AND TECHNOLOGY. Ljubljana, Slovenia: Inštitut za kovinske materiale in tehnologije, Ljubljana, Lepi pot 11, Ljubljana, Slovenija, 2014. s. 111-111. ISBN: 978-961-92518-7- 4.

KRIŠTOF, O.; SVĚRÁK, T.; KEJÍK, P.; BULEJKO, P.; SIKOROVÁ, K. CO2 absorption to the NaOH solution using pilot- plant wet shower scrubber. 21st International Congress of Chemical Engineering CHISA 2014 and 17th Conference PRES 2014, 23 - 27 August 2014, Praha, Czech Republic, Czech Society of Chemical Engineering. 2014. ISBN: 978-80-02-02555- 9.

KRIŠTOF, O.; SVĚRÁK, T.; BULEJKO, P.; KEJÍK, P.; SIKOROVÁ, K. PILOT- PLANT SHOWER SCRUBBER FOR CLEANING POLLUTED GAS. 22nd INTERNATIONAL CONFERENCE ON MATERIALS AND TECHNOLOGY. Ljubljana, Slovenia: Inštitut za kovinske materiale in tehnologije, Ljubljana, Lepi pot 11, Ljubljana, Slovenija, 2014. s. 128-128. ISBN: 978-961-92518-7- 4.

SVĚRÁK, T.; Baker, G. J. CH.; SIKOROVÁ, K.; KEJÍK, P.; BULEJKO, P.; KRIŠTOF, O. Progress of the IR measurement in the area of the fine particulate material water content. In Proceedings of the 2nd International Conference on Advances in Applied Science and Environmental Engineering. USA: Institute of Research Engineers and Doctors, 2014. s. 20-23. ISBN: 978-1-63248-033- 0.

BULEJKO, P.; SIKOROVÁ, K.; KEJÍK, P.; KRIŠTOF, O.; SVĚRÁK, T. Filtration Membranes Based on Secondary Materials: Preparation, Characterization, and Properties. 22nd

INTERNATIONAL CONFERENCE ON MATERIALS AND TECHNOLOGY. Ljubljana, Slovenia: Inštitut za kovinske materiale in tehnologije, Ljubljana, Lepi pot 11, Ljubljana, Slovenija, 2014. ISBN: 978-961-92518-7- 4.

KEJÍK, P.; SVĚRÁK, T.; SIKOROVÁ, K.; KRIŠTOF, O.; BULEJKO, P. Specific grinding energy and phase changes of the limestone and corundum ground stock in the ultrafine activated comminution process. 21st International Congress of Chemical Engineering CHISA 2014 and 17th Conference PRES 2014, 23 - 27 August 2014, Praha, Czech Republic, Czech Society of Chemical Engineering. 2014. s. 1 (1 s.). ISBN: 978-80-02-02555- 9.

BULEJKO, P.; SVĚRÁK, T.; KEJÍK, P.; KRIŠTOF, O.; SIKOROVÁ, K. The potential use of geopolymer- based materials in filtration applications. 21st International Congress of Chemical Engineering CHISA 2014 and 17th Conference PRES 2014, 23 - 27 August 2014, Praha, Czech Republic, Czech Society of Chemical Engineering. 2014. ISBN: 978-80-02-02555- 9.

SVĚRÁK, T.; KEJÍK, P.; SLANINA, O.; SIKOROVÁ, K.; BULEJKO, P.; KRIŠTOF, O. Bulk properties of micro- fine ligneous fillers. In 21st International Congress of Chemical and Process Engineering CHISA 2014 and 17th Conference PRES 2014, Authors of papers. Praha: Orgit Ltd., 2014. s. 1-10. ISBN: 978-80-02-02555- 9.

2013

SVĚRÁK, T.; KEJÍK, P.; SLANINA, O.; KRIŠTOF, O.; SIKOROVÁ, K.; FEKETE, R. Mletí a sypné vlastnosti netypických dřevinových plniv. In Sborník CHISA 2013. 1. Srní: ČSCHI, 2013. s. B2.5- 1 (B2.5-10 s.)ISBN: 978-80-02-02500- 9.

KEJÍK, P.; SVĚRÁK, T.; SLANINA, O. MILLING AND BULK PROPERTIES OF SPECIAL VERY FINE WOOD POWDERS. In Selected processes at the wood processing. Zvolen, Slovakia: Department of Chemistry and Chemical Technologies, 2013. s. 1-10. ISBN: 978-80-228-2534- 4.

2012

SVĚRÁK, T.; KEJÍK, P. Mechanochemistry changes of the calcium carbonate grinding stock under the dry mode of the ultra- fine grinding conditions. In CHoPS 2012, 7th International Conference for Conveying and Handling of Particulate Solids, 10. - 13. September 2012, Friedrichshafen/ Germany. Friedrichshafen: 2012. s. 1-10. ISBN: 9781629935362.

13.2 PATENT

2015

SVĚRÁK, T.; MAYEROVÁ, K.; KEJÍK, P.; HORSKÝ, J.; RAUDENSKÝ, M.; DOHNAL, M.; TYŠER, L.; ŠTEVULOVÁ, N.; Vysoké učení technické v Brně, Brno, CZ: Způsob kontinuálního měření vlhkosti jemných sypkých materiálů a zařízení pro tento způsob měření. 305570, patent.

13.3 CREATIVE ACTIVITIES

2013

HORSKÝ, J.; KEJÍK, P.; KRIŠTOF, O.: FV10/LPTP/12/2013; Stend na měření chlazení hliníkových vzorků. LPTP/D3.

2012

HRAZDIL, V.; KRIŠTOF, O.; KEJÍK, P.: FV07/12/2012; Vertikální stend. LPTP/ D3/0010.